

Beyond Thin Films: Manufacturing Layer by Layer Assembled Composites into Tunable Architectures

by

Christine M. Andres

A dissertation submitted in partial fulfillment
Of the requirements for the degree of
Doctor of Philosophy
(Chemical Engineering)
in the University of Michigan
2013

Doctoral Committee:

Professor Nicholas A. Kotov, Chair
Professor Erdogan Gulari
Associate Professor A. John Hart
Professor Joerg Lahann

© Christine M. Andres 2013

All Rights Reserved

To my parents, *Dave and Annette*

ACKNOWLEDGMENTS

First and foremost I would like to acknowledge the support and guidance of my advisor, Professor Nicholas Kotov. You have been my biggest proponent. Your generous humility has repeatedly given me ownership for ideas and accomplishments that undoubtedly would not have been realized without your support. While many have the ability to motivate, few have the ability to inspire. The guidance you provided left room for the creativity and growth that has allowed me to experience a sense of gratification that can only be realized through the maturation of one's own thoughts. You have helped me to realize my capabilities as a scientist, and inspired me to reach beyond my preconceived limits. I am deeply grateful for your patience and support in my quest to define myself as a professional. Without any direct benefit to you, you selflessly allowed me to explore the depths of science policy, teaching strategies, and the international scientific community. By example you have shown me how to have the courage to be a leader and innovator who steps beyond previously defined limits.

Mentorship and support has come from many places across the University. I would like to specifically point out valuable conversations with Prof. Sulijo Linic and Prof. John Hart that have directly inspired part of the vision of this document. Prof.

Phil Savage and Dr. Susan Montgomery have relentlessly supported me with recommendations for numerous opportunities, including funding sources from the National Science Foundation and Intel, which have supported this work. There are many past and present members of the Kotov group who have contributed to this work with their time, expertise, and inspiration. This includes Hunan Zhang, Dr. Meghan Cuddihy, Dr. Paul Podsiadlo, Dr. Ashish Agarwal, Dr. Daniel Lilly, Dr. Sudhanshu Srivastava, Dr. Inigo Alvarez, Mary Fox and Connor Flynn. Of specific mention is Jian Zhu, who without a need for the spotlight works humbly behind the scenes to maintain the lab equipment, provide new skill sets to his peers, and perpetually serves as a friend to all in need. I could not possibly give him enough praise for all the contributions he has unselfishly made to my success.

Finally I would like to acknowledge my support system throughout this thesis. First, my parents who have led me through many of life's greatest lessons with unwavering support throughout my pursuit of happiness. Meghan & Tom, Courtney, and Easton have been great listeners and provided me with invaluable insights into life and happiness. Dan's unconditional love and support has meant more to me than words could ever express. Last, but certainly not least Caitlin and the "MSDA" have always been there to celebrate the good times and pull me up from life's disappointments. I am very grateful for the support that each and every one of you have offered.

TABLE OF CONTENTS

DEDICATION	ii
ACKNOWLEDGEMENTS	iii
LIST OF FIGURES	viii
ABSTRACT	x
CHAPTERS	
I. Introduction	
1.1 Motivation: Materials for Innovation	1
1.2 Current State of the Art in Material Processing.....	3
1.3 Characteristics of Broad Impact Material Processing.....	6
1.4 Broader Impacts.....	8
1.5 Nanocomposites from Layer by Layer (LBL) Assembly.....	9
1.6 LBL as a Broad Impact Material Processing Approach.....	12
1.7 Focus of Thesis.....	13
II. Inkjet Layer by Layer	
2.1 Advanced LBL Material: Carbon and Gold Nanocomposites.....	15
2.2 The Rinsing Step.....	17
2.3 Inkjet Technology as a Solution.....	19
2.4 Inkjet Deposition of LBL Nanocomposites.....	23
2.4.1 Nanoscale Assembly of Gold Nanocomposites	23
2.4.2 Structural Control Over Nanophase Coverage.....	26

2.4.3	Multi-Dimensional Structural Control.....	28
2.4.4	Carbon Nanotubes and Alternative Substrates	31
2.5	Conclusion.....	38
2.6	Experimental.....	39
2.6.1	Materials.....	39
2.6.2	Inkjet LBL Deposition of Gold Nanocomposites.....	40
2.6.3	Inkjet LBL Deposition of Carbon Nanotube Composites	41

III. Shape Morphing of LBL Nanocomposites

3.1	Shape Morphing Background	43
3.2	Advanced LBL Material: Stimuli-Responsive.....	46
3.3	Humidity Induced Shape Morphing of Nanocomposites	47
3.4	Temperature Induced Shape Morphing of Nanocomposites	51
3.5	Control Over Stimuli-Responsive Architecture	55
3.6	Conclusion.....	60
3.7	Experimental.....	61
3.7.1	Fabrication of LBL Nanocomposites	61
3.7.2	Analysis of Thermal Expansion Properties	62
3.7.3	Inkjet Deposition of Polyelectrolyte Multilayers	63
3.7.4	Characterization of Shape Morphing	64

IV. LBL Nanocomposite Microcontainers

4.1	Current State of Microcontainer Fabrication.....	66
4.2	Advanced LBL Material: Clay Nanocomposite.....	68
4.3	Nanocomposite Microcontainer Fabrication	69
4.4	Microcontainer Loading.....	72
4.5	Conclusion.....	73
4.6	Experimental.....	74
4.6.1	Materials.....	74
4.6.2	PDMS Mold Preparation	74
4.6.3	Microcontainer Fabrication	75
4.6.4	Synthesis of Nanoparticles	76

V. Three Dimensional Layer by Layer Assembly

5.1	A Need for Hierarchical 3D Structures	77
-----	---	----

5.2	Advanced LBL Material: Synthetic Bone.....	79
5.2.1	Fabrication of Synthetic Bone Mineral.....	79
5.2.2	Mechanical and Biological Properties	81
5.3	Approaches to Multiscale 3D Structural Control.....	85
5.4	Hierarchical Structural Control for Layer by Layer Assembly	87
5.5	Conclusion.....	91
5.6	Experimental.....	92
5.6.1	Calcium Phosphate Nanoparticle Synthesis.....	92
5.6.2	Fabrication of Synthetic Bone Material.....	93
5.6.3	Cell Culture Studies.....	94
5.6.4	Colloidal Crystal Template Synthesis.....	95
5.6.5	Three Dimensional Nanocomposite Assembly.....	96
 IV. Conclusion		
6.1	Improvements to LBL Processing for Broad Impact Use.....	99
6.2	Future Directions	102
 BIBLIOGRAPHY		104

LIST OF FIGURES

<u>Figure</u>	<u>Page</u>
Chapter I	
1.1 Transistors: then and now	4
1.2 Hierarchical structure of bone	7
1.3 Layer by layer assembly	11
Chapter II	
2.1 Schematic of inkjet layer by layer assembly	21
2.2 Nanophase coverage of traditional LBL	25
2.3 Nanoscale growth with inkjet technology	25
2.4 Controlled nanophase coverage with inkjet technology	27
2.5 Control over line width	28
2.6 Nanocomposite patterns	30
2.7 Functional inkjet printed nanocomposites	35
2.8 Schematic of microfabrication integration	36
2.9 Inkjet LBL combined with microfabrication techniques	37
Chapter III	
3.1 Schematic of bilayer hinge actuation	48
3.2 Humidity induced shape morphing	50
3.3 Thermal expansion of polyelectrolyte multilayers	53
3.4A Temperature induced shape morphing	54
3.4B Temperature induced shape morphing (continued)	55
3.5 Influence of thickness on shape morphing	57
3.6 Spatially controlled actuation	58
3.7 Spiral actuations	60

Chapter IV

4.1	Schematic of LBL microcontainer fabrication	69
4.2	Template assembly of microwells	70
4.3	Loaded microcontainers	71
4.4	Transparency and stability of microcontainers	73

Chapter V

5.1	Characterization of synthetic bone mineral	79
5.2	LBL deposition of synthetic bone	81
5.3	Osteoblast compatibility	83
5.4	Deposition of LBL in three dimensions	88
5.5	3D hierarchical structures from LBL	90

ABSTRACT

Materials with enhanced performance and unique property combinations provide promising solutions to our challenges in clean energy, national security and human welfare. As material properties emerge from both chemical and structural features, independent structural control across multiple length scales enables the realization of novel materials. Layer by layer (LBL) assembly provides nanoscale structural control for the fabrication of polymer-nanocomposites with exceptional material properties. However, the planar deposition technique limits the incorporation of alternative structural features as is required for advanced applications. Here several approaches to introduce multi-dimensional and multiscale architectures to LBL assembled nanocomposites are developed with an emphasis on sustainability and versatility.

First, inkjet technology is employed to sequentially deliver precise volumes of each LBL component for the accelerated production and simple direct-write patterning of gold nanocomposites. Expanded to carbon nanotube composites, the integration of inkjet LBL with paper-based electronics and traditional microfabrication techniques is explored. Next, reversible shape transformations are achieved in carbon nanotube composites driven by the stimuli-responsive behavior of polyelectrolyte multilayers. The responsive material is printed on the

nanocomposite to form a hinge structure that can deflect $\sim 37^\circ$ out of plane with temperature or humidity variations. Determined by the thickness and placement of the responsive material, various environmentally stimulated actuations are achieved. Finally, clay nanocomposites are assembled onto templates for the realization of permanent three-dimensional (3D) structures. First the high-strength, optically transparent material provides advanced functionality to microcontainers with potential applications in high-throughput analysis, controlled release, and smart packaging. Second, a novel deposition machine and a 3D template are used to create a macroscale and hierarchically tunable porous material that is discussed as a potential tissue-engineering scaffold. The fairly independent structural control of each technique provides the opportunity for future development of structure-property relationships and integration of LBL nanocomposites into next generation devices.

CHAPTER I

Introduction

1.1 Motivation: Materials for Innovation

Materials and the ability to shape them into tools that provide increased efficiency has been fundamental to the development of civilization, dating back to the dawn of our existence.^[4] The earliest evidence of toolmakers dates back 2.5 million years ago, when the method of controlled fracture was used to shape stone into tools.^[5] The Stone Age ended around 4,000 B.C. with the realization that bronze and later iron could be produced from ore and used to make tools and weapons that were able to withstand greater impact than those of stone.^[6] Through the development of advanced metal processing techniques the world was transformed. Mankind followed the history of metals as we built the world of today with technical advancements in transportation, infrastructure, and machinery.^[7] This was until recent history, when the introduction of synthetic plastics transformed our world yet again. With processing inventions like injection molding, and derivations of equations to describe the viscous flow of polymer melts,^[8] plastic became the new medium of choice for many modern innovations. Technological advancements such as in film, electronics, and prosthetics can be linked to this almost infinitely

moldable material and development of processing techniques to produce well-controlled, high-quality parts. In 1979 the global volume of steel production was surpassed by that of plastic in what has come to be known as the Plastic Age.^[9] Looking toward the future, many have proposed that nanotechnology will serve as the next material revolution, further driving innovation.^[10, 11]

The significance of nanomaterials, materials on the nanometer scale (one billionth of a meter), is not just another step towards miniaturization. Rather it is the scale at which atoms and molecules, the fundamental building blocks of materials assemble. Manipulation of materials at this scale allows for unique control of the material properties and present unexpected phenomena that are not present in the same materials on a larger scale.^[10] For example, carbon nanotubes (CNT),^[12] one-atom-thick sheets of carbon rolled into long hollow structures, can exhibit an electrical conductivity as high as copper, thermal conductivity as high as diamond, and strength at least 100 times greater than steel at only one sixth of the weight.^[13] Such remarkable properties can not be found in larger-scale carbon-based materials. Beyond CNT, nanomaterials have been prepared in many different shapes and compositions with unique optical, electrical, biological, thermal, and mechanical properties.^[11] These unique properties are of interest for new technological innovations that outperform current technologies and provide novel functionalities.

The technological advancements of the Stone, Metal, and Plastic Ages were feasible not only because of the revelation of the existence of a new material, but also the development of techniques to process the materials into something of value. Until mankind figured out how stone could be shaped into a hand-axe to more

efficiently cleave animal hide, it remained as just a stone. With the development of new materials, comes the demand for technology to process these “raw” materials into usable structures. Nano-scale materials hold the potential to contribute non-traditional solutions to the global challenges we face today. This includes energy generation, storage and conversion; lower-cost and more-accessible healthcare; and environmental sustainability amongst others.^[14] Their ability to contribute to societal change will depend on our ability to transfer nanomaterials out of the research lab and into consumer applications. In fact, the United States’ National Nanotechnology Initiative, a cooperative of nanotech activities across 25 Federal agencies, lists sustainable nanomanufacturing as one of three signature initiatives created to target resources toward critical challenges and significant gaps in research and development.^[15] The focus of this work is to address the pressing need for advanced processing technologies to take full advantage of the impressive, often times record-breaking, material properties of nanomaterials for technological innovation.

1.2 Current State of the Art in Material Processing

One of the greatest technological advancements of the modern world has been the transistor, a semiconducting material device that can both switch and amplify the flow of electrons. The transistor has been the building block of the digital revolution, enabling some of mankind’s greatest achievements. However, the true champion behind these achievements has been the material processing technologies able to fabricate transistors at decreasing scales. Considering the

original transistor built by Bell Labs in 1947 was assembled by hand (**Figure 1.1A**), and that the modern computer requires millions if not billions of transistors working together to complete a task, miniaturization and advancement of material processing was key to many advanced applications.

Photolithography is the material processing technique used to transfer geometric shapes onto the surface of silicon wafers by the semiconductor industry.^[16] It employs optical projection through a stencil (mask) to selectively activate a photosensitive material (resist). Light changes the solubility of the resist through cross-linking so that upon development, the parts of the resist exposed to light are insoluble and left behind while the soluble sections are washed away. This allows for a pattern of transistors and other components such as resistors and capacitors to be patterned together



Figure 1.1 A) A model of the first transistor assembled by hand at Bell Labs in 1947.^[1] B) Intel's 22nm Trigate transistors.^[2]

into one integrated circuit, or computer chip. With continuous improvements to shrink feature size, the lithography process now enables commercial products with feature sizes as small as 22nm (**Figure 1.1B**). In addition to size reduction, the combined output of the chip fabrication plants owned by Intel, currently the world's largest chip manufacturer, totals over five billion transistors every second.^[2] The ability to pattern materials on the nanoscale in such a large capacity is truly a state-of-the-art technology.

While there have been very impressive advancements in the material processing techniques of the semiconductor industry, there are several limitations that prevent it from being the “go-to” approach for nanomaterial processing. First, photolithography is not able to pattern a wide variety of materials and is limited to a specific surface area. The approach is specialized to pattern only materials with specific photo-reactive properties and the most advanced tooling to date is optimized to create patterning on silicon wafers of only 450mm in diameter. Second, the use of masks to provide patterning is inherently planar and typically only patterns features in a single plane. There are examples of three-dimensional (3D) structures fabricated with photolithography, however they are created based on an extensive series of steps.^[17] The mask approach also creates an obstacle to design, as each pattern prototype requires the fabrication of a new mask. Finally, the manufacturing process requires significant amounts of time, energy and resources. From the start of the process to the realization of packaged chips the process requires over 200 sequenced processing steps that take six to eight weeks for completion. This takes place in highly specialized fabs that demand high-energy input to provide high temperatures, extreme pressures, and clean room environments pressurized with filtered air to remove any small particles capable of interfering with chip performance. In addition, only a small percentage of the starting materials ultimately make it into the final product, suggesting that the majority of manufactured materials are waste products.^[18] In general, the current material processing methods of the semiconductor industry do not provide the diversity of new materials, dimensions, scales and sustainability to serve as a broad-

impact material processing technique for the realization of the full potential of nanomaterials.

1.3 Characteristics of Broad Impact Material Processing

Drastically new approaches to material processing are required if widespread technical innovation is going to be realized from the fabrication of nanomaterials.^[15] The three characteristics of a nanomaterial processing technique that will allow for such innovation are: 1) versatility, 2) multiscale and multi-dimensional structural control, and 3) sustainability.

Versatility is the most obvious characteristic as the greater the amount of both nanomaterials and other building blocks that can be processed, the greater the probability that a broad impact across multiple technologies, sectors, and products can be made. A less obvious implication of processing building blocks with a wide variety of material properties is the opportunity for new practical applications by allowing for the realization of unusual combinations of properties that previously have not been achieved. A versatile material processing technique will have the ability to incorporate nanomaterial building blocks of different shapes, sizes, and compositions, along with polymeric, biological and renewable building blocks, onto a wide variety of substrates such as paper, cloth, flexible plastics or even biological surfaces. This will allow for widespread and novel applications, as well as the opportunity for a nearly unlimited combination of material properties.

Of equal importance as the varied structure and composition of the building blocks, is the architecture in which they are assembled. The second characteristic

needed for a nanomaterial processing approach is the ability to control the placement of the different building blocks across multiple length scales and dimensions. As demonstrative by the hierarchical structure of human bone, a nanocomposite comprising nanoscale bone mineral and collagen, the control of composition and structure across multiple scales (**Figure 1.2**) allows for the unique combination of high material strength and toughness to be realized in a single material.^[3, 19] The introduction of 3D architecture, controlled across multiple length scales, provides an opportunity to also impart unique characteristics to materials such as special deformation patterns,^[20] negative Poisson's ratio,^[21] negative thermal expansion,^[22] controlled biological interactions,^[23] and mass transport properties.^[24, 25] Finally, it aids in scalability and ultimately bridging the gap between nanoscale materials and macroscale applications, as is one of the most significant challenges in material science.

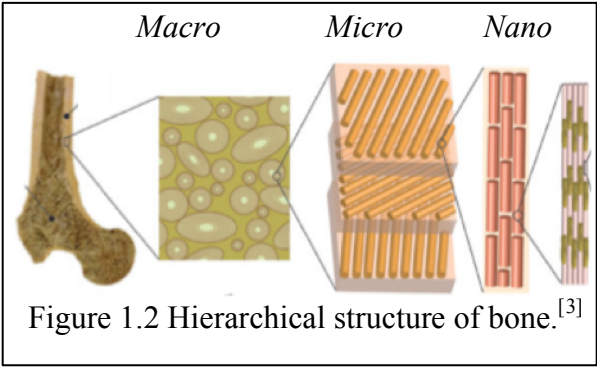


Figure 1.2 Hierarchical structure of bone.^[3]

Finally, in order for approaches to next generation processing of nanomaterials to be ubiquitous, they must be both sustainable and economic by design. This includes fabrication techniques that as much as possible employ ambient temperatures, atmospheric pressures and water-based systems and incur as little waste and cost as possible. For example, additive patterning techniques allow for the majority of the material used in production to make it into the final product, decreasing material costs and wastes as compared to subtractive

patterning techniques.^[26] Similarly, direct-write fabrication allows for a pattern to be produced electronically, eliminating the need for the use of stamps, molds or masks for pattern formation.^[27] Of additional interest, manufacturing solutions that allow for retooling and/or decreased time for design and scaling aid in reducing the economic cost and time associated with process development. The discovery of material processing technologies that are versatile, allow for multiscale controllability, and are sustainable, is not only of interest within the scope of this thesis, but rather holds the potential to play a very prominent role in the revitalization of the American manufacturing sector.

1.4 Broader Impacts

In June of 2011, the United States President's Council of Advisors on Science and Technology released the report "*Ensuring American Leadership in Advanced Manufacturing*", which brought to attention the need for manufacturing innovation policy.^[28] President Barack Obama responded by launching the Advanced Manufacturing Partnership to investigate investment opportunities to transform American manufacturing. Co-Chaired by Andrew Liveris, President, Chairman, and Chief Executive Officer of the Dow Chemical Company, and Susan Hockfield, now President Emerita of Massachusetts Institute of Technology, the steering committee consisted of several leaders from leading U.S. manufacturers and top engineering universities. Over the next year the committee solicited ideas from over 1,200 stakeholders representing industry, academia, and government at all levels on how best to promote U.S. leadership in manufacturing and innovation performance.^[29]

The committee's report on "*Capturing Competitive Advantage in Advanced Manufacturing*" detailed recommendations for enabling innovation, securing the talent pipeline, and improving the business climate.^[30] One recommendation called for an increase in funding for research and development in top crosscutting technologies. Among the technologies identified for widespread innovation were *Advanced Materials Design, Synthesis and Processing*, along with technologies for *Sustainable, Nanoscale and Additive Manufacturing*. Another recommendation called for a National Network of Manufacturing Innovation Institutes (MII) to serve as a bridge between basic research performed in national universities and laboratories, and the manufacturing industry. In August 2012, a multiagency partnership led by the Department of Defense awarded funding for a pilot MII focused on additive manufacturing. Industrial partners expressed their interest in the development of advanced material processing innovations by matching the federal investment with \$40 million.^[29]

1.5 Nanocomposites from Layer by Layer (LBL) Assembly

As technological advancements in electronic, biomedical, optical and magnetic applications demand novel functional materials with vastly enhanced and diversified properties, hybrid inorganic-organic nanocomposites have become a fast growing area of materials science research.^[31] Hybrid nanocomposites are a class of materials fabricated by dispersing inorganic nanomaterial building blocks into a macroscale organic matrix as a means of translating the unique nanoscale properties of the building blocks to the macroscale where humans can easily

interact. For example, the automotive industry has created a lightweight, yet high-strength material by homogeneously dispersing individual clay nanoplates (1nm thick) into a continuous polymer matrix for mechanical reinforcement.^[32]

The final properties of the nanocomposite that are transferred to the macroscale depend not only on the material properties of each component, but several other structural factors. Most obvious, the ratio of nanomaterial to polymer matrix plays a significant role as increased reinforcement sites provide enhanced mechanical properties. However, while it seems intuitive that a greater weight percent of the nanoscale building blocks would allow for greater realization of the nanoscale properties, this is not always the case. Nanomaterial additives have a tendency to aggregate, losing their nanoscale size and corresponding properties. Incomplete dispersion of a high weight percent of nanomaterials can actually lead to a decrease in material strength.^[33] Therefore, the extent to which the nanoscale building blocks are dispersed within the polymer matrix significantly impact the number of reinforcement sites and therefore the material properties of the nanocomposite.^[34] In addition to the composition and dispersion, the characteristics of the interfacial phase between the two components plays a significant role. Nanomaterials have a very high surface area to volume ratio that provides a tremendous amount of interface between the separate components when finely dispersed. The chemical interactions at this interface determine to what extent the two will interact and how much stress will be transferred from the weaker polymer matrix to the stronger nanomaterial. Finally, the 3D architecture of the

nanocomposite across multiple length scales will determine the final macroscale material properties of the nanocomposite.

Among the many techniques to fabricate nanocomposites, layer by layer (LBL)^[35] assembly stands out due to its ability to finely control nanomaterial dispersion and interfacial interactions. Traditionally the technique utilizes oppositely charged materials and a repetitive four-step dipping process to assemble nanocomposites one layer at a time (**Figure 1.3**).

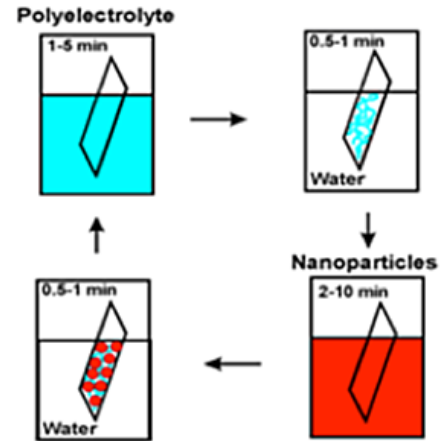


Figure 1.3 Schematic of layer by layer (LBL) deposition.

For example, first a negatively charged substrate is dipped into a positively charged polyelectrolyte solution where electrostatic, thermodynamic and kinetic interactions drive the adsorption of the polyelectrolyte onto the substrate.^[36] Second, the substrate is rinsed in deionized water to remove any excess or loosely bound material, leaving behind only a single molecular layer. The adsorption of the polyelectrolyte reverses the surface charge^[37] allowing for negatively charged nanoparticles to be adsorbed onto the surface upon dipping in the third step of the process. Here insoluble complexes are formed between the polymer and nanomaterial so that upon rinsing the surface in the fourth step, a single layer of polymer and nanomaterial is deposited and the surface charge switched to allow for repetitive deposition of the nanoscale-controlled and uniform nanocomposite layer. Throughout this document, a LBL nanocomposite fabricated from z repetitions of this cycle will be notated as (polymer/nanomaterial) _{z} . The

immobilization of the macromolecular compounds and strong interdigitation of the nanoscale layers allows for nearly perfect dispersion of the components^[38] at a nanomaterial weight percent unavailable by other means (>65wt%).^[39] This specific quality of LBL is reflected in the very distinctive mechanical, electrical, biological, thermal and optical properties of its nanocomposites.^[39-44] For example, in the case of clay nanocomposites, those produced by LBL assembly are found to have a significantly higher maximum tensile strength and Young's modulus than any other clay-polymer nanocomposite.^[39]

1.6 LBL as a Broad Impact Material Processing Approach

Besides the exceptional material properties of LBL-assembled nanocomposites, LBL exhibits many other qualities desired for a next-generation material processing technique. First, LBL is a very versatile technique. Originally demonstrated with the growth of oppositely-charged polyelectrolytes,^[45] LBL has now been significantly expanded to include alternate chemistries, biological materials and nanomaterials of different shapes, sizes, and compositions.^[44, 46-53] Second, the thermodynamically limited assembly of monomolecular layers allows for precise control of layer thickness on the nanometer scale.^[39, 54] Considering the LBL deposition process is very similar for nanomaterials of different dimensions, this control has allowed for optimization or gradients of the nanophase material.^[55, 56] For example, controlled-release coatings with stratified spatially separated reagents have been realized with LBL.^[57-59] Lastly, but certainly not of least importance, the simplicity of LBL provides a rather sustainable approach to material

processing. Performed at room temperature, under atmospheric pressure, and in aqueous-based solutions, the conditions are such that even the biological activity of LBL deposited macromolecules can be retained.^[48, 60] The combination of these properties makes LBL an excellent starting point for the development of a versatile, controllable, and sustainable material processing approaches for the realization of the potential of nanomaterials.

1.6 Focus of Thesis

While the alternating chemical adsorption of thermodynamically controlled layers with LBL provide structural control over thickness in one direction on the nanoscale,^[46] the incorporation of these materials into advanced applications will require both two-dimensional (2D) and 3D structural control. In addition, the volume of water required in the rinsing steps and the current time for film fabrication create sustainability concerns for the broad use of LBL as a material processing technique. The focus of this work is to develop material processing solutions to introduce multiscale and multi-dimensional architectures into LBL materials for the realization of the enormous potential of nanotechnology. To as much as possible, the inherent versatility of the technique will be preserved and lower-demand approaches developed for an improved sustainability outlook.

First, a direct-write approach based on inkjet technology is employed to significantly accelerate the LBL assembly process while allowing for simple additive patterning of LBL nanocomposites. The technique allows for strict control over building block coverage and provides opportunity for the deposition of LBL patterns

onto alternative substrates, including those of interest for incorporation with flexible electronics and traditional microfabrication techniques. Next, the stimuli-responsive behavior of LBL assembled polyelectrolytes is investigated for the application of reversible shape-morphing of nanocomposites in response to both humidity and temperature stimuli. When patterned with inkjet deposition onto LBL nanocomposites, the polyelectrolyte multilayers drive reversible and prescribed 3D shape transformations with applications in soft robotics and environmentally responsive materials. Third, a template-based LBL approach for the fabrication of nanocomposite microcontainers with a permanent 3D shape is introduced. Here the incorporation of unique material properties offered by LBL assembly is incorporated into the walls of the microcontainer to provide advanced functionality with applications in high-throughput analysis, controlled release, and smart packaging. Finally, the template-based approach is advanced to macroscale and hierarchically tunable porous materials with the creation of a novel 3D deposition machine. Fairly independent structural control of each of these techniques provides the opportunity for extensive structure-property relationships to be obtained, and unique combinations of material properties applied and incorporated directly into next generation devices.

CHAPTER II

Inkjet Layer by Layer

2.1 Advanced LBL Material: Carbon and Gold Nanocomposites

Many technological innovations require materials with unique combinations of material properties. Transparent conductors for solar cells and touch-screen display applications require high transparency combined with electrical conductivity, two properties that are inherently opposite of each other.^[61] In addition, flexible or potentially wearable devices will also require a material that can maintain conductivity over a high strain percentage. The aviation industry requires materials that exhibit high toughness, high electrical conductivity, and low density, while materials for next generation batteries and fuel cells need to provide high ionic conductivity, a high shear modulus, and a high temperature resilience.^[62] Materials that are capable of demonstrating such orthogonal properties are challenging to produce.

Layer by layer (LBL)^[35] assembly however has successfully produced materials with unique combinations of very impressive and in some cases record-breaking material properties. For example, a carbon nanotube (CNT) composite

prepared with LBL has shown a stiffness, ultimate strength, and toughness of 16GPa, 500MPa, and 130J/g respectively. This represents one of the strongest and stiffest CNT composites made to date; outperforming other bulk composites by 2–10 times and exceeding the toughness of Kevlar threefold.^[63] Meanwhile CNT coatings assembled by LBL with a π -conjugated polymer showed optical transparency of 86.7% at a wavelength of 550nm and a temperature resilience up to 500°C, all while approaching the conductivity of metals at 1.1×10^5 S/m and maintaining conductance up to a failure strain of 120%.^[64] Gold LBL nanocomposites with a polyurethane matrix showed a conductivity as high as 1.1×10^6 S/m that only drops to 2.4×10^6 S/m at 110% strain.^[65] These unique combinations of material properties make LBL materials very desirable for incorporation into advance devices.

One specific application, where both gold and CNT LBL nanocomposites have shown great success is with neural devices.^[66, 67] Neural devices utilize electrodes to interact with neurons to create a brain-to-computer interface with applications in prosthetics, pain management and signal recording.^[68, 69] Current devices are rigid and present a large mismatch in mechanical properties with neural tissues. Combined with the normal microscale motions typical of the brain, this can cause a significant inflammatory response.^[70] As a result the scar formation and accumulation of immune cells prevent the device from maintaining a prolonged electrical connection with the surrounding neural tissue leading to device failure.^[71] The thin, flexible and conductive nature of LBL nanocomposites allow for a much smaller footprint. Along with a less rigid structure, this evokes less of an

inflammatory response for prolonged electrical interactions and device functionality to be achieved.^[66]

2.2 The Rinsing Step

Many other composite materials produced via LBL possess impressive mechanical, electrical, optical and biological properties that would be advantageous for macro-, meso-, and microscale devices in emerging technologies.^[39-43] However, the multiple fluid cycles required for multilayer preparation make this otherwise promising method for the design and fabrication of customized materials time consuming and often impractical. The abundance of fluids used in the process make it challenging to couple LBL deposition with other processing steps during device fabrication. From this perspective, it is quintessential to investigate other means to produce LBL materials that maintain a similar nanoscale control over structure while accelerating the composite build-up and evolving the technique for better integration with device manufacturing.

Formation of the sequentially adsorbed monolayers is traditionally carried out by alternate dipping of a substrate between two reservoirs of oppositely charged macromolecular compounds, for example a positively charged polyelectrolyte solution and a negatively charged nanoparticle dispersion,^[72, 73] with intermediate rinse steps that remove excess fluid and loosely adsorbed components. The self-limiting nature of the growing film results in a layered pattern transversal to the substrate and a homogenous assembly of the combined materials, which would otherwise phase separate when directly mixed. Often times the impressive

properties of the resulting LBL materials can be attributed to these useful structural features. In large part, these features are due to the presence of rinsing steps believed to prevent the formation of large aggregates with variable composition that destroy the materials' essential qualities, for instance, homogeneity, electrical conductivity, or mechanical strength.

The rinsing steps also appear to be quite important from the perspective of the stability of the multilayers.^[54, 74-77] A substantial portion of the Gibbs free energy associated with multilayer formation (and therefore the adhesion strength between the LBL components) originates from the hydration/solvation of ions^[54, 74] and from entropic contributions originating from the release of low molecular weight counter ions into the media^[75-77] during the formation of insoluble complexes. Therefore, the rinsing steps appear to be a significant component of LBL assembly and necessary from the point of view of basic thermodynamics. Nevertheless, the rinsing steps dramatically limit the practical applications of the LBL technique and add processing time and waste. Modifications to the technology have been developed that accelerate the process with spraying and/or spin coating,^[78-82] but rinsing steps are still required for film production and structural control. Therefore, as it has attracted very little attention thus far, it would be very useful and fundamentally interesting to obviate the intermediate rinsing steps. In doing so, one needs to resolve the issue of the excess material left on the surface during dip coating and the low molecular weight inorganic salts released during complex formation.

2.3 Inkjet Technology as a Solution

Encouraged by the development of the dewetting technique where the salt and excess material is removed by the retreating liquid,^[83] we investigated alternative approaches to satisfy the hard-to-cheat thermodynamic requirements while still reaching substantial simplification of the process. We hypothesized that *if the proper amount of material necessary for film growth is delivered to the surface without large excess*, constant rinsing after every adsorption step may no longer be necessary. In this way, one can still retain the high level of structural control of the LBL composite, reasonably high homogeneity of the resulting material, and universality of the deposition, *i.e.* the freedom of mixing and matching the components to gain a unique set of properties. With respect to the release of low molecular weight salts, the actual amount required for multilayer formation is quite small. Since there is substantial diffusion transparency of the LBL films for small ions,^[84, 85] its removal might potentially be achieved in a final (single) rinse at the end without the destruction of the multilayer assembly. Thermodynamic restrictions on multilayer formation and concerns of fast decomposition of the entire film still likely remain in this process, however if implementation of this idea is possible, it will be exceptionally convenient for a variety of applications and expand the basic understanding of LBL.

Here we demonstrate the preparation of LBL films using inkjet printing as a practical method to alternately deliver precise amounts of each component for the formation of LBL films without intermediate rinsing. The replacement of the numerous rinsing steps with one final rinse was feasible in this case, indicating that

the kinetics of low molecular weight salt removal from the films is fast enough to prevent decomposition of the entire assembly. The technique offers nanoscale control over layer thickness, variable nanoparticle coverage of the surface, and compatibility with additive schemes of device manufacturing, which set it apart from previous methods of combining inkjet and LBL multilayers.^[86-90] In addition, the vast range of materials that can be deposited with this patterning method is currently unavailable with patterning techniques such as traditional lithography or inkjet printing of conventional materials.^[43, 91-95] This work leads to the development of a convenient method of patterning a variety of surfaces with composite materials that is expected to be quite useful for the development of advanced materials and devices.

Previously there have been successful combinations of LBL assembly with inkjet technology,^[86-90] however their purpose, scientific rationale, and results are different. For instance, Rubner *et al* dispersed water via inkjet to selectively destroy portions of traditionally deposited LBL multilayers that were pH sensitive.^[87] It resulted in a useful patterning method that can be applied to a variety of hydrogen-bonded multilayers, but is not suitable for nanocomposites. LBL and inkjet printing were also combined to selectively activate the surface of a multilayer film for electroless metal plating.^[89, 90] In this case a single polyelectrolyte from the multilayer pair was printed for the purposes of patterning chemical functionalities. More recently, Limem *et al* demonstrated that pairs of self-assembling or reactive polymer solutions could be printed to form insoluble gels.^[86] This work also described simple patterns but obviated the questions of the accurate control over

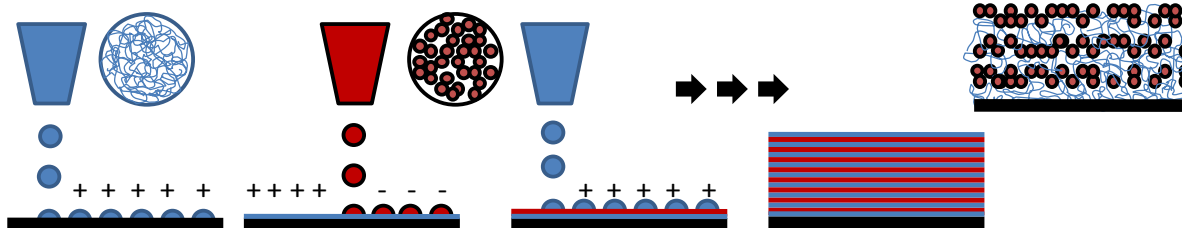


Figure 2.1 Schematic of multilayer film production by inkjet layer-by-layer assembly.

the multilayer growth that is essential for material design and application of multilayer films. Multilayer films were also used to modify the print surface for enhanced adhesion and controlled wettability.^[88, 89]

The deposition and build-up of LBL multilayers with inkjet technology that is explored herein can be taken advantage of in several ways. The mode that is considered here begins with the delivery of an appropriate amount of positively charged polyelectrolyte ink onto a negatively charged substrate via inkjet deposition (**Figure 2.1**). Due to the small volume size of the droplet the solvent is evaporated leaving behind an insoluble film of polymer on the surface and a positive surface charge. A second nozzle is then used to deliver a measured amount of a suspension of negatively charged nanoparticles. The nanoparticles interact with the positively charged polymer forming a nanocomposite. After evaporation of the solvent, the surface charge is then negative again and the process of dispensing each component is repeated until the desired overall thickness is obtained. Several passes of the inkjet printing head dispersing smaller quantities of an LBL component can be used to accurately vary the amount of the deposited polyelectrolyte or nanoparticles. Overall, the idea addresses the significant

challenges of LBL mentioned above by delivering *precise amounts of the selected polyelectrolyte and nanoparticles or any other LBL component* to the surface in order to reduce the need for rinsing steps to one final or only a few intermediate rinse step to remove the accumulation of low molecular weight salts. This mode of inkjet deposition has the potential to significantly accelerate the preparation of the films while retaining the advantageous layered and homogenous structures characteristic of LBL deposition. Considering the potential applications of LBL composites in micro-scale devices, inkjet LBL should also make it possible to pattern surfaces using direct-write methods rather than by different types of etching. Note also that the ability of LBL to make gradient structures^[56] will remain and will only require a simple change of ink during pattern build-up.

One can compare inkjet LBL as described in **Figure 2.1** to spray LBL deposition, where overcoming the diffusion limitations found in traditional LBL with the direct delivery of material to the surface significantly decreases processing times.^[78, 96] Films of equivalent quality, adhesion, composition and morphology to those prepared with traditional LBL techniques have been created with spray LBL despite the fact that the adsorption occurs under non-equilibrium conditions.^[78, 96] While significantly decreased rinsing times can be implemented with spray LBL, rinsing of the substrate between depositions is still necessary. Also, while excellent for large-scale coatings, spray LBL lacks control over the size, velocity, and density of the droplet, which are crucial for precise material preparation. Alternatively, drop-on-demand inkjet printing delivers picoLiter volumes of ink from a reservoir, ejected through a nozzle with highly controlled size and placement.

As compared to the standard notation, (polymer/nanomaterial)_z, which represents bilayers deposited with the traditional dip-coating approach, the notation (polymer^x/nanomaterial^y)_z will be used for LBL films deposited with inkjet printing to discriminate between different printing programs. To reflect the new possibility of printing small quantities of one LBL component several times until the desired amount is deposited, *x*, will denote the number of overprints of polymer jetted on the substrate before *y* overprints of nanomaterial are applied to make up a single bilayer. The entire cycle is then repeated *z* times. Typically greater number of overprints, *x* and *y*, of a solution of lower concentration of the components should result in a more uniform deposition that can overcome the structural disturbances caused by the singularity of each droplet. Ideally, of course, *x*=*y*=1 will result in faster film growth with the concentration adjusted to provide monomolecular or monoparticulate coverage of the substrate. One might point out that not all traditionally grown LBL films give uniform dense coatings in the dip cycles and that multiple inkjet passes can definitely improve the film's structure. The possibility of using a concentration that results in a higher coverage than that corresponding to monolayer coverall can also be considered as long as the stoichiometry between the components is retained.

2.4 Inkjet Deposition of LBL Nanocomposites

2.4.1 Nanoscale Assembly of Gold Nanocomposites

The introduction of gold nanoparticles (GNP) into organic matrixes using LBL assembly has been used to significantly improve the mechanical, optical and

electrical properties of polymeric materials with potential applications in, for example, microelectronic devices, electrochemical sensors and bioanalysis.^[97-99] As spray LBL was successfully used to produce GNP multilayer films,^[100] we investigated the capability of the inkjet LBL technique to create multilayered GNP nanocomposites. To test the performance and capabilities of inkjet LBL we chose standard GNPs made with citrate ions stabilizers,^[101-103] average diameters of 13 ± 2 nm and 20 ± 2 nm, and a negative surface charge. They are assembled with poly(diallyldimethylammonium) chloride (PDDA), a positively charged polyelectrolyte.

For proof of concept we deposited five lines of increasing thickness of $(\text{PDDA}^1/\text{GNP}^1)_z$ onto a silicon wafer by alternating inkjet printing of single print cycles ($x=y=1$) of the positively charged PDDA and negatively charged GNP for $z = 5, 10, 15, 20$ and 25 bilayers. Despite the patchiness (which is also present in traditional dip-coated LBL films with rinsing, **(Figure 2.2)**), the averaged thickness of the multilayer film grows linearly with the number of depositions, similar to LBL films assembled by dip-coating, spin-coating or spraying **(Figure 2.3)**. The average thickness per layer as determined by dividing the average total thickness by the number of bilayers is 1.38 ± 0.34 nm. The thickness per bilayer is less than the diameter of the GNPs due to the GNP surface coverage of the films. As the number of bilayers increases, the content of gold on the surface steadily increases allowing for the average thickness to rise **(Figure 2.3)**. Notably, the printed multilayers demonstrate denser and more uniform GNP coverage compared to films produced using traditional dip-coating LBL **(Figure 2.2)**. Note that one can adjust the surface

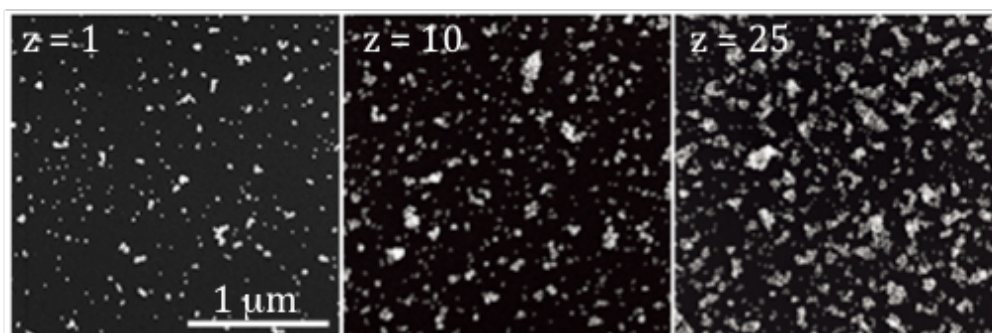


Figure 2.2 Surface coverage of GNPs in a $(\text{PDDA}/\text{GNP})_z$ film produced using standard dip-coating LBL with $z = 1, 10$ and 25 bilayers

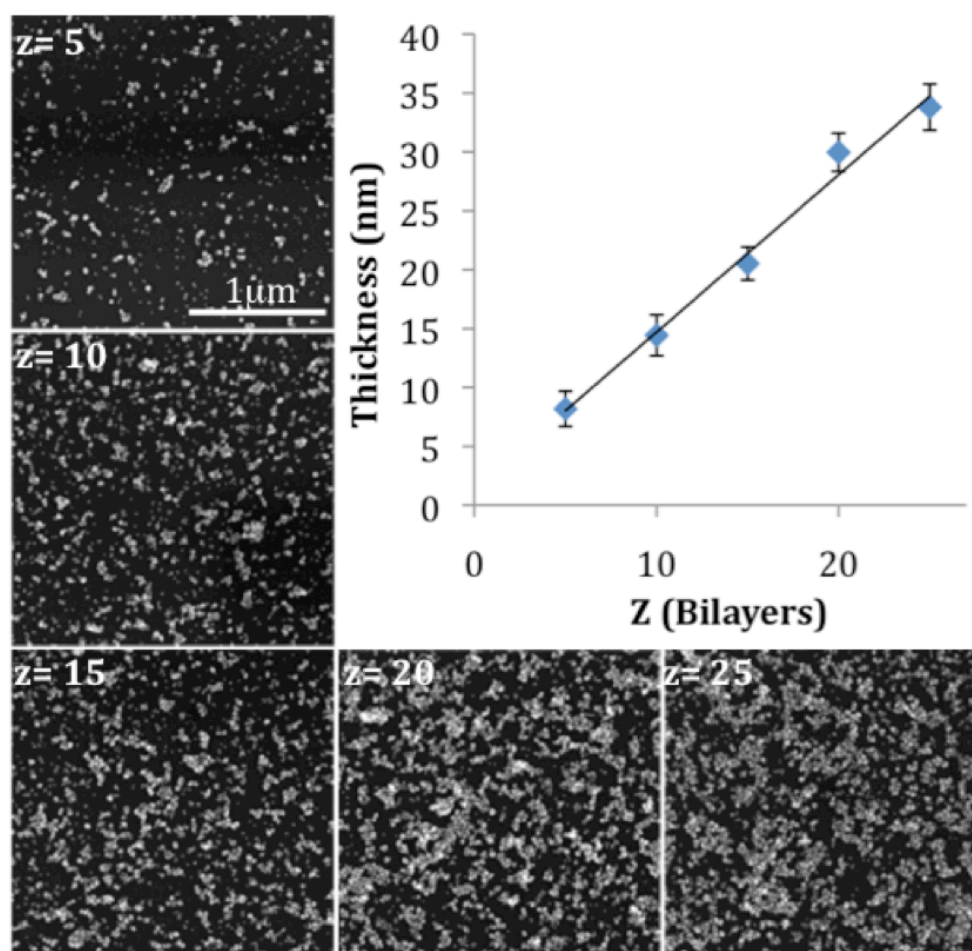


Figure 2.3 Increasing thickness of $(\text{PDDA}^1/\text{GNP}^1)_z$ and scanning electron microscopy images of GNP coverage after deposition of z bilayers by inkjet.

density of nanomaterials in dipped LBL films to reach complete and uniform coverage by different means, however, we did not optimize the conditions of the traditional LBL or inkjet modality in order to investigate the use of relatively standard conditions with direct use of the as-made GNPs. This is a clear demonstration of the advantageous performance characteristics of inkjet LBL.

2.4.2 Structural Control over Nanophase Coverage

The GNP coverage of the inkjet LBL films can be purposely improved further by increasing the number of prints of gold delivered per bilayer. To investigate the range of surface coverage available with the technique, a single layer of 0.25wt% PDDA was applied to a silicon substrate using dip-coating LBL before six lines of width 318 μ m in Adobe Photoshop were printed onto the substrate. The number of prints of gold per line was increased over the following values: $y= 1, 10, 25, 50$ and 75. The washed and dried (PDDA/GNP)₁ lines were imaged at different length scales (**Figure 2.4**). Comparative surface coverage of GNPs with traditional LBL can be achieved after one print (**Figure 2.22**, $z=1$ and **Figure 2.4**, $y=1$). With greater number of overprints, the GNP coverage gradually increases reaching a complete multi-NP thick layer at about $y=50$. Further increase in overprints did not strongly affect the layer morphology. The concentration of the GNP dispersion can be altered to adjust the coverage and the number of prints needed to obtain the desired GNP coverage and potentially thickness of the NP film. This indicates a much-improved degree of control over the multilayer structure with inkjet LBL over the dip modality.

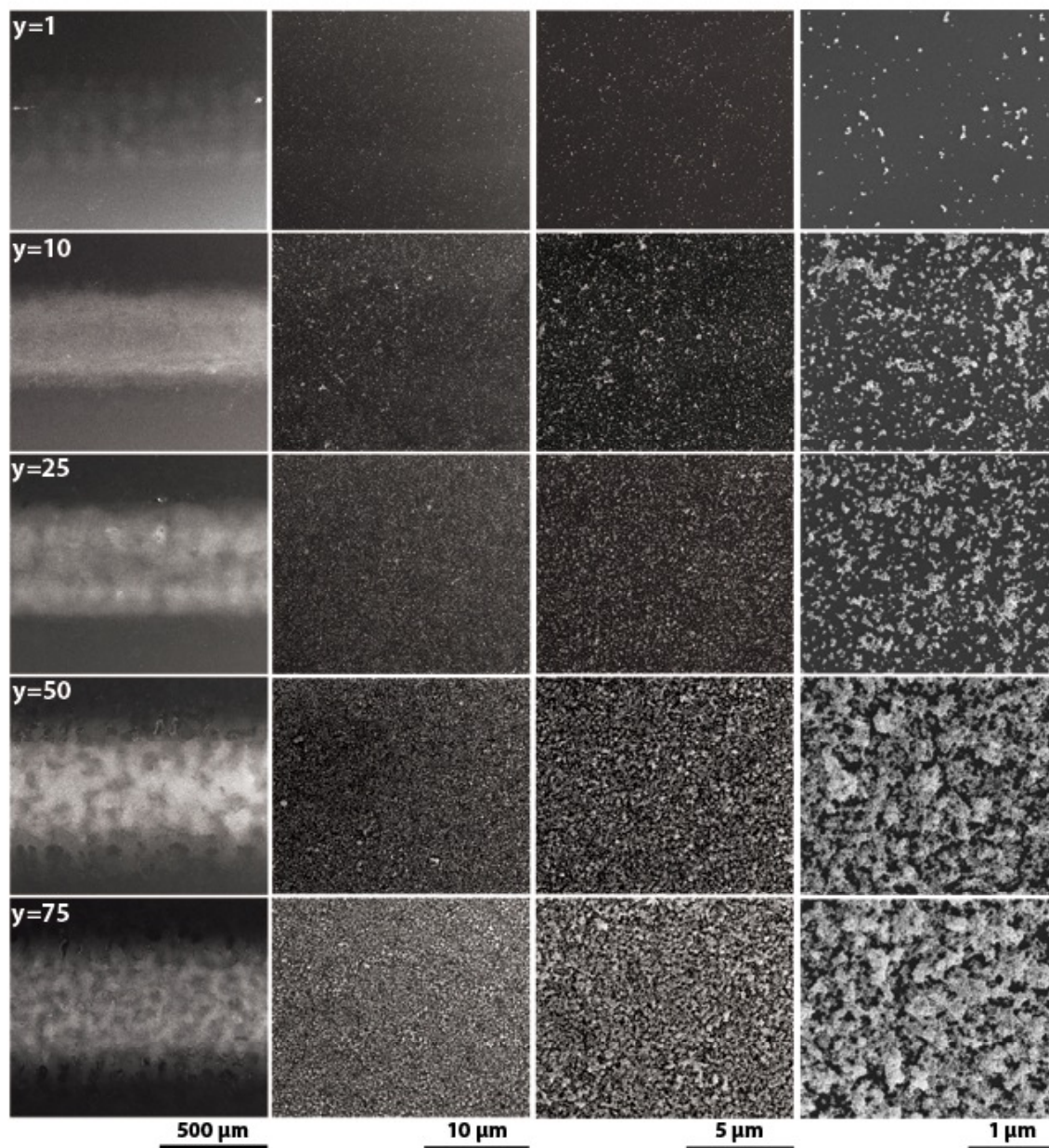


Figure 2.4 Images of a single bilayer of $(\text{PDDA}/\text{GNP}^y)_1$ LBL films with $y= 1, 10, 25, 50$ and 75 prints of gold.

The distribution of NPs in the printed layer that was observed without any special effort was quite uniform, which is often times not the case for many inkjet patterned surfaces due to the fairly large droplet size and “coffee ring” effect during

drying.^[104-106] Progress continues to be made towards high-precision patterns and elimination of the “coffee ring” effect,^[107] however one needs to point out that regardless of the absence of the effects in our case of $(\text{PDDA}^x/\text{GNP}^y)_z$ (**Figure 2.4**), the possibility of its occurrence will need to be considered for optimal structural control.

2.4.3 Multi-Dimensional Structural Control

In addition to controlled droplet delivery, inkjet printing provides the opportunity for additive patterning with simple introduction of multiple computer-generated patterns and components that are attractive for advanced material manufacturing. As a demonstration of this capability, we deposited GNP features of various sizes by printing four lines of decreasing computer-generated widths of 425, 283, 168, and 66 μm with 3 prints of 0.0025wt% PDDA and 75 prints of the GNP dispersion *i.e.* $(\text{PDDA}^3/\text{GNP}^{75})_1$ onto a silicon substrate (**Figure 2.5**). The goal of this test was to establish the limits of patterning well-resolved lines with a simple desktop printer and the LBL technique. As expected, the smaller the computer-generated features become, the less precise the actual deposited line. Interestingly

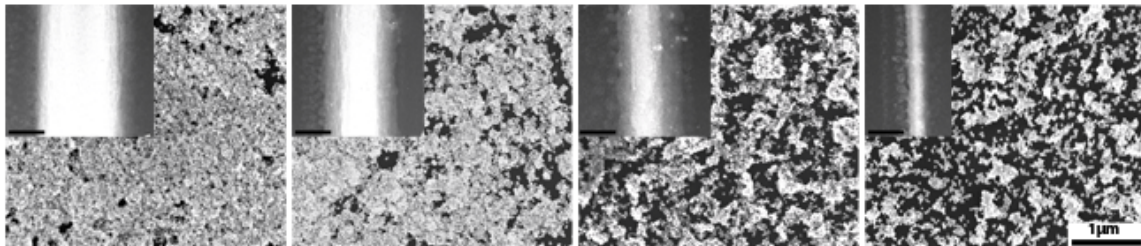


Figure 2.5 Inkjet printed $(\text{PDDA}^3/\text{GNP}^{75})_1$ lines of decreasing computer designed widths from left to right of 425, 283, 168, and 66 μm . (Scale bar of inset images =250 μm).

the reduction of the line width is accompanied by a lower average density of GNPs, which is attributed to specific droplet size control programs employed by Epson (**Figure 2.5**). Although this patterning effect is printer-specific and much higher resolution and droplet control can be obtained with advanced inkjet systems, it is still quite important to realize that some structural parameters of the coatings can become coupled in the inkjet modality of LBL while being fairly independent in the dip-coating LBL technique. Interesting to point out based on **Figures 2.4 and 2.5**, there is apparently no strict and specific ratio of polymer to NPs that results in stable layers; we believe that wide range of ratios could be used. At the same time, if only one component is deposited multiple times, the pattern is washed immediately off during the single final rinse step.

In order to demonstrate the ability of the inkjet technique to simultaneously produce and control the spatial arrangement of multilayered nanocomposites, a grid pattern designed with 0.3mm line width was printed from 0.0025wt% PDDA and GNP LBL (**Figure 2.6A**). Each bilayer was composed of $x=3$ prints of PDDA followed by $y=10$ prints of GNPs. Light transmission at 700nm was observed three times during each bilayer to observe the growth of the film; after the deposition of 3 prints of PDDA, and after 5 and 10 prints of gold. UV-vis transmission data were then plotted against the number of prints (N) to demonstrate the continued growth of the film (**Figure 2.6B**). The nanocomposite LBL grid was then washed and dried, leaving behind a multilayer composite with not only controlled GNP composition in each layer, but controlled 3D spatial arrangement as well. Although, the transmission of the pattern rose from $34.6 \pm 0.4\%$ to $43.4 \pm 0.5\%$ after washing, this

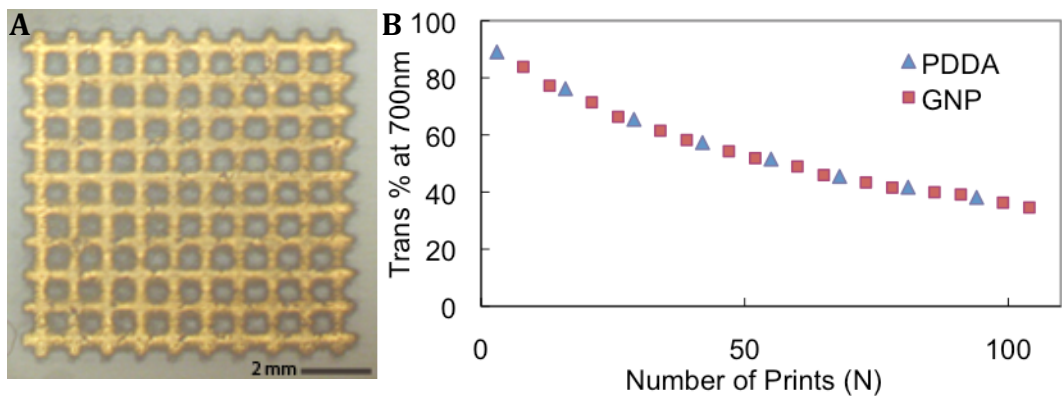


Figure 2.6 A) Photograph of $(\text{PDDA}^3/\text{GNP}^{10})_4$ nanocomposite multilayer formed using LBL assembly and patterned with inkjet printing. B) Dependence of optical transmission of the grid pattern on the total number of printed layers, N. Measurements were taken after every 3 prints of PDDA and 5 prints of GNP.

test clearly demonstrates the ability of inkjet LBL to create insoluble, multilayered nanocomposite patterns without the need for intermittent rinsing steps.

When considering the case of simple $(\text{polymer/nanomaterial})_z$ composite films deposited onto a relatively small area (4cm^2), targeted here as a base for elements of potential everyday devices produced by LBL, one can find a significant improvement in production time with the use of inkjet LBL as compared to using traditional dip-coating LBL (approx. 7 times faster when estimated bilayer deposition times of 4 minutes for inkjet LBL and 28 minutes for dip coating are considered). Processing times should be significantly enhanced with advanced printing systems and automation. When subsequent patterning of traditional LBL films is considered, which will need to include additional steps, such as, photoresist deposition, masking, UV exposure, photoresist removal, *etc*, improvements in production times with the use of inkjet LBL are even more radical. One of the

disadvantages of inkjet LBL is that it is primarily applicable when the total area of LBL coating is relatively small. The task of coating of large and highly curved areas with continuous LBL multilayers is probably better served by one of the traditional LBL approaches.

2.4.4 Carbon Nanotubes and Alternative Substrates

A number of approaches to spatially control LBL-assembled multilayers to create lateral patterning have been explored.^[43] For example, patterned surface chemistries created by microcontact printing,^[108-110] dip-pen nanolithography,^[111] nanografting,^[112] and electron-beam lithography^[113] were used to guide the spatially-selective growth of LBL assembled multilayers. Electric-field-directed LBL assembly^[114] and spin-assisted LBL combined with microfluidics^[115] were also each employed for selective deposition of LBL multilayers. Alternatively, spatially-selective removal of LBL multilayers was used for patterning based on the selective dissolution of pH sensitive films with inkjet printing,^[87] assembly atop patterned substrates with selective removability created by nanoimprinting^[116] or photolithography,^[117] selective photocrosslinking^[118, 119] and traditional lithographic patterning.^[120] Finally, stamps used either in compression^[121, 122] or for multilayer transfer printing^[123] have also successfully created multilayer patterns.

In respect to the characteristic size of the features, traditional lithography and nanoimprinting have better X-Y. However, unlike them and most LBL patterning modalities mentioned above, inkjet is a continuously additive technique with corresponding advantages and disadvantages. It is also exceptionally simple and can be realized with minimal hardware investments and immediate results. The

additive approach of inkjet LBL printing can in many cases reduce the number of processing steps while increasing process flexibility where patterns are generated from electronic data rather than premade templates. The combined versatility of LBL and inkjet has the capability to serve as a universal patterning technique for LBL as it does not rely on specific chemical functionalities or templates such as stamps or masks that limit the material choice, number of components, and designs currently possible.

Many of the above approaches to patterning LBL materials, including the demonstration of patterned gold nanocomposites with inkjet technology, have been realized on flat, nonporous surfaces. As discussed in section 2.1, the material properties of CNT composites prepared with LBL make them of interest for incorporation into many next generation electronics.^[63, 64] In many cases, this will depend on the ability of LBL materials to be patterned onto a variety of different substrates and incorporated with well-established microfabrication techniques. For example, paper electronics for disposable environmental monitoring^[124] and wearable fabrics that monitor and report health indicators such as the presence of blood on body armor^[125] are both innovations that could benefit from the properties of LBL nanocomposites. It is likely that such technologies will only evolve into actual functional devices if controlled spatial arrangement of the materials can be achieved. Similarly, for technologies such as neural probes^[66] that rely on traditional microfabrication techniques for some of its components, integration with existing microfabrication technologies will be imperative for the benefits of LBL to be realized.

Here we demonstrate the conceptual possibility of inkjet technology to pattern LBL nanocomposites onto alternative substrates. Single-walled CNTs dispersed with negatively charged polyelectrolyte poly(sodium 4-styrene-sulfonate) (PSS) will be deposited in sequence with PDDA to form functional electronic pathways on paper. In addition, as integration with existing technologies is important for the launch of new technologies, the combination of inkjet LBL with photolithographically patterned substrates and focused-ion-beam lithography will also be demonstrated.

Currently, most electronics are fabricated on very clean, flat surfaces as required by traditional material processing.^[16] Coming in at around 0.1 cent/dm², paper provides an opportunity for low cost electronics that would not be economically feasible on silicon (~5cents/dm²).^[126] Paper also serves as a renewable material that is readily available and inherently biodegradable. However, it has a relatively high roughness and high porosity that readily absorbs liquids, making patterning materials onto the surface challenging using traditional approaches. Inkjet printing has long provided a successful approach to produce patterns of pigment on paper. Inkjet technology has been expanded to a very impressive variety of materials, including nanomaterials such as CNT, all sorts of different natural and synthetic polymers and even live cells.^[91, 93, 95, 127] While the potential health risks and cost of nanomaterials must be considered independently, the versatility of inkjet technology has made it a very realistic processing technique for the production of paper-based electronics.^[126]

The realization of the versatility of inkjet technology is rooted in the ability to finely tune the droplet ejection mechanism for the specific properties of different material systems. Drop-on-demand inkjet printing relies on a pulsed pressure wave to eject ink droplets. One approach to generating this pulsed pressure wave is with piezoelectric materials; materials that reversibly change shape with the application of an electric field. Behind each nozzle is a small ink chamber made of a piezoelectric material such as lead zirconate titanate. First a negative voltage is applied to expand the volume of the chamber, allowing it to be filled with ink. Next a positive voltage causes the chamber to contract, causing a pressure wave that travels through the fluid with a force that depends on the amount of friction, i.e. the viscosity of the ink. If the force is greater than the surface tension holding the ink in the nozzle, a droplet will be ejected. After ejection, the positive voltage is retracted in a recovery period where the chamber is allowed to go back to its original shape, ideally without the influx of air. The repeated pulse of these three different distributions of voltage is referred to as the ejection waveform. For optimal droplet delivery, the ejection waveform must be finely tuned to the specific viscosity and surface tension of the ink to be deposited.^[128]

Standard desktop printers such as the Epson printer used above for the deposition of gold nanocomposites, commonly come with a default waveform that has been finely tuned for the specific print head and brand of ink. Alternatively, the Dimatix DMP-2800 (Fujifilm) system provides a waveform editor and drop-watch camera that enables waveform optimization, allowing for a wide variety of inks to be deposited in a highly controlled fashion.^[129] Here the Dimatix system is employed

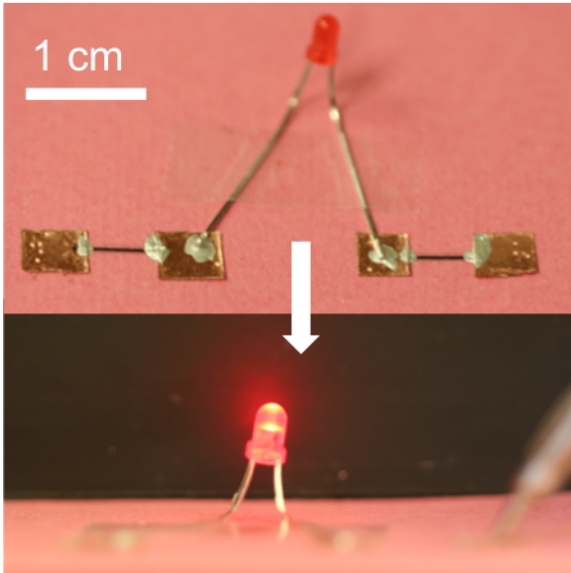


Figure 2.7 Inkjet deposition of LBL carbon nanotube composites is applied as electrical contacts on paper for illumination of an LED device.

to deposit CNT and 0.025wt% PDDA. The deposition of $(\text{PDDA}^2/\text{CNT}^6)_2$ onto paper and silver paste electrodes is able to conduct a voltage applied to copper touch pads and illuminate a three volt LED light (**Figure 2.7**). Following additional optimization, such structures could be employed for the application of binary sensors or advanced paper electronics with the introduction of multi-component features.

The patterning and stability of inkjet LBL films also indicate that this method can provide a promising alternative for multilevel patterning with nanoscale control over stratification. In traditional inkjet printing of electronic devices there is a long-standing problem in the production of multi-component, layered structures. The common solvents of many inks with electro- or photoactive components results in re-dissolution and mixing with pre-deposited layers. Low temperature phase-changing inks, polymer binders, UV curing or reacting inks, thermal treatments and orthogonal solvents^[130-132] were used to prevent redistribution of the solute between layers. However, even under special conditions the thickness of individual strata that can be deposited with these approaches is seldom smaller than $100\mu\text{m}$ ^[130, 133-135]. Inkjet LBL allows multilayers to be assembled into stratified multilevel structures with accuracy determined by the thickness of the individual

bilayer (**Figure 2.3**) and diameter of nanomaterial (if any) without any problems associated with re-dissolution or complex chemistry associated with the use of orthogonal solvents or special inks.

In addition, these approaches to multilayer ink insolubilization correspond to a relatively small set of systems and often times significantly change material properties. When considering the combination of inkjet with current microfabrication processes, many of these approaches may interfere rather than contribute. For example, the use of ultra violet curing after each layer deposition will interfere with any undeveloped photo-sensitive materials laid down for photolithographic patterning. Alternatively, the insoluble complexes formed during LBL assembly serve as a built in approach to insolubilize the ink, allowing for multilayer inkjet printing to be combined with traditional photolithography. To demonstrate the feasibility of combining inkjet LBL with traditional techniques, SPR220 photoresist was deposited onto a silicon wafer and selectively cross-linked to insolubilize specific sections. Before development of the pattern, inkjet deposition of $(\text{PDDA}^1/\text{CNT}^1)_{12}$ was performed on the surface, which comprised both soluble

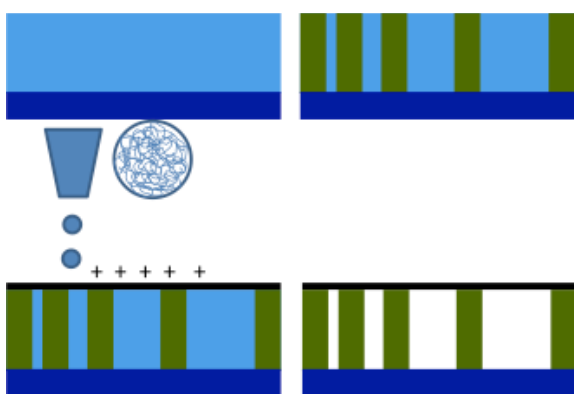


Figure 2.8 Schematic of inkjet deposition onto lithographically patterned substrates prior to development, allowing for microscale channels to be fabricated beneath.

and insoluble photoresist (**Figure 2.8**). Here the walls of the Dimatix printer were coated with yellow film to protect the soluble portion from light exposure. Upon completion of the inkjet deposition of CNT nanocomposite, the structure was exposed to a developer that selectively removed the soluble resist. From 3D confocal imaging, one can observe the channels developed by photolithography and note that the insoluble complexes making up the LBL composite remain in place after development (**Figure 2.9A**).

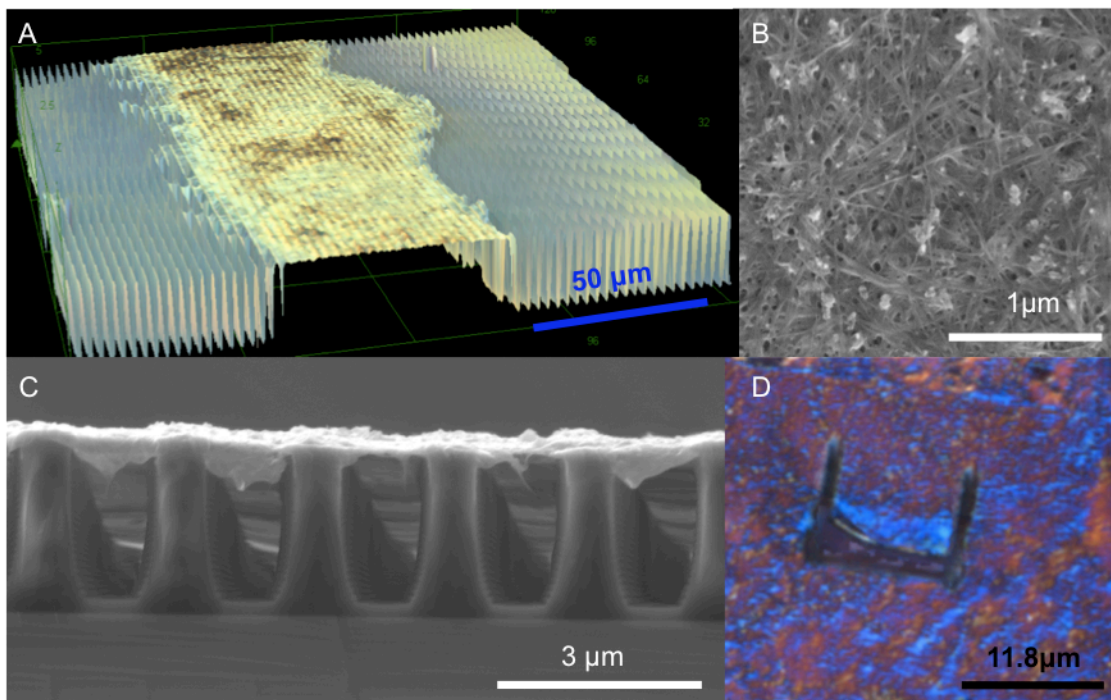


Figure 2.9 A) 3D confocal imaging and B,C) SEM of LBL nanocomposite deposited on top of photolithographically patterned substrate with inkjet technology. D) 3D confocal image of window cut with focused-ion-beam lithography.

Closer inspection with scanning electron microscopy (SEM) shows that the CNT film remains in tact and suspended over the channels that have been hollowed out below (**Figure 2.9B,C**). Further advancing the structure, the CNT composite can be selectively ionized with a focused ion beam to create select access to the channels

below (**Figure 2.9D**). As CNT based materials have been extensively investigated as sensors and actuators,^[136] the feasibility of such structures being activated by a wide variety of stimuli is quite feasible for future applications. In Chapter III, we will discuss the principles and fabrication of an LBL composite that actuates in response to external stimuli. Such principles could potentially be applied here as well.

2.5 Conclusion

As a result of this study, it has been demonstrated that inkjet technology can be successfully used to modify LBL assembly by eliminating most intermediate rinsing steps with accurate dispensing of the LBL components to the surface. Besides providing some insight into the basics of LBL, the data collected indicate the ability of this approach to provide structural control by varying the surface coverage of GNPs while retaining the overall linearity of GNP deposition characteristic of traditional LBL methods. The comparison of $(\text{PDDA}^x/\text{GNP}^y)_z$ and $(\text{PDDA}/\text{GNP})_z$ multilayers also shows that (at least in some cases) the localized dispensation of the required amounts of LBL components will lead to marked improvements in the surface density of nanomaterials. It can also lead to a wider ranges of particle-polymer ratios. The versatility of inkjet technology was explored with the deposition of CNT-based composites onto paper and integrated with traditional microfabrication approaches. Further optimization of the inkjet LBL technique toward advanced material production and better understanding of the methods of structural control in such multilayers are anticipated. Investigation of applying

advanced functionality to LBL materials with inkjet technology will be explored in Chapter III.

2.6 Experimental

2.6.1 Materials

High molecular weight poly(diallyldimethylammonium) chloride (PDDA) was purchased from Aldrich and diluted to 0.25, 0.025 and 0.0025wt% in deionized water. Citrate stabilized gold nanoparticles (GNP) with diameters 13 ± 2 nm and 20 ± 2 nm were synthesized using previously published techniques.^[101-103] Briefly, for 13 ± 2 nm GNPs for example, HAuCl₄ in deionized water (0.0005M, Aldrich) was brought to a boil on a hot plate. Under vigorous stirring sodium citrate in deionized water was added (1wt%, Aldrich). Vigorous stirring and heat were then added for an additional 15 minutes. The concentration of the GNPs was increased via centrifugation (Sorvall Legend Mach 1.6R, 10,000rpm, 30min) and cellulose membrane dialysis tubing (Sigma) was used to remove the excess salt after two days in deionized water changed every 5-10hours. Finally, the solution was filtered through a 0.22 μ m filter to remove aggregates and a final concentration of approximately 2480 GNP per pL of water was obtained. High-purity P2 single wall carbon nanotubes (CNT) were purchased from Carbon Solution, Inc., and dispersed at 0.5 mg/mL in 2 mg/mL poly(sodium 4-styrene-sulfonate) (PSS; MW 100k; Aldrich) solution by ultrasonication overnight. The CNTs are estimated to be 1nm in

diameter by 2 μ m in length. The dispersed CNT were centrifuged three times at 10,000rpm for 10 minutes to remove aggregation.

2.6.2 Inkjet Layer by Layer Deposition of Gold Nanocomposites

For the GNP system, a drop-on-demand Epson R280 photo printer with the capability to print onto CDs was equipped with an external continuous ink system. A CD was modified to allow for placement of various substrates (glass, silicon, plastics), paying attention to the location of the rollers on the printer to prevent contact with the actual sample. The continuous ink system and Epson nozzles were cleaned several times with deionized water and the yellow and black cartridges were refilled with 0.0025wt% PDDA and the GNP dispersion respectively. Patterns designed in Adobe Photoshop (CS4 Adobe Systems Inc) were printed first in yellow (PDDA) for a set number of overprints, x , before being printed in black (GNP) for y overprints onto piranha-washed silicon and glass substrates. The printer was set to operate under the Epson *best photo printer* setting at normal speed with integrated color management and no color adjustment. The bilayer comprising x layers of PDDA followed by y prints of GNP was then repeated z times until the desired film thickness of $(\text{PDDA}^x/\text{GNP}^y)_z$ was obtained. The substrate was then removed from the printer set up, washed under a stream of deionized water for 1 minute and dried with compressed air.

The growth of the film was evaluated by light transmission measurements obtained using an Agilent 8453E UV-visible spectrometer and thickness measurements obtained using a single wavelength (532 nm) EP3-SW imaging ellipsometer (Nanofilm Technologie). Four-zone nulling experiments were

performed at an angle of incident of 60° and the ellipsometric parameters ψ and Δ were modeled with a two-coefficient Cauchy dispersion law ($A= 1.45$, $B=0.01$). Measurements were taken from five different areas of each sample and averaged. Scanning electron microscopy images were obtained with an FEI Nova 200 Nanolab.

For traditional dip-coating LBL, a piranha-washed silicon substrate was first soaked in 0.25wt% PDDA solution for 10 minutes. It was then rinsed under a stream of deionized water for 1 minute and dried with compressed air. The substrate was then soaked in the concentrated GNP dispersion for 10 minutes before being rinsed and dried again. The four-step sequence was repeated for each of the z bilayers.

2.3.3 Inkjet Layer by Layer Deposition of CNT Composites

For the CNT system, a FUJIFILM Dimatix material printer (DMP-2800) was used with disposable 10pL droplet size cartridges with 16 piezoelectric nozzles. A typical voltage cycle (waveform) for 0.025wt% PDDA included two steps at a duration of $5.056\mu\text{s}$. First a slew rate of 0.9 was applied to reach a level of 87% followed by a slew rate of 0.19 decreasing to 0%. The waveform was fired at a frequency of 5kHz. For CNT a slew rate of 0.77 for a level of 87% was applied for $6.4\mu\text{s}$ followed by a slew rate of 0.12 to decrease to a level of 27% over $7.53\mu\text{s}$ with a firing frequency of 2kHz. For both inks, the cartridge settings were set to a print height of 0.5mm, a vacuum meniscus set point of 3.5 inches H_2O and ambient temperatures. For LBL deposition, the cartridge and cleaning pad were alternately loaded. Before each deposition, a cleaning cycle of a 3 second purge was applied. In all cases droplets were delivered to the surface with $5\mu\text{m}$ spacing. All patterns were printed lengthwise as to allow for brief drying between printing as the printer

repositioned along the y-axis. For the deposition onto paper, the pattern was designed to be nine droplets wide to account for the absorptive behavior of the substrate, whereas the deposition integrated with photolithography was only one droplet wide. While the droplets are delivered at 5 μ m intervals, it is estimated that each droplet adds ~50 μ m in width to the line.

For activation of the three volt LED, LBL nanocomposites was deposited between silver paste electrodes attached on one side to a copper tape pad and the other to the wire of the LED. The resistance of the system was quite high, requiring 40V for illumination. Positive photoresist (SPR-220 3.0, Rohm and Haas) was patterned for 500nm spacing and developed using standard photolithography practices, with the exception of the additional processing step of inkjet deposition prior to development. The Dimatix was coated with yellow foil to prevent unintended exposure to crosslinking wavelengths. A LEXT OLS4000 laser scanning confocal microscope was used for 3D imaging and an FEI Nova 200 Nanolab Dualbeam Focused Ion Beam was applied for ionization.

The material in this Chapter has been adapted with minor modifications from the following peer-reviewed, published article:

Andres, C. M. & Kotov, N. A. Inkjet Deposition of Layer-by-Layer Assembled Films. *Journal of the American Chemical Society* 132, 14496-14502, (2010).

CHAPTER III

Shape Morphing of LBL Nanocomposites

3.1 Shape Morphing Background

Stimuli-responsive materials able to reversibly convert external stimuli to three-dimensional (3D) mechanical motion have attracted significant attention for their potential to enable controllable and programmable shape morphing.^[137, 138] Great success has been achieved in utilizing stimuli-responsive materials for the self-assembly of 3D structures^[17] and the realization of shape-memory polymers.^[139] However, in many cases the self-assembled 3D structures are not designed to disassemble, and shape-memory polymers require a reprogramming cycle for repeated response.^[17, 139] Dynamically tunable materials capable of *repeatedly* and *reversibly* converting simple environmental stimuli into mechanical motion are of interest for developments in adaptable clothing,^[140] climate-responsive buildings,^[141] controlled encapsulation/delivery,^[142] and actuation of soft-robotics.^[143]

Most living systems are capable of repeatedly responding to changes in their environment with a series of mechanical reconfigurations. The ability to fabricate

synthetic materials that meet or exceed these capabilities is a substantial and significant engineering challenge.^[144] While some biological movements require complicated chemical and biological mechanisms, several plants demonstrate mechanical responsive behaviors for seed dispersal that are deceptively simple and cellular independent.^[145-149] For example, investigation into the mechanism of unfolding/folding of pine cones,^[145, 150] and ice plants,^[146] has revealed that it is based on a simple mechanism of differential swelling in response to variations in relative humidity. The simple introduction of humidity is able to create a complex mechanical response due to the controlled composition and structural attributes of the plant material. Here a cellulosic inner layer, organized in a stratified structure is capable of absorbing large amounts of water. Paired with an opposing tissue that has a different cellulose fibril orientation that restricts the swelling behavior, a bending moment is generated.^[146] Similar to the uniform heating of bimetallic strips,^[151] the difference in expansion coefficients do not allow for uniform expansion and the internal stresses are equilibrated with a bending moment. The location of the bimorph within the plant creates a hinged structure where origami-like folding is realized. Upon removal of the stimulus, the bimorph will return to its original shape, providing a straightforward way to create reversible and repeatable shape-morphing structures.

Reversible shape transformations from the differential swelling of synthetic bimorph structures in solution have been widely observed.^[152-156] Differential swelling in hydrogel-based materials is a prominent example. In solution their elastic networks allow for significant volume change based on polymer hydration

and chain mobility.^[157-159] On the other hand, such response to humidity outside of solution^[160] is difficult for solid synthetic networks as they often have greater mechanical properties that impose larger restrictions on chain mobility within the network, directly limiting responsiveness.^[161]

The nanoscale structural control and versatility of layer by layer (LbL) assembly^[35] has repeatedly been proven to be a simple technique for the fabrication of solid functional materials that respond to a variety of external stimuli.^[162] In most cases these materials have been applied to trigger morphological changes on flat surfaces or to control permeability of capsules within solution. Surprisingly, very little investigation into freestanding structures that can generate mechanical motion outside of solution has been performed.^[163-165] In addition to the fabrication of stimuli-responsive materials, LBL has also been employed to fabricate a wide variety of nanocomposites with very distinctive mechanical, electrical, biological, thermal and optical properties.^[39-44] While traditionally a technique to fabricate planar thin films, the introduction of multiscale and multi-dimensional patterning to create permanent shapes^[43, 166-168] has been developed as an important step towards the incorporation of such materials into advanced functional devices. An obvious next step is the investigation of producing advanced stimuli-responsive functionality into such nanocomposite structures.

Herein we present LBL assembled solid polymeric multilayers capable of driving shape transformations of LBL assembled nanocomposites in response to environmental humidity and temperature variations. A hydrophilic polyelectrolyte multilayer is stacked with a less responsive LBL assembled carbon nanotube (CNT)

composite prepared with polyurethane, a considerably water resistant material. The differential swelling of the two LBL layers results in repeatable and reversible out-of-plane deformations. The sorption properties of polyelectrolyte multilayers is then revealed to drive a pseudonegative thermal expansion^[169] that is applied to drive similar shape-morphing with temperature variations. In agreement with a theoretical model, the ability of LBL assembly to control thickness on the nanoscale allows for the responsive behavior of the material to be strictly controlled. LBL deposition by inkjet^[166] is employed to pattern the active material onto the base in order to localize the stresses for programmable folding. Finally, a biomimetic structure is fabricated for the realization of a 3D responsive structure as inspired by the awn of wheat grass.

3.2 Advanced LBL Material: Stimuli-Responsive

Several features of layer by layer (LBL)^[35] assembled polyelectrolyte multilayers (PEM) make them attractive for solid stimuli-responsive materials that can drive reversible and repeatable shape-morphing. First, during LBL assembly of polyelectrolytes, the formation of polyanion-polycation complexes provides an electrostatically cross-linked structure capable of holding water in ambient conditions.^[170] Changes in environmental humidity drive the sorption and desorption of water resulting in repeatable and reversible volumetric fluctuation.^[165, 170] Second, as a solid material with a Young's modulus, E , around 1 GPa ^[171, 172], LBL polyelectrolyte composites provide greater mechanical integrity than, for example, high performing hydrogels with sub-MPa moduli.^[173] Third, while

the increased mechanical integrity of a solid limits the swellability, the nanoscale structural control of LBL assembly may provide the means to allow for optimal volumetric expansion to be realized. When exposed to the same change in relative humidity, polyelectrolyte films assembled by LBL experienced a greater change in film thickness as compared to complexes prepared by simply mixing the same polyelectrolytes together.^[170, 174] Fourth, the presence of nanoscale pores^[175-177] and success of LBL-based humidity sensors^[178, 179] suggest that such dimensional changes may be able to occur rather quickly as would be desirable for stimuli-responsive structures. Finally, LBL materials are prepared in ambient conditions with nanoscale control over thickness and can be deposited directly into specific patterns without additional processing.^[166] This provides the potential to easily develop unique patterns for the prescribed 2D to 3D transformation of many different materials, including LBL assembled nanocomposites.

3.3 Humidity Induced Shape Morphing of Nanocomposites

In order to investigate the performance of LBL polyelectrolyte multilayers as stimuli-responsive materials capable of driving reversible and repeatable shape-morphing, poly(diallyldimethylammonium) chloride (PDDA) and poly(sodium 4-styrene sulfonate) were prepared in a bilayer structure with a less responsive carbon nanotube (CNT) composite. The CNT composite was fabricated by the LBL deposition of 200 layers of cationic polyurethane (PU) and single walled CNTs. It was removed from its glass substrate and a thin strip (15mm x 3mm) was removed to serve as the shape-morphing platform. Inkjet LBL assembly^[166], an LBL

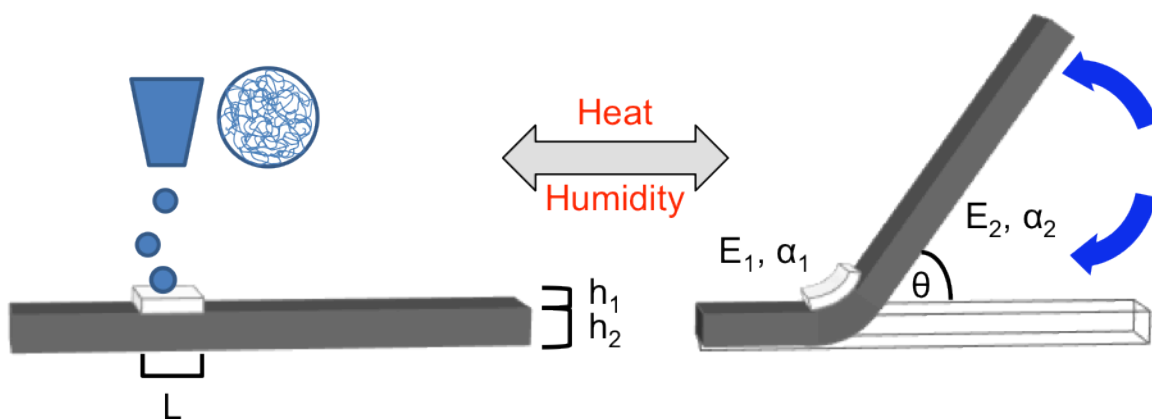


Figure 3.1 Schematic of the $(\text{PU/CNT})_{200}$ strip with inkjet deposited $(\text{PDDA}^2/\text{PSS}^2)_{10}$. When exposed to humidity and temperature stimuli, the bimorph responds by bending, creating an angle of deflection of θ in the longer arm. Here θ depends on the thickness (h), stiffness (E) and expansion coefficient (α) of each layer, along with the total length of the bimorph (L).

patterning approach that allows for the direct-write and strictly additive patterning of LBL materials in an accelerated manner, was used to selectively deposit the stimuli-responsive LBL polyelectrolytes onto a CNT strip. In this case, 10 bilayers of $(\text{PDDA}^2/\text{PSS}^2)$ were deposited in a line $\sim 300\mu\text{m}$ in width that perpendicularly traversed the entire width of the strip. The PEM was deposited 3mm into the 15mm $(\text{PU/CNT})_{200}$ strip creating a short arm and long arm separated by a small bilayer that will serve as a hinge to actuate the long arm of the CNT strip (**Figure 3.1**). After deposition there is no need for additional adhesives or processing as the same electrostatic forces used for their assembly also holds the two layers of the bimorph together. This adhesion will allow for the expansion/contraction of the stimuli-responsive LBL material to apply stress to the CNT layers below, resulting in out-of-plane deformation as the lowest stress configuration is achieved. In fact, before any introduction of controlled stimuli, the stress generated during fabrication as the inkjet deposited $(\text{PDDA}^2/\text{PSS}^2)_{10}$ layers dry on the $(\text{PU/CNT})_{200}$ film is reflected in

an initial deflection angle, θ , of $43.9 \pm 1.5^\circ$ at an ambient humidity of 24%. Here θ is a measurement of the trajectory of the large CNT arm at 0.5mm with respect to the plane of the short CNT arm.

The stimuli-responsive behavior of the hinged film was first investigated at constant temperature with variations in environmental humidity. The sample is placed into a quartz chamber and the shorter arm of the hinged film weighed down to allow for any out-of-plane actuation of the bilayer hinge to be realized in the long arm of the LBL nanocomposite. The weight was placed no closer than 0.5mm to the bilayer hinge as to not influence the location of fold. A stream of nitrogen was introduced into the chamber to decrease the relative humidity and drive desorption of water from the internal structure of the film. After five minutes, $t= 5\text{min}$, the nitrogen exposure led to greater volumetric contraction of the (PDDA/PSS)₁₀ layer due to the desiccation of water. The different extents of contraction in the two layers generates an internal stress that increases the deflection angle of the hinged bilayer to $\theta= 80.9 \pm 1.5^\circ$ (**Figure 3.2A**). Upon termination of the nitrogen stream, the ambient humid air diffuses into the chamber and hydrates the structure initiating a decrease in θ . After twenty minutes, $t= 25\text{min}$ the nitrogen stream is reintroduced and the cycle is repeated a total of three times for the realization of repeatable and reversible actuation of the bilayer hinge (**Figure 3.2**).

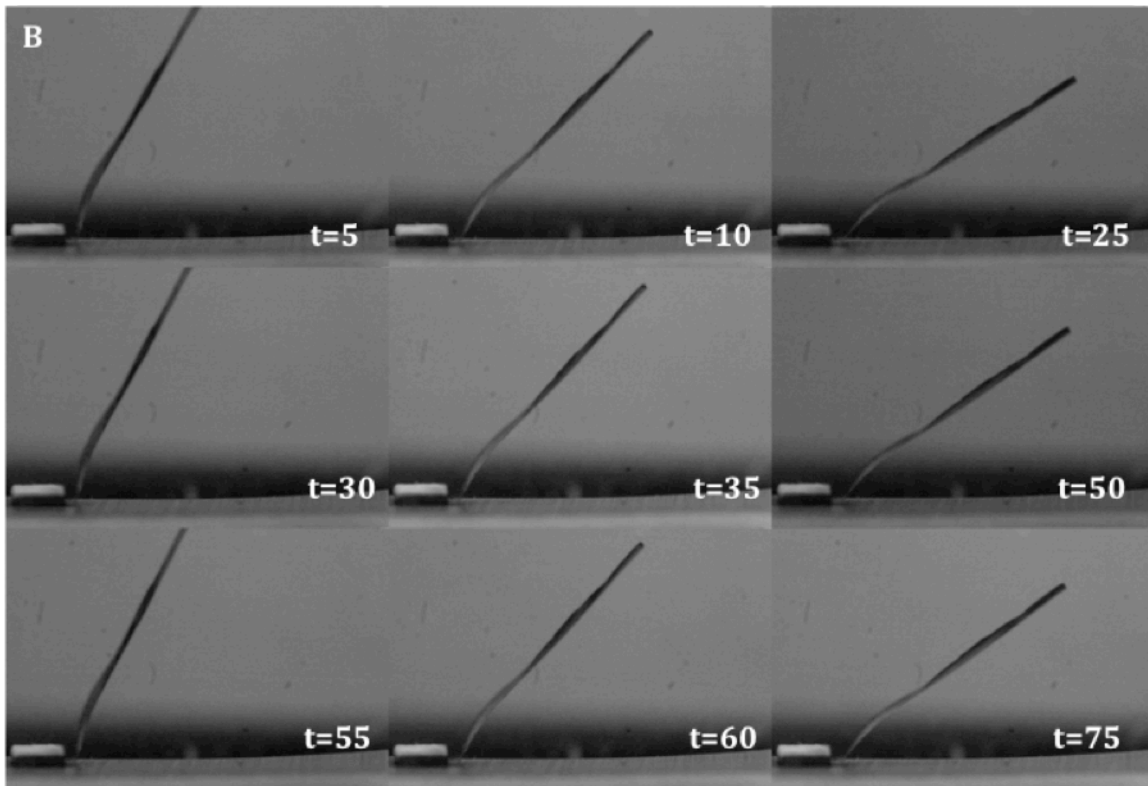
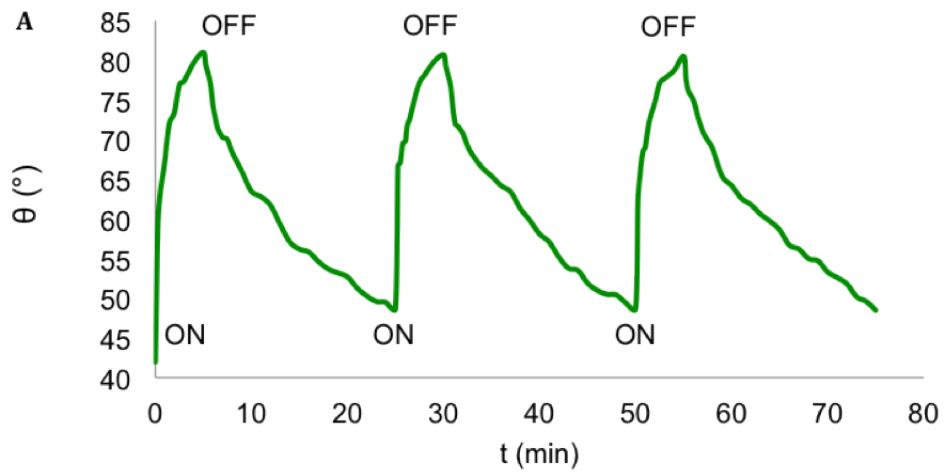


Figure 3.2 A) Graphical and B) Image representation of the dependence of the angle of deflection, θ , of the hinged film over time, t . Nitrogen was turned ON at $t=0, 25$ and 50 and turned off at $t=5, 30$ and 55 . Introduction of nitrogen causes the θ to increase and removal of nitrogen allows θ to return to a lowered position.

Note that while the hinged film recovers to $\theta = 49.0 \pm 1.5^\circ$ consistently when exposed to the same conditions, the recovery time of 20 minutes is not sufficient for a full return to the θ observed immediately after fabrication. However, when allowed to equilibrate for one hour, the film makes a completely reversible recovery to $\theta = 43.9 \pm 1.5^\circ$ as will be employed to investigate temperature induced shape morphing below.

3.4 Temperature Induced Shape Morphing of Nanocomposites

Next, we investigated the stimuli-responsive behavior of the hinged film in response to temperature, **T**. As compared to a humidity chamber, tools to manipulate temperature are much more transportable, readily available, and simple, allowing shape-morphing structures that respond to temperature to be highly versatile. While the response of LBL PEMs has been established for humidity variations,^[163, 164, 170] their response to temperature variations outside of solution has received little attention. Recent investigation of the thermal response of layered graphene oxide assemblies suggests that materials with nanoscale channels that respond fairly quickly to a decrease in environmental humidity may respond to temperature variations with a *pseudonegative thermal expansion* (PNTE).^[169] Here the thermodynamically required decrease in relative humidity with an increase in temperature, drives the desiccation of water and a corresponding decrease in dimension that overcomes the intrinsic positive thermal expansion of the material. The fairly quick response to humidity observed in **Figure 3.2A**, prompted us to

investigate (PDDA/PSS) multilayers as a PNTE material for the widespread application of LBL PEMS for temperature induced shape morphing.

The coefficient of thermal expansion, α , of LBL PEMS was evaluated with a stack of four (PDDA/PSS)₂₅₀ films fabricated with traditional LBL techniques and hot pressed together. The sample was exposed to a temperature ramp of 5°C per minute over a ΔT of 30°C to 80°C while the linear displacement was monitored with a thermal mechanical analyzer (Perkin-Elmer)(**Figure 3.3A**). The LBL PEM exhibits a PNTE effect with a repeatable and reversible response to temperature that occurs almost immediately following the environmental change. At an ambient relative humidity of $24 \pm 1\%$, the apparent linear coefficient of thermal expansion of the LBL PEM was calculated to be $\alpha_1 = -368 \pm 9 \text{ ppm}^\circ\text{C}^{-1}$ over the temperature increase from 35°C to 75°C. The extreme extent of contraction can be realized in comparison to the LBL CNT composite, which displays an apparent α of only $\alpha_2 = -6.5 \pm 4 \text{ ppm}^\circ\text{C}^{-1}$ at ambient humidity.

To investigate the role of water, a continuous flux of ultrapure helium was applied during thermal mechanical analysis to incrementally decrease the environmental humidity around the sample. As observed in the graphene oxide assemblies, the extent of contraction and apparent α of the LBL polyelectrolyte multilayers became less extreme as the source of water vapor (relative humidity) was decreased (**Figure 3.3B**). Also similar to the PNTE graphene oxide assemblies^[169] the LBL film shows a quicker dimensional response to heating as compared to cooling. As unequal water sorption and desorption rates have been predicted in other polyelectrolyte systems^[180, 181] it is likely that water is playing a

significant role in this behavior. Even at a relative humidity of 0.37%, the lowest possible humidity that we could obtain within the TMA sample chamber, the LBL PEM still displays a negative expansion coefficient of $-5.3 \pm 2.7 \text{ ppm}^\circ\text{C}^{-1}$. While this inherently seems unexpected, previous investigation into the relationship between water content and expansion of LBL PEMs suggests a complicated mechanism of water sorption where the volumetric expansion is greater than required for the

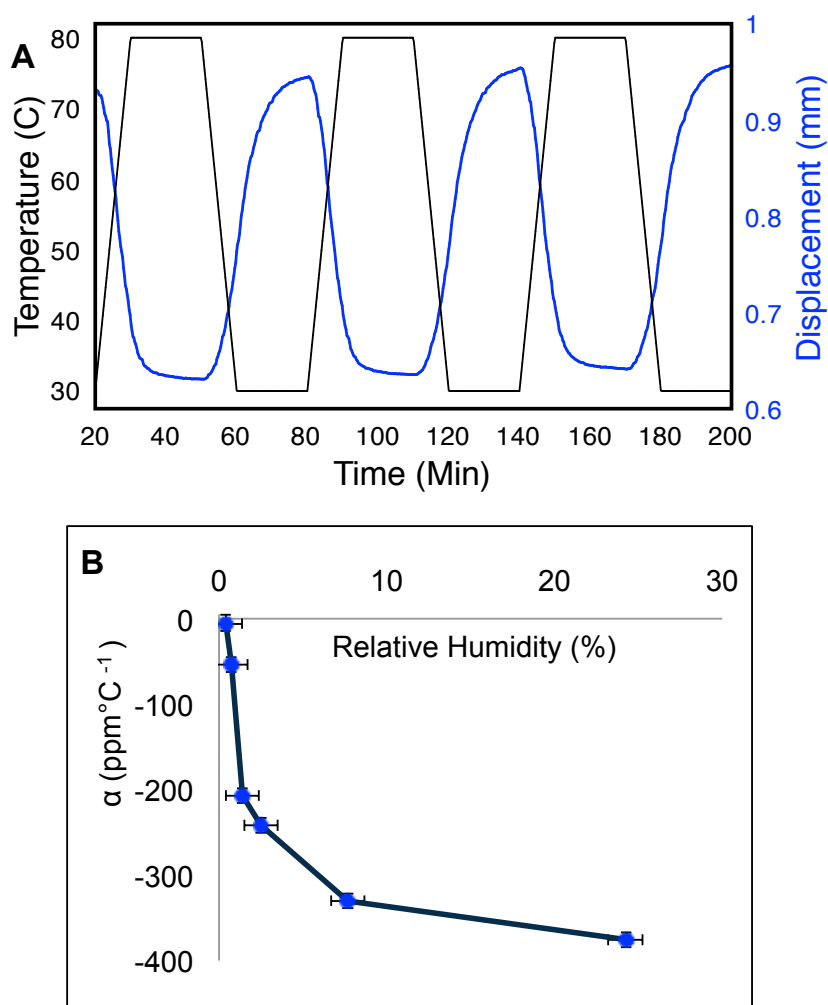
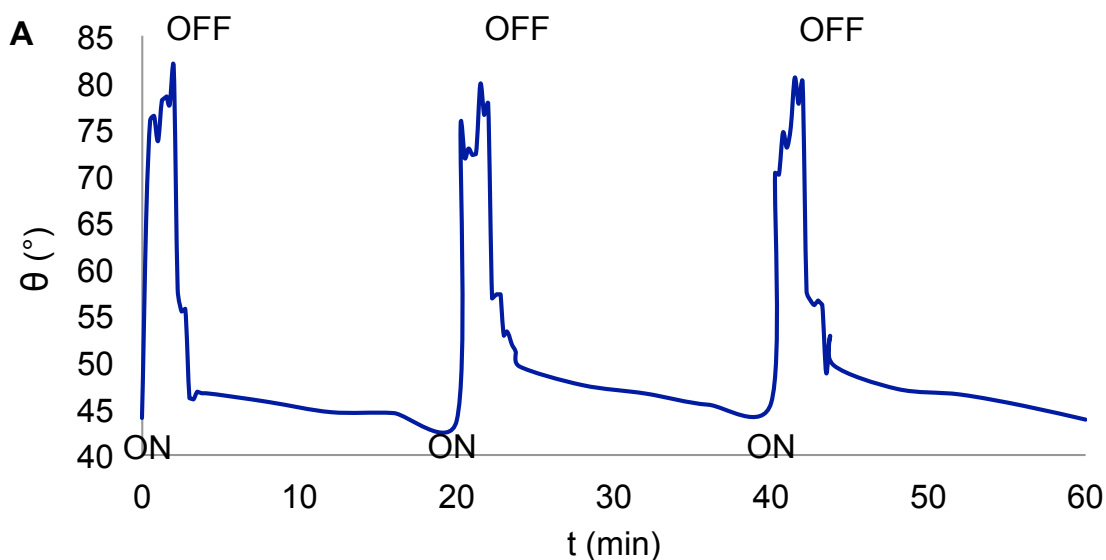


Figure 3.3 A) Thermal mechanical analysis of stimuli responsive LBL PEM showing an apparent negative thermal expansion that reversibility and repeatedly responds. B) The expansion relies on the relative humidity of the environment. A less drastic contraction occurs while heating with less available water vapor (relative humidity).

volumetric displacement of the increased water content.^[170] The exaggerated volumetric contraction with increased temperature, along with the quick, reversible, and repeatable response (**Figure 3A**) makes the LBL PEM an excellent candidate for the active material in a solid, stimuli-responsive bilayer that transforms shape with temperature stimuli.

To demonstrate the feasibility of temperature based shape-morphing with LBL PEM, the same (PDDA/PSS)₁₀ and (PU/CNT)₂₀₀ hinged film actuated above was heated remotely from 20.5 to 37 °C with a 250W heat lamp. As the presence of the CNT composite aids in the efficient absorption of near-IR radiation^[156] the hinged film responds within five seconds of exposure to the lamp, reaching an average peak $\theta = 79.9 \pm 2^\circ$ within two minutes (**Figure 3.4A**). The hinged film recovers completely after 18 minutes ($t=20$), when the environmental temperature under the heat lamp returns to 20.5 °C. Subsequent cycles of actuation of the heat lamp show reversible and repeatable shape morphing (**Figure 3.4**). The heat lamp set up provides a faster



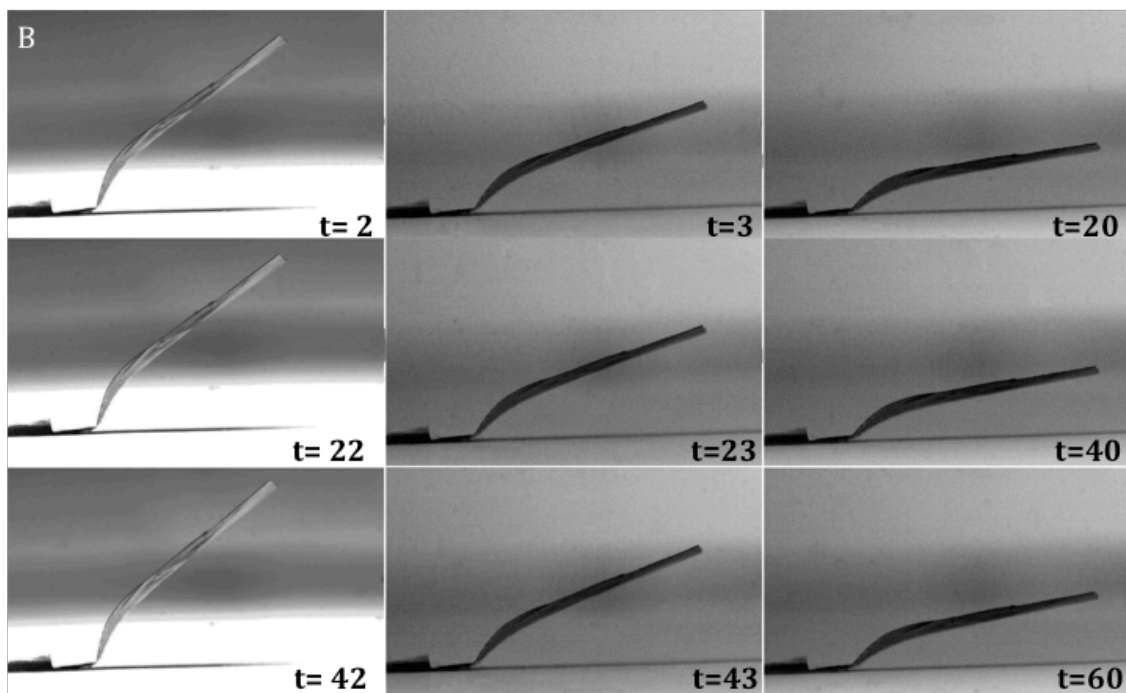


Figure 3.4 A) Graphical and B) Image representation of the dependence of the angle of deflection, θ , on temperature variations over time, t . The heat lamp was turned ON at $t=0, 20, \text{ and } 40$ and turned off at $t=3, 23, \text{ and } 43$.

response than the humidity chamber, however some instability is realized due to the convection currents generated as the surrounding air is heated.

3.5 Control Over Stimuli-Responsive Architecture

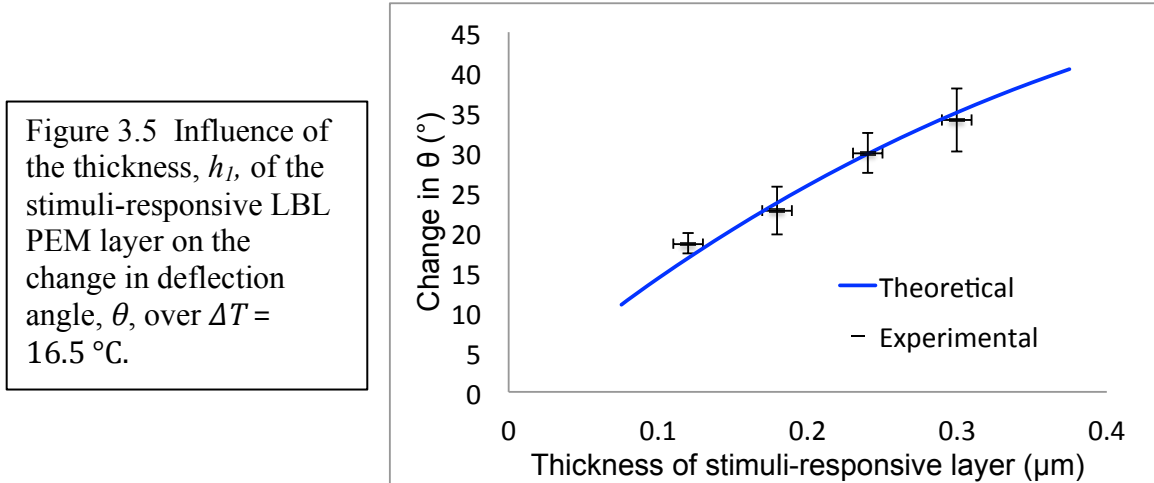
The out of plane deformation under ambient humidity is driven by the difference in expansion coefficients ($\alpha_1 = -368 \pm 9 \text{ ppm}^\circ\text{C}^{-1}$, $\alpha_2 = -6.5 \pm 4 \text{ ppm}^\circ\text{C}^{-1}$) over the temperature change delivered remotely from the heat lamp of $\Delta T = 16.5^\circ\text{C}$. The greater contraction of the (PDDA/PSS)₁₀ layer generates a compression stress upon the (PU/CNT)₂₀₀ layer of the bimorph hinge, which delivers an opposing tensile stress onto the LBL PEM. The material and structural properties of the

components allow for the internal stresses within the bilayer hinge to balance through an out-of-plane deformation. Originally derived by Timoshenko,^[151] a force balance can be performed to estimate the radius of curvature, ρ , of the bending moment. In the case where the bilayer is employed as a hinge, the unsecured arm can be assumed to follow a trajectory that is tangent to this curvature when in close proximity to the hinge. This tangent extends at an angle of displacement that is geometrically equivalent to the angle subtended by the curved bilayer. Combining Timoshenko's equation for ρ with the geometric definition of arc length allows for the angle of displacement to be expressed in the following manner, where the variables m and n are defined as the ratio of layer thickness, h_1/h_2 , and elastic moduli, E_1/E_2 , respectively.

$$\theta = \frac{L}{\rho} = L \left[\frac{6(\alpha_2 - \alpha_1)(1+m)^2 \Delta T}{(h_1 + h_2) \left[3(1+m)^2 + (1+mn)(m^2 + 1/mn) \right]} \right]$$

The theoretical model enables one to investigate and optimize how the angular deflection depends on the material and structural properties of each component. While assuming that n and the value of $(\alpha_2 - \alpha_1)$ remain constant over the temperature range explored, we can mathematically investigate how variations in thickness of the PEM layer influence θ (**Figure 3.5**). From previous studies,^[171, 172] E_1 is assumed to be 1 GPa and E_2 and h_2 were measured to be ~ 1.8 GPa and ~ 1.5 μm respectively. The thickness of the LBL PEM, h_1 was varied while L was held constant at $300\mu\text{m}$. Here we see that nanoscale control over PEM thickness can provide strict

control over the morphology of the actuated structure. One of the many benefits of LBL assembly over alternative composite fabrication techniques is its nanoscale control over thickness. When the thickness of the PEM layer is varied, the angle of deflection can be strictly controlled as expected by the theoretical analysis (**Figure 3.5**). While the theoretical model assumes that the bilayer is uniformly heated/cooled, curvature is only occurring in one direction, and neglects any shear or external forces, over the range of thicknesses explored the model fits quite well.



Not only is inkjet LBL capable of controlling the thickness of the stimuli-responsive bilayer, but it can also be used to specifically pattern stresses into localized regions of the nanocomposite. An attractive but relatively unexplored area^[182] is the fabrication of reconfigurable or stimuli responsive polymeric structures that can fold or un-fold in specified patterns. While theoretical models exist for simple hinge type structures the introduction of additional and multidirectional hinges into one structure quickly complicate the balance of internal forces within the nanocomposite. **Figure 3.6A** shows a square (PU/CNT)₂₀₀ strip

with orthogonal prints of $(\text{PDDA}^2/\text{PSS}^2)_z$ where $z=10$ is printed in the vertical direction and only $z=6$ is printed in the horizontal direction. Upon exposure to the heat lamp, the structure folds in a manner where the $(\text{PDDA}^2/\text{PSS}^2)_{10}$ dominates and only slight bending is realized across the $(\text{PDDA}^2/\text{PSS}^2)_6$ hinge (**Figure 3.6B**). Additional stimuli-responsive material can then be added to make both hinges the same thickness $(\text{PDDA}^2/\text{PSS}^2)_{10}$. As shown on the right, the folded structure of the film is completely different as both hinges provide approximately the same stress onto the LBL nanocomposite (**Figure 3.6C**). Such structures are of interest due to the numerous applications that can benefit from precise control over 3D actuation. Of possible greater impact, the controllability provided by inkjet LBL opens the door for opportunities to investigate the fundamental mechanics of complex folding so that the development of prescribed 2D to 3D transformations can be widely applied.

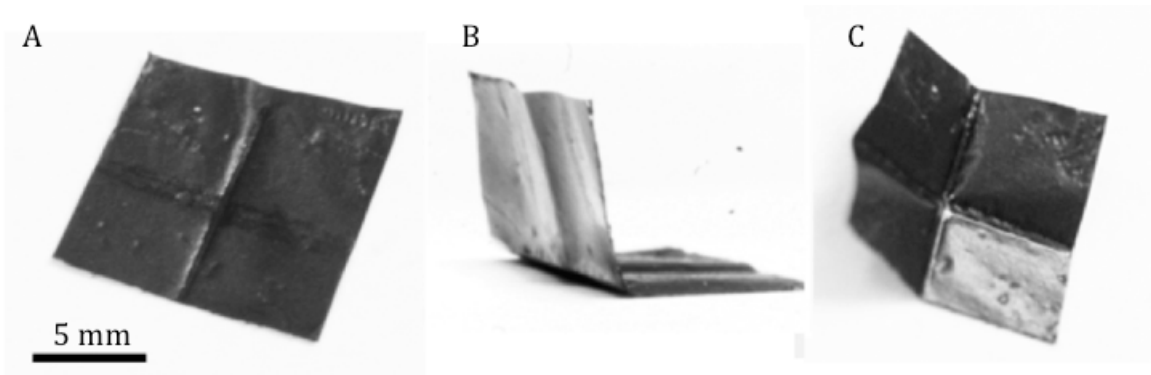


Figure 3.6 A) A cross-shaped hinge is printed onto an LBL nanocomposite square. The vertical hinge is $(\text{PDDA}^2/\text{PSS}^2)_{10}$, while the horizontal hinge is $(\text{PDDA}^2/\text{PSS}^2)_6$. B) Upon exposure to heat the structure folds into a structure where the thicker film dominates. C) With the addition of extra layers of PEM to make both parts of the hinge the same thickness, the structure now transforms into a completely different shape.

In nature, an example of a structure that relies on actuation methods beyond that of a single hinged bimorph, is the dispersion mechanisms of awns.^[149] Select seeds of grass and wheat have long awns attached to them that aid in dispersing the seeds through a coil and uncoil motion driven by humidity.^[147, 148] Here the functionality of the awn is achieved through very subtle yet highly precise twisting movements based on the spatial arrangement of the cellulose fibrils. While traditional machinery can offer great strengths and frequencies, the ability to make subtle, gentle and precise movements is often challenging. Materials such as wheat awns serve as a source of inspiration for the design of adaptive and stimuli-responsive materials, with applications in soft robotics.

To investigate the opportunity to create a nanocomposite material capable of a controlled and stimuli-responsive twisting motion, a spiral-like structure was prepared from the LBL nanocomposite, where PEM hinges of $(\text{PDDA}^2/\text{PSS}^2)_{10}$ were specifically patterned onto the corners of the spiral as shown in **Figure 3.7A**. When hung within the humidity chamber, the CNT spiral stretches out into a long coil. Upon exposure to nitrogen the structure responds in a very subtle, yet predictable fashion. The stress generated by the bimorph hinges causes the structure to rotate just enough for the central panel to face a different direction before returning back to its original direction when the nitrogen flow is discontinued. (**Figure 3.7B**). As LBL serves as a universal approach for the fabrication of nanostructured materials, the simple addition of additional materials to make the structure responsive to multiple stimuli for alternative shape transformations could easily be imagined.

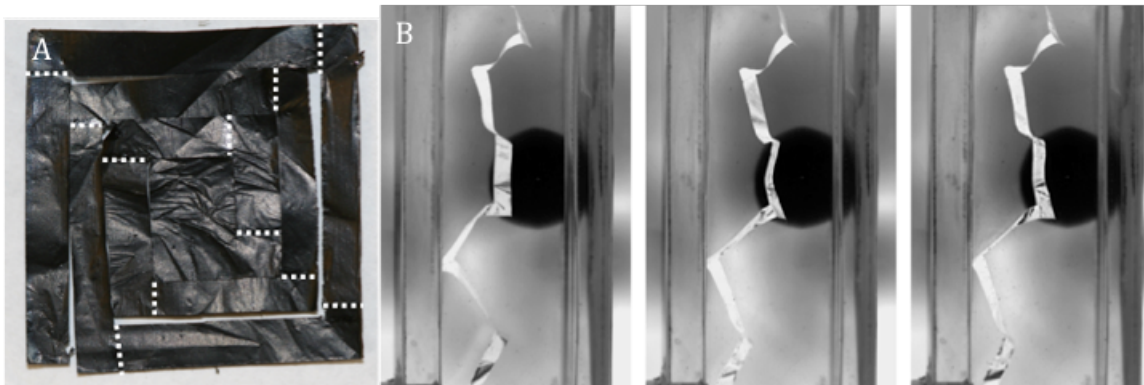


Figure 3.7 A) A spiral is cut into an LBL nanocomposite that has stimuli-responsive hinges inkjet printed into the edges of the spiral (drawn in as dotted lines) Complete structure is 1in^2 when flat. B) When hung from a support and introduced to nitrogen, the structure responds with reversible and subtle twisting motion.

3.6 Conclusion

Nature frequently produces solid materials capable of repeatedly and reversibly transforming shape in response to variations in environmental temperature and humidity. Mimicking these motions achieved in nature in synthetic materials provides opportunities for inducing controllable motion into novel materials that display enhanced properties such as LBL nanocomposites. LBL PEMs provide stimuli-responsive swelling with changes in humidity that also allow for actuation based off temperature due to the unique pseudonegative thermal expansion effect.^[169] When patterned with inkjet technology onto a CNT nanocomposite, the two form a bimorph structure capable of controllable and reversible shape transformations with fairly advanced complexity.

A number of challenges remain on both the theoretical and experimental front of shape-morphing structures. Further, integration with diverse materials is required to enable electronic, optical, and biomedical functionalities. Widespread application will require further miniaturization and scaling of the self-folding mechanisms. In terms of theoretical challenges, further investigation into the mechanism of swelling, especially in the case of pseudonegative thermal expansion will need to be developed for optimization of responsive behavior. The application of LBL and inkjet technology however serves as a promising approach to investigate several of these challenges based on the high level of structural control granted with the combination of the two technologies.

3.7 Experimental

3.7.1 Fabrication of LBL Nanocomposite

In a typical LBL cycle, glass slides cleaned by piranha solution for 24 hours were immersed in 1% cationic polyurethane (Hepce Chem Co., South Korea, Mw ~92000) for 5 min, rinsed with deionized water, and then dried with compressed air. Subsequently, these slides were dipped into the 0.25mg/ml P3 single walled carbon nanotube (SWNT, Carbon Solution Inc.) aqueous dispersions for 5 min, followed by rinsing and drying. The P3 SWNT were well dispersed in water by sonicating for 20 min. 200 bilayer films were deposited on a glass substrate by a NanoStrata robot. The(PU/CNT)₂₀₀ films were then removed with brief exposure to hydrofluoric acid.

3.7.2 Analysis of Thermal Expansion Properties

High molecular weight poly(diallyldimethylammonium) chloride (PDDA) and poly(sodium 4-styrene sulfonate) (PSS, MW 70,000) were purchased from Aldrich and diluted with deionized water. A (PDDA/PSS)₂₅₀ film was fabricated onto a Teflon substrate with 1wt% solutions of each polyelectrolyte using the typical LBL cycle described above. Upon removal from the Teflon, the films were stacked 4-fold before hot pressing under four tons at 80°C for five hours to obtain a film thick enough to withstand characterization. The hot pressed (PDDA/PSS) film and the (PU/CNT)₂₀₀ film were cut into 2 mm wide and 15 mm long strips for thermal mechanical analysis.

The coefficient of thermal expansion, α , of the film was measured in extension mode by a Perkin-Elmer TMA7 following the ASTM test method for linear thermal expansion of solid materials by thermomechanical analysis (E 831) and slightly modified to measure thin films.^[183, 184] The extension probe and grips were customized by RT Instruments, Inc. to minimize the expansion of the grips during the measurement. Ultrapure helium was used as purge gas to give an inert atmosphere and facilitate heat transfer. Cooling of the chamber was accomplished by circulating water at 8 °C provided by a chiller. The TMA instrument was calibrated using an aluminum standard; the experimental error for α of aluminum was 7.6% for temperatures as high as 300 °C. The α of Kevlar fibers from DuPont was also measured as an additional calibration for negative expansion, yielding a value of $-4.58 \text{ ppm } ^\circ\text{C}^{-1}$, which is in agreement with data reported elsewhere.^[185]

The strips were stretched under 45 mN of force, and the length changes were recorded by monitoring probe displacement for temperature ramps of 5 °C/min. The sample was initially heated from 30 up to 80 °C and then stabilized for 2 h to remove free water and residual stress. The length change for both cooling and heating segments was used to calculate the α , represented by the slope of the curve normalized by the initial length at 30 °C. Average α were calculated from the 75-35 °C interval. More than three samples were measured for each data point. For varied humidity testing relative humidity values of approximately 7.7, 2.5, 1.4, 0.7, and 0.4% were achieved with the controlled flow of ultrapure 99.9995% helium.

3.7.3 Inkjet Deposition of Polyelectrolyte Multilayers

PDDA and PSS were diluted in deionized water to 0.025wt% and sent through 0.22 μ m filters. Two 10pL droplet size cartridges with 16 piezoelectric nozzles were loaded separately with each polyelectrolyte. A FUJIFILM Dimatix material printer (DMP-2800) was used to deliver both polyelectrolytes to the surface with a typical voltage cycle (waveform) with two steps at a duration of 5.056 μ s each. First a slew rate of 0.9 was applied to reach a level of 87% followed by a slew rate of 0.19 decreasing to 0%. The waveform was fired at a frequency of 5kHz. Cartridge settings were set to a print height of 0.5mm, a vacuum meniscus set point of 3.5 inches H₂O and ambient temperatures. For LBL deposition, the cartridge and cleaning pad were alternately loaded. Before each deposition, a cleaning cycle of a 3 second purge was applied. Two overprints of each polyelectrolyte were alternately deposited to produce a (PDDA²/PSS²)_z film where z was varied between 4 and 10.

All samples were aligned and patterns developed to print lengthwise as to allow for a brief drying moment between printed drops as the printer repositioned along the y-axis. Patterns with lines in both the x and y direction were printed in two separate patterns with sample rotation in between to allow for all lines to be printed in this fashion. All hinged structures were fabricated with lines six droplets in width. While the droplets are delivered at 5 μ m intervals, it is estimated that each droplet adds \sim 50 μ m in width to the line. In the case of the multi-fold structure (PDDA²/PSS²)₁₀ was printed in one direction before the sample was rotated and (PDDA²/PSS²)₆ was printed orthogonally. After imaging, 4 additional layers were deposited so that both hinges had the thickness of (PDDA²/PSS²)₁₀. In the case of the spiral, each hinge was made up of (PDDA²/PSS²)₁₀. The hinges were patterned prior to cutting of the spiral structure with a razor blade.

3.7.4 Characterization of Shape Morphing

For humidity controlled investigation, a quartz chamber, 1 inch by 1 inch and 6 inches in height was fabricated to have two openings, one at the very top and one at 3 inches high. Nitrogen was switched on and off at 3 psi where it was allowed to flow into the top opening while the bottom opening remained open to ambient conditions. The chamber was placed onto a small square of rubber to minimize leakage. In the case of temperature analysis, a 250 Watt heat lamp was set up at a distance of 15 cm above the sample. A small magnet was used to hold the sample in place to allow for imaging. Temperature and ambient humidity were monitored with Hanna Instruments hygrometer HI 8064. All images were taken with an EOS 20D Cannon digital camera.

The Material in this Chapter is being adapted with minor modifications for submission for peer-reviewed publication. Contributing authors include Christine M.

Andres, Jian Zhu, Connor M. Flynn, and Nicholas A. Kotov

CHAPTER IV

LBL Nanocomposite Microcontainers

4.1 Current State of Microcontainer Fabrication

Microcontainers have many applications in smart packaging for pharmaceuticals, electronics, biological materials, and food products. They can be used as microreactors for expensive or media sensitive components, or used to encapsulate chemical agents, cells, particles, *etc* to prevent premature reactions based on a carefully controlled flux.^[17, 186] This property also allows for their use as sensors based on selective permeation of components through their sidewalls. Arrayed microcontainers can aid in high throughput analysis and fast optimization of component concentrations, sensing protocols, or (drug) delivery condition.

The fabrication of the majority of three-dimensional (3D) microcontainers is currently achieved using complex, multistep, two-dimensional (2D) lithographic processes predominantly using silicon or plastics. More advanced methods include elements of self-assembly where patterns are fabricated on planar surfaces and upon release are folded along pre-patterned hinges based on specific stimuli.^[187-189] Some methods of encapsulation also use templates made with molds or stamps

fabricated by lithography.^[17, 190] These variations of 2D lithography allow for variable micron scale porosity,^[186, 191] while subnanometer sized pores have been etched into the lids of some microcontainers by nanoimprinting.^[192] Such structures are generally geared toward the encapsulation of cells for therapeutic purposes and have high perfusion rates. Microcontainers with slow release rates are desirable for implantable drug carriers and microreactors. Beyond controlled porosity and mechanical properties, microcontainers also often need transparency at different electromagnetic frequencies, for example for high-throughput analysis.^[193]

While quite exciting and still under intense development, the current methods to make microcontainers have two significant limitations:

(1) the choice of materials available for sidewalls and other parts of microcontainers and therefore the range of transport, optical, mechanical, and biological properties available is quite limited; and

(2) the choice of microcontainer contents is strongly restricted by chemicals/solvents or temperatures used during fabrication/assembly and by the limited compatibility between the solvents used for loading and the walls of the microcontainer.

Both of these issues result in significant delays in the development of most applications mentioned above as well as substantially increase the cost of microcontainer fabrication, which also affects their potential, for instance, for high-throughput reaction optimization or sensing.

Considering these problems, nanocomposites offer unique combinations and an exceptionally wide range of chemical and physical properties that can be easily

adapted to specific applications. Here we demonstrate a methodology for microcontainers to be made from layer by layer (LBL)^[35] nanocomposites rather than silicon or polydimethylsiloxane (PDMS).

4.2 Advanced LBL Material: Clay Nanocomposites

Among the many techniques to fabricate nanocomposites, LBL stands out due to the universality, simplicity and unlimited combinations of remarkable material properties possible by the thermodynamically limited assembly of high molecular weight materials^[43, 194-199] and high performance.^[200, 201] The technique can be applicable to a very broad range of polymer-polymer or polymer-nanoparticle combinations. The well-known ability of the LBL technique to make controlled-release coatings with stratified spatially separated reagents^[57-59] and spherical microcapsules^[202, 203] adds to the versatility of the method. Here we will look at clay nanocomposites from polyvinyl alcohol (PVA) and sodium montmorillonite clay nanoplatelets (MTM) as they present a particularly attractive nanomaterial for microcontainer walls.

Due to the controlled orientation of the anisotropic clay nanoplatelets, (PVA/MTM) multilayers provided excellent barrier properties for low permeability of small molecules such as oxygen, which is particularly suitable for drug carriers.^[204] The high weight percent of highly dispersed inorganic material provides a high flexibility and tensile strength for microcontainer stability.^[39, 41] The highly dispersed nature of the film also ensures that the spacing is significantly less than the wavelength of optical light (390–780 nm), making them optically

transparent.^[39, 41] (PVA/MTM) multilayers also have high biocompatibility,^[205] and are resistant to both hydrophilic and hydrophobic solvents. They can provide inert packaging with slow/controlled release for virtually any type of encapsulating material. Finally, they can also be made in high yield and rather inexpensively.

4.3 Nanocomposite Microcontainer Fabrication

All together, the current material limitations of microcontainers and the exceptional material properties of LBL nanocomposites prompted us to demonstrate the conceptual possibility of fabricating arrays of well-and-lid microcontainers from LBL clay nanocomposites. To generate 3D patterns from a traditionally planar material, we used a template approach with a PDMS mold

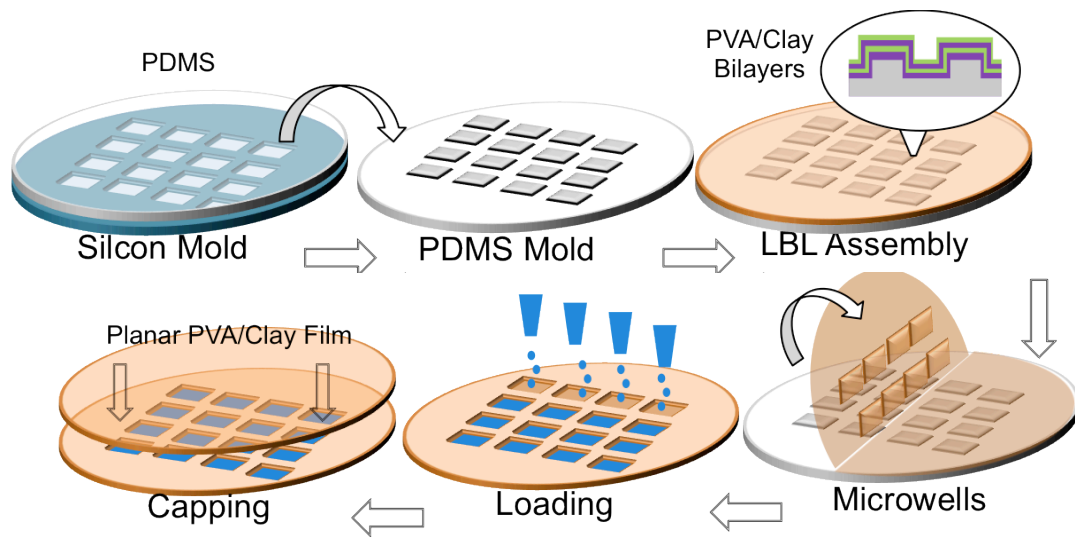


Figure 4.1. A PDMS mold with microtowers is fabricated from a silicon mold. Alternate deposition or the PDMS mold into PVA and MTM with intermediate rinsing and drying steps, results in the growth of an LBL assembled film onto the surface. This film is then peeled off to reveal nanocomposite microwells that can be loaded by micropipetting. After loading, a planar LBL film is then pressed on top of the microwells to form a lid sealed by hydrogen bonding.

(Figure 4.1). Initially, a 1 cm thick layer of PDMS was cured onto a silicon wafer with patterned 0.18 μ L capacity microwells (3mm x 3mm x 20 μ m) to create a PDMS mold with microtowers **(Figure 4.2A)**. (PVA/MTM)_z was deposited onto the released PDMS microtower mold and a planar PDMS sheet to make the wells and the lids of the microcontainers, respectively. Due to the conformal and self-limiting nature of LBL assembly, the film takes on the shape of the PDMS microwell template and does not fill in the cavities as would be expected for other methods of thin film

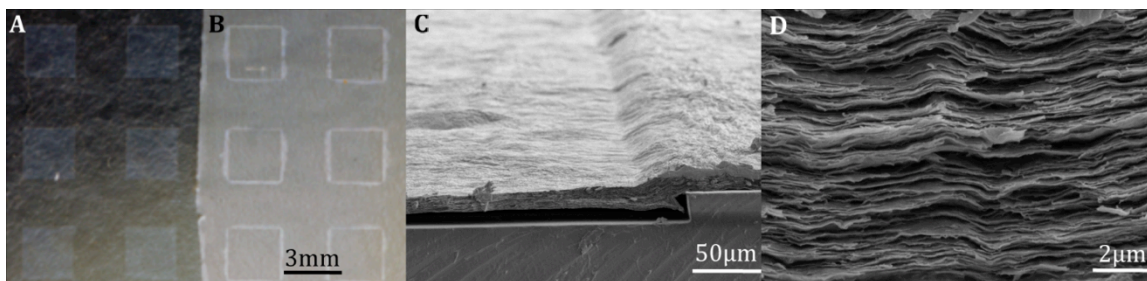


Figure 4.2 A) Photograph of PDMS mold with microwell shape. B) Clay nanocomposite film deposited on PDMS template with LBL assembly. C) SEM image of clay nanocomposite LBL film with the contour of the PDMS microwell. D) SEM image of the layered structure of the LBL clay nanocomposite that contributes to the unique properties of the material that are advantageous for microcontainer walls.

fabrication *i.e.* spin coating or blade-spreading **(Figure 4.2B,C)**. This results in the realization of a controlled 3D pattern in the LBL film without the need for additional processing.

Importantly, the (PVA/MTM)₁₀₀₀ film maintains the layered structure **(Figure 4.2D)** that is often granted responsibility for the excellent mechanical, optical, and barrier properties of the material.^[41] The same layered structure, especially for the “lid” of the microcontainer, will also offer unique control over gas/liquid permeability. As such, a lid was made from (PVA/MTM)₁₀₀₀, however its

thickness and composition can be varied widely to regulate, for instance permeation and/or response to external stimuli, e.g., magnetic field.^[56] The assembly of the microcontainer array was achieved by placing the planar (PVA/MTM)₁₀₀₀ sheet on to the (PVA/MTM)₁₀₀₀ sheet with patterned wells followed by application of pressure onto the back of the planar substrate to allow for hydrogen bonding to occur between the PVA/MTM multilayers of each sheet and a sealed microcontainer to be fabricated **(Figure 4.3A,B)**. Mechanical properties of the (PVA/MTM)₁₀₀₀ allow this transfer to occur with ease. Previously microchambers have been fabricated from the LBL assembly of polyelectrolytes,^[206, 207] however having a Young's modulus, E , of $\sim 4\text{GPa}$ and other mechanical properties substantially weaker than LBL clay nanocomposites with $E=125\text{GPa}$ ^[39] can be quite restrictive. For instance, they were reported to exist only while being supported by a solid substrate. Also while loading has not been demonstrated with these chambers, it is likely due to the mechanical properties that solvent-exchange methods would be required, as is done in many cases with microcapsules.^[198]

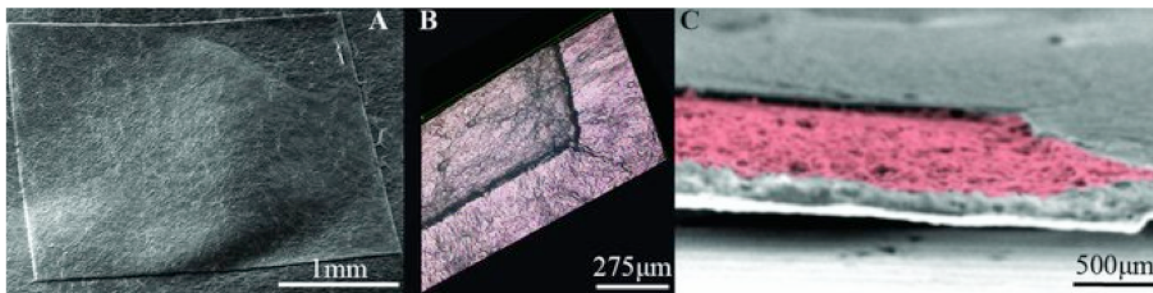


Figure 4.3 A) SEM image and B) three-dimensional confocal microscopy image of capped clay nanocomposite microcontainer. C) SEM image of micro-well filled with CdSe NPs (the color has been artificially added).

4.4 Microcontainer Loading

Besides the fabrication of the microcontainer itself, it is important to consider the methodology of its loading. To further investigate the nanocomposite microcontainers as an advanced packaging technology, trioctylphosphine oxide stabilized CdSe nanoparticles (NPs) or citrate stabilized gold NPs, synthesized according to previously published procedures,^[101, 208] were loaded into the microwells by micro injection (**Figure 4.3C**) before the lid was sealed. The microinjection loading procedure used here does not rely on self-loading equilibrium conditions or special thermal or chemical treatments and allows for a wide variety of materials to be loaded into the microcontainers. It can also be integrated with inkjet technology,^[166] allowing for controlled mixtures, live cells, or even reacting species to be loaded into the nanocomposite microcontainers.

The fluorescence of the Cd-Se NPs was clearly observed under UV-light through the transparent nanocomposite walls (**Figure 4.4A**). The robustness of the microcontainers was tested by exposure of an array of six sealed microcontainers to chloroform, a solvent capable of dispersing the TOPO-stabilized NPs. After soaking for several hours, the fluorescence of the NPs loaded into the microcontainers submerged in chloroform was observed to be localized exclusively in the original wells, suggesting that they are well protected and sealed (**Figure 4.4B**). The walls of the nanocomposite container were not compromised nor any detectable release of NPs observed after the sealed microcontainers were placed in vials filled with water, ethanol, or acetone. Similarly, when the microcontainers were loaded with citrate stabilized gold NPs, a water dispersible nanomaterial, and submerged in water for

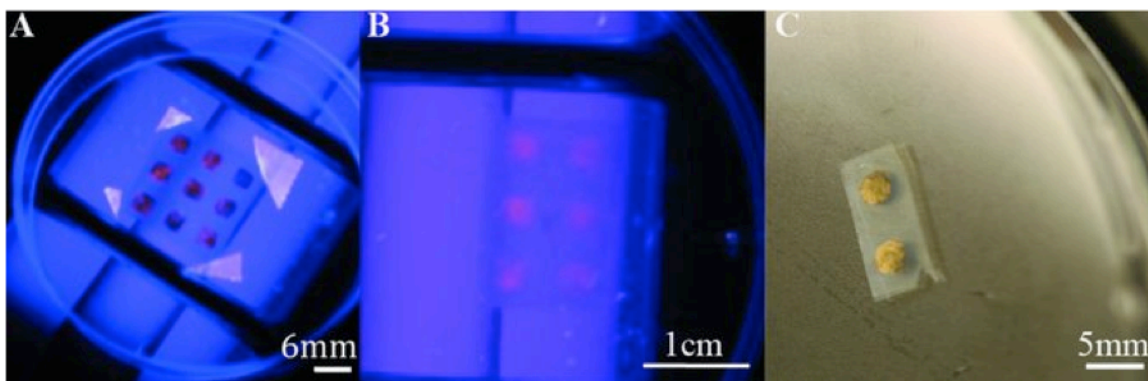


Figure 4.4 A) Photograph of nine CdSe-filled micro-containers in the presence of UV light demonstrating transparency to optical and ultraviolet wavelengths. B) Photograph of clay nanocomposite microcontainer filled with CdSe NPs under UV-light in the presence of chloroform and C) gold NPs in the presence of water.

24 hours, the NPs remained localized in the well of the microcontainer (**Figure 4.4C**) suggesting the ability of the microcontainers to retain a variety of different materials in numerous solvents.

4.5 Conclusions

Beyond clay nanocomposites, LBL offers a wide variety of materials that can be incorporated into the walls of microcontainers as the technique is not limited by lithographic processing of the material or special conditions required for folding. The strict control over material stratification provided by LBL allows for control over the interior and exterior surface properties of the microcontainer as well as for the simple incorporation of other materials into the MTM nanocomposite such as silver NPs for antimicrobial action,^[209] magnetite NPs^[47] or the growth of carbon nanotubes within LBL assembled films.^[210] The simple, low cost, and universal LBL

deposition operates at low temperature and mild conditions outside of a clean room, providing a sustainable option for universal microcontainers.

4.6 Experimental

4.6.1 Materials

Polyvinyl alcohol (PVA) with a molecular weight of $MW \approx 70,000$, Selenium powder (Se), Cadmium Oxide (CdO), trioctylphosphine (TOP), trioctylphosphine oxide (TOPO), hexadecylamine (HDA), stearic acid, trichloro(3,3,3-trifluoropropyl)silane, chloroauric acid, sodium citrate, n-hexane, chloroform and methanol, were purchased from Sigma-Aldrich and used as received. Poly(dimethylsiloxane) (PDMS) Sylgard 184 was purchased from Dow Corning (Michigan, USA). Na⁺-montmorillonite (MTM) powder was purchased from Southern Clay Products (Gonzales, TX) and was exfoliated via extensive stirring in aqueous solution. The average diameter of the platelets is 110 nm and thickness is approximately one nm as described by the supplier.

4.6.2 PDMS Mold Preparation

A silicon wafer containing 64 squared 0.18 μ L wells with 3 mm edges and a depth of 20 μ m (Lurie Nanofabrication Facility, UofM), was vapor-coated with Trichloro(3,3,3-trifluoropropyl)silane. PDMS pre-polymer was mixed with a curing agent in 10:1 proportion and poured onto the specified Silicon wafer in order to form 1 cm thick mold. The PDMS was cured at 80^oC overnight. A flat PDMS (without pattern) mold was similarly produced on a glass substrate. Both PDMS templates

were removed from their substrates and washed with acetone before using for layer by layer deposition (LBL).

4.6.3 Microcontainer Fabrication

The patterned and non-patterned PDMS molds were sequentially immersed in a 1wt% aqueous solution of PVA for 5 minutes and in a 1wt% aqueous dispersion of MTM. Each polymer and clay adsorption step was followed by a rinse in deionized water for two minutes followed by drying under an air stream for two minutes. The deposition procedure was realized with a robotic manipulator (DR-1, R&K Technologies, Germany) programmed to carry out all the operations automatically for a number of cycles, n , to produce a $(\text{PVA}/\text{MTM})_n$ film. Both the patterned and planar molds were coated with $n = 1000$ bilayers, with fresh solutions of each component used after every 20 bilayers. After multilayer fabrication, the PVA/MTM films were gently peeled from the PDMS molds. The microcontainer was produced by combining the planar and patterned LBL nanocomposite films with a droplet of water in between and applying gentle pressure to allow for hydrogen bonding to seal the planar lid in place. In some cases, prior to sealing, the microwells were filled with a CdSe or gold nanoparticle solution by micropipetting. The samples were analyzed by scanning electron microscopy (Philips XL30 Environmental Scanning Electron Microscope and FEI Nova 200 Nanolab) after gold coating and confocal microscopy (Olympus LEXT Interferometer).

4.6.4 Synthesis of Nanoparticles (NPs)

The synthesis of CdSe nanoparticles was based on the previously reported procedure.^[208] A three necked rounded bottom flask 0.04g of CdO and 6g of stearic acid were combined and heated under argon to 250°C, at which point the mixture became colorless. The solution was then cooled to room temperature and 5.67g of HDA and 5.67g of TOPO were added while stirring. The solution was heated up again to 250°C and a solution of Se powder (0.025 g) and TOP prepared under an inert atmosphere was added drop wise. In order to control the NP growth, the fluorescence of aliquots of dispersed NPs in chloroform was measured. The reaction was stopped when a maximum of 650nm absorbance was reached. After the reaction reached room temperature, the NP's were purified by dispersion in a 1:1 hexane/methanol solution followed by centrifugation for 15 minutes at 6000 rpm and repeated three times. Fluorescence was realized based on photography in the presence of a UV light source.

As previously reported,^[101] citrate stabilized gold NPs were fabricated by bringing chloroauric acid (0.005M) to boil before adding sodium citrate (1% w/w) under vigorous stirring. Heat and stirring was applied for an additional 15 minutes before cooling.

The Material in this Chapter has been adapted with minor modifications from the following peer-reviewed, published article:

Andres, C. M., Larraza, I., Corrales, T. & Kotov, N. A. Nanocomposite Microcontainers. *Advanced Materials* 24, 4597-4600, (2012).

CHAPTER V

Three Dimensional Layer by Layer Assembly

5.1 A Need for Hierarchical 3D Structures

Over 1.3 million procedures are conducted to treat bone deficiencies in the U.S. each year.^[211] Defects of bone wounds above a critical size are naturally replaced with a weaker fibrous connective tissue unless a repair strategy is used. Replacements for such defects include: bone grafts, which are limited by a lack of donor tissue, rejection, and susceptibility to infection, and material implants, which are limited by lack of biocompatibility and fatigue.^[212, 213] Alternatively, cell scaffolds aim to temporarily securing the defect site while facilitating bone regeneration and slowly degrade as natural bone takes over. Production of a successful bone tissue-engineering scaffold requires a unique combination of material properties. This includes biocompatibility, biodegradability, porosity to enable mass transport of components required for cell life, mechanical properties to meet the mechanical demands in-vivo upon implantation, and a controlled 3D environment, including nanoscale morphology, suitable for bone regeneration.^[214, 215] While metals and ceramics provide excellent mechanical support, limitations due to brittleness, limited processability, biodegradability, and adaptability to environmental changes

have been cited.^[214] Biodegradable polymers can overcome many of these deficiencies; however often lack the mechanical properties necessary for providing support during tissue regeneration. The tensile strength of the solid components of the human tibia or femur ranges between 66-170 MPa^[216] while poly(lactic acid) for example possesses a tensile strength of only 28-50 MPa, depending on its molecular weight.^[217] The matching of the mechanical properties of a scaffold to that of bone is one of the most essential requirements for successful implant design so that sufficient strength and stiffness is maintained as a gradual shift of mechanical load takes place from the scaffold to the strengthening, maturing tissue.^[212] Therefore, it is clear that the mechanical properties of biodegradable polymers must be improved if a successful bone tissue-engineering scaffold is to be derived from polymers. Naturally, we will again look to nanocomposites to provide a unique combination of material properties.

This appears to be an appropriate choice considering natural bone is itself a nanocomposites. The extra cellular matrix of bone comprises nanoplates of primarily hydroxyapatite (HAP: $\text{Ca}_{10}(\text{PO}_4)_6(\text{OH})_2$), arranged along an organic material; mainly Type 1 collagen fibers^[218]. Similar to many nanocomposites, the nanophase within the collagen matrix is believed to supply bone with it's mechanical integrity.^[218] Several examples of the incorporation of calcium phosphate nano-fillers for improved mechanical properties have been realized for applications in bone tissue engineering, however the realization of biomimetic mechanical properties has not yet been achieved.^[219] In part, this is related to the fact that bone is an organic-inorganic composite with a high inorganic content of

~65%. This is very hard if not impossible to reach by traditional methods of composite preparation, however easily realized with layer by layer assembly (LBL).[39]

5.2 Advanced LBL Material: Synthetic Bone

5.2.1 Fabrication of Synthetic Bone Material

Natural bone mineral exists as anisotropic plate-like crystals 20–80 nm long and 2–5 nm thick^[220]. The nanoplates' advantageous, 2D symmetric shape allows for uniform, multidirectional reinforcement when two dimensionally aligned. Their continuous 2D surface may also give rise to a deeper interaction with the surrounding matrix.^[221] Therefore, relatively monodispersed biomimetic calcium phosphate nanoparticles (CP NP) were synthesized from aqueous calcium nitrate and phosphoric acid in the presence of 2-carboxyethylphosphonic acid (CEPA) to be used in preparation of biodegradable polymer nanocomposites. The particles have a platelet shape similar to that of natural bone mineral. Under transmission electron microscopy (TEM), their diameter was observed to be between 20-40nm (**Figure 5.1A,B**). Atomic force microscopy (AFM) was used to find a nanoplate height

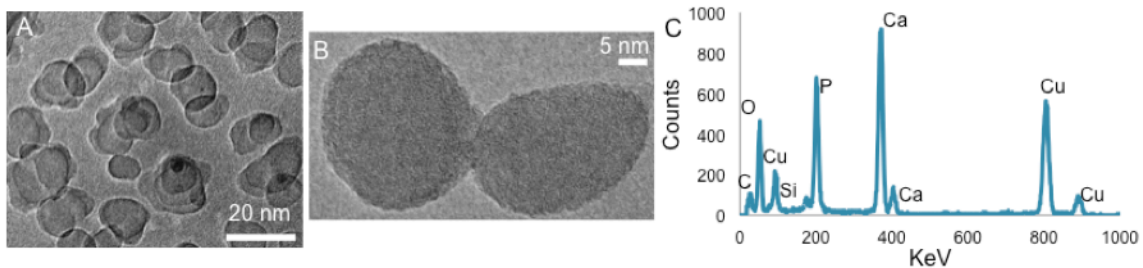


Figure 5.1 Characterization of calcium phosphate nanoparticle suspension by A,B) TEM and C) Elemental Analysis

ranging between 7-15nm (not shown). Energy dispersive X-ray analysis during TEM of the air-dried samples demonstrates the presence of calcium, oxygen and phosphorous as expected for CP (**Figure 5.1C**). Finally, X-ray diffraction of the freeze-dried powder confirmed the composition of the CP NPs, demonstrating reflections corresponding to HAP and amorphous calcium phosphate. The average particle diameter calculated from the half-peak width was 40.64 nm, corresponding nicely with that of TEM.

CEPA serves as a functionalizing agent to protect the suspension from aggregation through electrostatic repulsion. The surface charge generated from the functionalizing agent was approximately -41.4mV as estimated from dynamic light scattering. Not only does this surface charge serve to prevent agglomeration of the CP NPs so that the inherent nanoscale properties of the particles can be conserved, but also provides an excellent system for LBL assembly. LBL assembly, described as the sequential adsorption of oppositely charged solutions alternating with rinse water to yield monolayer control over surface properties, was used to create biodegradable nanocomposites with the CP NPs. Poly(diallyldimethylammonium chloride) (PDDA), a strong polycation, was alternated with the dispersion of negatively charged nanoplates to prove that nanocomposites could be created with the nanoplates in such a manner.

Ellipsometry data demonstrates the steady growth of the film thickness as well as the capabilities of the technique to control thickness on the nanoscale (**Figure 5.2A**). A single bilayer is defined as a complete cycle of deposition, including one layer of polycation and one of nanoplates with intermediate rinsing and drying. Scanning electron microscopy (SEM) images of $(\text{PDDA}/\text{CPNP})_{100}$ demonstrate the uniform coating created by the LBL assembly, the capabilities of the technique to make thick films, as well as the high concentration of nanofiller present in the film (**Figure 5.2B**). Thermal gravimetric analysis reveals that the film is composed of 80wt% inorganic material, an unprecedented achievement in calcium phosphate nanocomposites.

5.2.2 Mechanical and Biological Properties

The mechanical properties of the $(\text{PDDA}/\text{CPNP})_{100}$ film were determined using nanoindentation with a maximum load of 2mN. The calculated elastic modulus under compression, Y_c , and hardness, H , of the film were 5.6 GPa and 0.21 GPa,

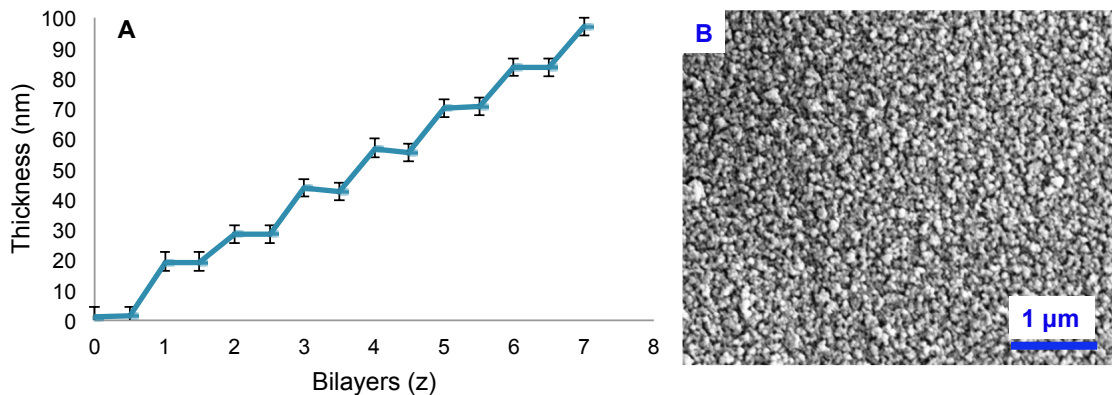


Figure 5.2 Characterization of CP NP and PDDA LBL Film: A) Ellipsometry thickness analysis of 7 bilayers B) SEM image of $(\text{PDDA}/\text{CPNP})_{100}$ film.

respectively. Nanoindentation testing of both trabecular and cortical bone suggests a range of 8 to 26GPa for Y_c and 0.4-0.7 GPa for H .^[222] As natural bone extra cellular matrix is composed of ~65% inorganic material, the somewhat brittle nature of the film due to the high inorganic component (80 wt%) of the nanocomposites may be leading to decreased mechanical properties. Due to the high level of control provided by the LBL technology, addition of additional organic material as well as manipulation of the polymer properties to optimize the mechanical properties of the film is simple. For example, successful LBL assembly of the biomimetic CP NPs with Type 1 collagen has also recently been achieved. Similarly the thermal aging time used in the synthesis of the CP NPs can be adjusted to vary the size of the nanoplates allowing for an additional level of adjustment.

In addition to enhancing mechanical properties, nanoscale molecules are often involved in cellular signaling mechanisms and interactions with the extra cellular matrix. Therefore, controlled surface chemistry with nanoscale morphology have demonstrated the ability to not only increase mechanical properties but to enhance bone formation within cell scaffolds by regulating properties of adsorbed proteins as well as cell adhesion, organization, morphology and differentiation.^[133, 223-227]

The bioactivity of the nanocomposites was tested with human osteoblasts (hFOB 1.19 cell line), cells responsible for bone generation. Several square centimeter glass slides were coated with either only one layer of PDDA (control) or (PDDA/CPNP)_{5.5} where the topmost layer of the test films was composed of PDDA. All samples were sterilized by soaking overnight in ethanol followed by exposure to

ultraviolet and rinsing with phosphate buffer solution (PBS). The coated glass squares were then placed in 24-well plates and rinsed with media, before 30k cells were seeded onto them and cultured as recommended by ATCC. The biocompatibility of the nanocomposite was demonstrated as over the eight day experiment the osteoblasts spread nicely over the surface as is typical for thriving osteoblasts (**Figure 5.3A**).

In order to investigate the ability of the nanocomposite film to stimulate bone growth with an *in vitro* study, the amount of osteocalcin, a protein produced by osteoblasts that is often used as a marker for new bone formation, was detected every other day of the eight-day study. To determine the amount of osteocalcin produced per cell, the amount of double stranded DNA (dsDNA) was also analyzed, which is representative of the number of cells present. The amount of bone producing protein produced per cell (ng of osteocalcin per ng of dsDNA) was

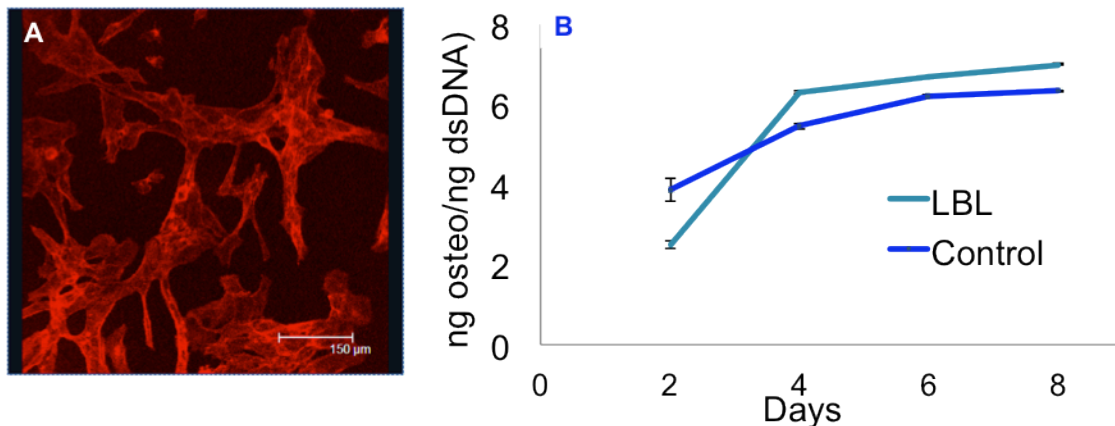


Figure 5.3 A) Stained osteoblasts spreading across a (PDDA/CPNP)_{5.5} surface imaged with confocal microscopy (scale bar 150μm). B) Summation of osteocalcin production versus amount of DNA over eight days of cell growth. Osteocalcin production per cell is greater with LBL nanocomposites.

calculated for the nanocomposites and control films (**Figure 5.3B**). As higher levels of osteocalcin are directly correlated with increased bone production, it can be concluded that the produced nanocomposite is not only biocompatible but may also stimulate bone production.

The mechanical and biological properties of the CP LBL nanocomposites make it an attractive material for bone tissue engineering scaffolds. However, in its current state, the nanocomposites does not have the 3D hierarchical organization that would improve conditions for cell growth by combining the nanoscale features with micro-scale interconnected pores necessary for adequate mass transfer of nutrients and metabolic wastes, vascularization, and cell migration.^[228] As, the overall material performance depends on the three-dimensional (3D) organization of the material across multiple length scales, it can generally be assumed that the introduction of controlled porosity will allow for greater performance as compared to random pore distributions, as such techniques will require a higher degree of porosity for complete pore interconnectivity. Therefore, a multi-scale design paradigm that controls the structure of LBL composites on the nano-, micro- and macroscale, will allow for a bone scaffold with optimal mechanical and tissue-regenerative properties to be synthesized. Beyond tissue engineering, a systematic approach to the synthesis of hierarchically ordered porous materials has become attractive in many other promising applications in material science including absorption, separation, drug delivery, catalysis, optics, sensing, and electrodes.^[229]

5.3 Approaches to Multi-scale 3D Structural Control

Development of material processing techniques that allow for structural control across multiple length scales is interesting for numerous reasons. First, it provides a systematic approach to investigate the effect of micro-scale architecture on the macro-scale properties of nanocomposites, allowing for structure-property relationships to be realized and applied for device optimization. Second, it aids in bridging the gap between nanoscale materials and macro-scale applications, as is currently one of the most significant challenges in material science. Third, it creates opportunities for new practical applications by allowing unusual *combinations* of properties that previously have not been achieved, as exemplified, for example, by the well-known Ashby diagrams.^[230] Fourth, the introduction of 3D architecture provides an opportunity to impart unique characteristics to materials such as special deformation patterns^[20], negative Poisson's ratio,^[21] negative thermal expansion,^[22] controlled biological interactions^[23] and mass transport properties.^[24, 25] Finally, while computational predictions of unique properties of 3D topological structures are quite abundant, actual methods for fabrication of controlled 3D architecture are quite limited and often restricted to multistep adaptations of 2D processes that introduce structural restrictions, are time consuming, and require expensive hardware.

Most 3D fabrication case studies have been carried out on materials sculpted by photolithography, folding of planar materials, and direct 3D lithography^[17, 231-234] or serial alternatives including free-form fabrication,^[235] micromachining,^[236] and direct-write with colloidal dispersions.^[237, 238] A lot of success has been achieved in

this area aimed predominantly toward applications in medicine and electronics.^[21, 23, 239-241] However, the variety of materials available to these techniques is quite limited, especially with respect to nanocomposites with unique properties that could be very beneficial to a variety of applications.^[39-43] In addition, for methods such as 3D direct-writing and 3D lithography that have produced microscale architectures, the transition to macroscale applications is envisioned to be challenging by requiring massively parallel micromanufacturing processes for example. Considering these technological needs and challenges, a simple and scalable technique to introduce controlled 3D architecture across multiple length scales to novel nanocomposites is quite interesting from both an academic and applied standpoint.

While the alternating chemical adsorption of nanoscale layers of different high-molecular-weight species (organic or inorganic) during LBL assembly provide thermodynamic control over thickness in one direction on the nanoscale,^[46] a number of approaches to spatially control LBL materials across multiple scales and dimensions for incorporation into advanced materials have been employed.^[43, 194] For example, micro- and nanoscale colloidal particles have been coated with LBL nanocomposites and later removed to create 3D hollow capsules for applications in drug delivery, sensing, catalysis and microreactors.^[202, 242] On the macro-scale, freestanding metal oxide/polymer hybrid membranes with random micro-scale architecture have been fabricated from cellulose templates.^[243, 244] While being very attractive for many advanced applications, macroscale examples of LBL *nanocomposites* with micro-scale structure or any LBL materials with *ordered*

microscale structure have not yet been demonstrated. In the next section of this chapter, the structures obtained on a newly developed LBL deposition system **(Figure 5.4A)** demonstrate the production of macroscale objects from LBL nanocomposites with millions of repeating structural units based on inverted colloidal crystal (ICC) architectures. This automated system greatly accelerates the process of LBL deposition onto porous substrates with the aid of suction to facilitate solution diffusion and decrease production time.

5.4 Hierarchical Structural Control for Layer by Layer Assembly

Colloidal crystal templates (CCT), composed of hexagonally packed arrays of spherical colloidal particles, have served as molds for the synthesis of hierarchically ordered networks with precisely controlled pore size, shape and order upon infiltration and subsequent removal of the CCT.^[229] This technology has been used to pattern and order inorganic nanoscale materials in three-dimensions through nanoparticle packing of the CCT voids.^[245, 246] The random dispersion of nanoparticles within the void leads to low-density packing and often requires annealing to form a mechanically stable 3D structure. Combining LBL deposition and CCT templates allows one to introduce controlled spatial distribution of a nanophase into the bulk of the ICC while retaining the structural control of the micro-scale architecture and simple scalability to macro-scale dimensions.

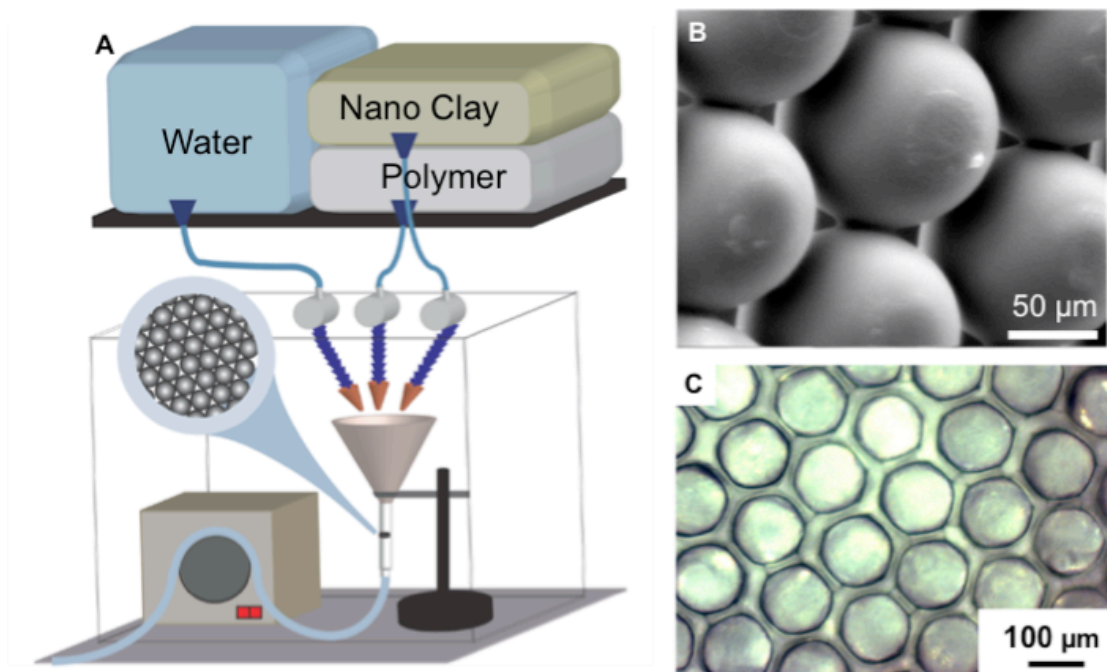


Figure 5.4 A) 3D LBL set up used to deliver alternating solutions via solenoid valves through a colloidal crystal template (CCT) secured within silicone tubing and accelerated by a peristaltic pump. B) SEM image of the annealed polystyrene CCT. Note the necks forming between the beads for pore interconnectivity. C) Optical microscopy image of the LBL clay nanocomposite on the CCT (B).

Uniform polystyrene spheres (diameter $\sim 100\mu\text{m}$) were assembled into hexagonally packed arrays via sedimentation and interconnected by annealing at 120°C to create a CCT as a mold for template LBL (**Figure 5.4B**). Interconnectivity of the colloidal spheres provides the structural stability needed for further processing and a template for pore interconnectivity for the final 3D LBL structure. The versatile and simple technique used to create the CCT^[247] can be employed to produce a variety of multi-dimensional shapes when alternative molds or sphere sizes are employed. Anneal times can also be varied to control the diameter of the sphere interconnectivity and later pore interconnectivity as desired.^[248]

As successful nanoscale control of montmorillonite clay nanosheets (MTM) within a polymer matrix has previously been performed two dimensionally with LBL assembly,^[39, 41] alternative depositions of polyvinyl alcohol (PVA), and MTM with intermediate rinse water were used to grow the layered nanocomposite within the void space of the CCT as a proof of concept. Scanning electron microscopy (SEM) was used to confirm the presence of the 300 bilayers of nanocomposite on the complex 3D substrate (**Figure 5.4C**). While the surfaces of ICC structures have been functionalized by LBL assembly post-production^[247, 249] and LBL has been used to introduce precursor materials or surface coatings into the voids of CCT,^[250, 251] to our knowledge, the highly organized and controlled bulk structure of LBL materials have yet to be employed to produce macro-scale structures with the controlled ICC micro-scale architecture.

Upon removal of the polystyrene CCT with tetrahydrofuran, an intact macro-scale structure with clear micro-scale pore definition and interconnectivity is achieved. While suspended in ethanol, optical and confocal microscopy was used to view the micro-scale architecture and the hierarchical organization of the LBL-assembled nanocomposite (**Figure 5.5A,B**). The combination of ICC and LBL assembly provides the systematic assembly of nanomaterials over several discrete length scales. The technique offers a multi-scale structure with designed pore size, interconnectivity and organization, wall thickness, and nanoparticle dispersion in the bulk. Controlled spatial arrangement of nanoparticles within the interstitial voids of the CCT and corresponding structure of the ICC is demonstrated for the first time as well as the advancement of freestanding LBL assembled organic-inorganic

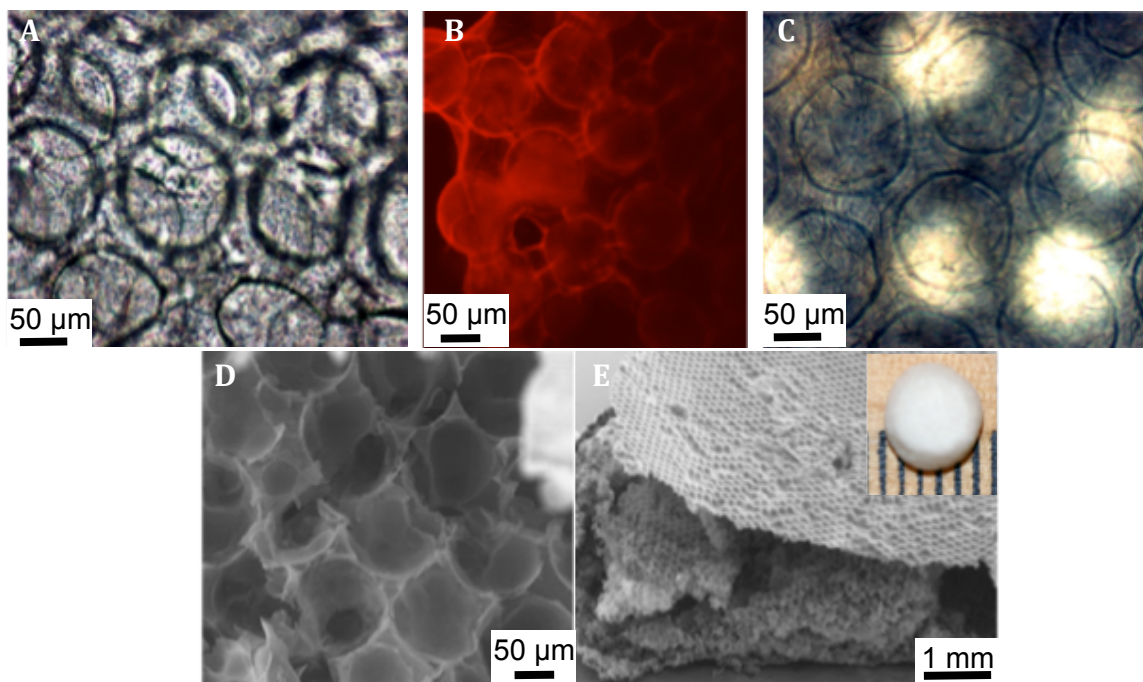


Figure 5.5 A) Optical and B) confocal microscopy images of the microscale architecture of the LBL clay nanocomposite material suspended in ethanol after dissolution of the CCT. C) Optical images of the microstructure after dried in air and D,E) SEM images of the freestanding freeze-dried LBL clay nanocomposite structure with an inset showing the macroscale size and shape before cutting in half (tick marks are 1mm).

hybrid nanocomposites to a reproducible 3D macroscale geometry with microscale architecture and the potential to be easily modeled *in silico*.

While 2D LBL films are quite flexible and not very rigid, the interconnected 3D geometry of the ICC structure provides the support needed to allow the structure to exist three-dimensionally with very little material usage. While beneficial for filling the CCT, the combination of the wall flexibility, presence of microscale voids/channels, and hydrophilicity result in structural collapse during simple air drying (**Figure 5.5C**). This problem was resolved with freeze-drying to create a self-supporting structure when the strong capillary forces present within the structure

during drying were overcome (**Figure 5.D, E**). The 3D controlled pore distribution, size uniformity and interconnectivity on the microscale are preserved in the dried sample composed of 300 bilayers of PVA and MTM. It is important to note in the case of fairly large clay sheets, the top of the structure becomes completely filled in at some point and prevents further infiltration of the CCT. Obstruction of the smaller channels connecting the interstitial voids during assembly leads to incomplete filling of the voids and insufficient penetration throughout all parts of the mold. The technique is limited by mass transport during the assembly of nanoplates and polymers on the complex template. The use of clay nanoplates presents advantages in respect to mechanical properties,^[252] catalysis, and drug delivery,^[253] however we expect by taking advantage of the LBL assembly of smaller nanoparticles the mass transport limitation could be overcome to some extent.

5.5 Conclusion

The fabrication technique presented allows for complex materials with well-controlled architectures on the macroscale and microscale to be created and integrated with nanoscale organization and surface functionalization. Besides the technological promise of such hierarchically organized structures, the fabrication technique presented allows for fundamental study of structure-property relations and the delivery of macroscale nanocomposites by design. Repeatable, controlled spatial arrangement of nanophase materials provides a strategy for tailoring the mechanical, thermal, optical and electrical properties to achieve specific performances. Additionally the wide variety of materials capable of being assembled

using LBL assembly allows for an extensive range of chemical compositions and material properties to be employed.

The future of 3D LBL for the development of macroscale nanocomposites with microscale architectures for advanced material applications will be dependent on the optimization of the automated fabrication device to provide the fluid mechanics and mass transport conditions for enhanced filling of the CCT, which is suspected to enhance the mechanical properties of the resulting structure, as will be required for many applications.

5.6 Experimental

5.6.1 Calcium Phosphate Nanoparticle Synthesis

Calcium phosphate nanoparticles (CP NP) were synthesized from the aqueous precipitation of calcium nitrate and phosphoric acid in the presence of 2-carboxyethylphosphonic acid (CEPA). A 2.89mmol calcium nitrate tetrahydrate (Sigma) and 6.75mmol 2-carboxyethylphosphonic acid (CEPA, Sigma) solution was adjusted to pH of 7 with ammonium hydroxide (Aldrich) and filtered with a 0.22micron filter. Meanwhile, phosphoric acid (Aldrich) at a concentration of 1.1mmol was also adjusted the same pH and filtered. The phosphoric acid was then added drop-wise over 30 minutes to the Ca/CEPA solution while stirring in a 4:3 Ca:P molar ratio. The mixture was heated to 60°C in an oil bath and allowed to age for 10 days.

The average diameter of the NPs was accessed with transmission electron microscopy (TEM, JEOL 3011) where spectral analysis was also performed with

EDAX's retractable-TEM detector and acquisition software. Samples were prepared by placing one drop on carbon coated copper grids and air-drying. The average height was determined with section analysis by atomic force microscopy (AFM, multimode scanning probe microscope with Nanoscope IIIa controller) in tapping mode with ultra sharp silicon cantilevers (NSC16/Cr-Au/50). X-ray diffraction (XRD, Rigaku Double Crystal) was applied for additional compositional characterization. Samples were freeze-dried to prevent structural change with heating. The zeta-potential of the particles was determined by dynamic light scattering (DLS, Malvern Zetasizer Nanoseries) on samples diluted ten times.

5.6.2 Fabrication of Synthetic Bone Material

In a typical LBL cycle, either glass slides or silicon wafers were cleaned by piranha solution for 24 hours were immersed in 1wt% Poly(diallyldimethylammonium chloride) (PDDA, high molecular weight, Aldrich) for five minutes, rinsed with deionized water, and then dried with compressed air. Subsequently, these slides were dipped into the CPNP solution for five minutes followed by rinsing and drying. The growth of the bilayer film was monitored with a J. A. Woolham Co. VASE spectroscopic ellipsometer. Film thickness was extracted by fitting to a Cauchy model. Scanning electron microscopy (SEM, FEI Nova NanoLab) was used to observe the uniformity of the film. A 100 bilayer film was made using a robotic NanoStrata (Tallahassee, FL) LBL deposition system onto glass slides. The mechanical properties of the coatings was assessed by Hysitron (Minneapolis, MN) nanoindenter for Y_c and H and the inorganic contents, X_{in} , was be evaluated by thermogravimetric analysis (X Pyris).

5.6.3 Cell Culture Studies

Using the methods above, one square centimeter glass slides were coated with either only one layer of PDDA (control) or (PDDA/CPNP)_{5.5} where the topmost layer of the test films was composed of PDDA. All samples were sterilized by soaking overnight in ethanol followed by exposure to ultraviolet light for 30 min. The samples were then rinsed with phosphate buffer solution (PBS) and placed in 24-well plates. A media solution of in 45% Ham's F12 medium, 45% Dulbecco's modified Eagle medium and 10% fetal bovine serum supplemented with 1% geneticin was used to rinse the samples. Each film was seeded with 30k human fetal osteoblasts (hFOB) from cell line 1.19 (CRL-11372 ATCC) and incubated at 37°C and 5% carbon dioxide. After the cells were allowed to attach for 30 minutes 1mL of media was added. The media was changed every day and samples were removed for analysis on days 2,4,6, and 8.

To visualize the attachment and spreading of the cells, samples were placed into clean well plates and fixed with 500µL of 4% formaldehyde for 10 minutes at room temperature. The films were then rinsed twice with PBS and were permeablized with 0.1% Triton X-100(500µL) for 5 min, rinsed twice more with PBS and incubated in rhodamine phalloidin for 30 min before visualization with a Leica SP2 confocal laser scanning microscope.

To investigate how the film impacted the cells ability to produce bone material the amount of osteocalcin, a protein produced by osteoblasts during bone production was detected and compared to the amount of double stranded DNA (dsDNA), which directly related to the number of cells present. Four of the test and

control samples were removing from incubation every other day and 1mL of media was removed from each well and kept at -70°C. The films were moved to clean well plates and soaked in trypsin for 10 min at 37°C to detached the cells from the film. The cells were centrifuged for 5 min at 900rpm, redispersed in PBS and centrifuged again. The cells were then sonicated in 500 µL of passive lysis buffer and stored at -70°C. After all samples were gathered the samples were thawed and centrifuged for 10 min at 10,000rpm. For ds DNA analysis 50µL of the supernatant was used to evaluate dsDNA following the Invitrogen protocol.^[254] For the osteocalcin assay, 25 µL of the previously collected media were analyzed separately with an intact human osteocalcin enzyme immunoassay kit (Biomedical Technologies, Inc, Stoughton, MA). Briefly, each aliquot was combined with 100 µL of anti-Hu OST conjugate into the provided wells and incubated for 2 hours at room temperature on a horizontal shaker set at 700 rpm. The wells were then washed three times and 100 µL of chromogenic solution and incubated for 30min at room temperature on the shaker. 200 µL of the stop solution was then added and the absorbance at 450 and 490nm was detected at a Synergy 2 Multi-Detection Microplate Reader (Biotek, Winooski, VT).

5.6.4 Colloidal Crystal Template Synthesis

Monodispersed polystyrene (PS) spheres with a diameter of $100 \pm 1.5\mu\text{m}$ were purchased from Duke Scientific. Based on the procedure previously reported,^[247] two drops of an aqueous suspension of highly monodispersed polystyrene spheres (3×10^4 particles per mL) were settled into a mold through a glass Pasteur pipette every 15 minutes. A 0.5mL plastic centrifuge tube mold was

placed into an ultrasonic bath (VWR) to aid the formation of a uniform, close-packed structure. After the mold was filled to the desired level, excess water was removed and the structure was dried at 60°C over night. The close-packed uniform spheres were then interconnected through annealing at 120°C for four hours to provide a single colloidal crystal template (CCT) with a diameter of 6mm and height ranging from 1-2mm.

5.6.5 Three Dimensional Nanocomposite Assembly

Poly(vinyl alcohol) (PVA; MW, 70,000 to ~ 100,000), Rhodamine, tetrahydrofuran (THF), and 95% ethanol were purchased from Sigma Aldrich. PVA was dissolved in hot deionized water at 0.25wt%. Clay nanosheets (average 1nm thick and 70-150nm in diameter) from Southern Clay Products were dispersed in deionized water at 0.25wt%.

LBL assembly was used to sequentially build up a PVA and clay nanosheet composites on the CCT surface. The PVA and clay nanosheet solutions were sequentially delivered to the CCT 5mL at a time, with 25mL of deionized rinse water in between. The four-step sequence was performed once for each bilayer desired up to 300 bilayers. In this case, hydrogen bonding between the -OH group and clay nanosheet surface was used to enable the LBL assembly of the components.^[39] An automatic 3D LBL assembly machine was developed and used to sequentially deliver and rinse each layer of material deposition. The machine employs a series of solenoid valves operated by a Texas Instrument data acquisition board and toggled with a labVIEW (National Instruments) program to allow for delivery of polymer, nanosheets and rinse water based on gravity (Figure 1A). The material is delivered

through nozzles to a funnel that leads to silicon tubing where the CCT is securely suspended. A peristaltic pump aids in providing the suction necessary to deliver each aliquot throughout the porous substrate, thoroughly remove the excess solution and provide adequate rinsing before the complimentary solution is applied.

The LBL coated CCT was dehydrated in 95% ethanol overnight before being transferred to THF for 3 days to selectively dissolve the PS CCT and produce a free standing LBL structure. The solvent was replaced as many times as necessary to remove the PS. THF was then replaced by ethanol for the purposes of characterization.

SEM images were taken with an FEI Nova Nanolab and an FEI Quanta 200. Prior to imaging, the CCT and LBL coated CCT were coated with gold for 90 seconds with a Denton Vacuum Desk 2 Model sputter coater. The freestanding LBL structure was dehydrated in 95% ethanol and freeze-dried overnight with a Labconco FreeZone before coating with gold. A razor blade was used to provide access to the internal architecture. Confocal images were taken with a Leica SP2 confocal microscope. Prior to imaging, the specimens were soaked overnight in a 1wt% rhodamine in ethanol solution, allowing the rhodamine to penetrate and embed within the LBL film. LBL films still attached to CCTs were rinsed with ethanol and imaged dry. Light microscopy images of both dry and submerged specimens were obtained with a Nikon Eclipse TS100 inverted microscope.

The Material in this Chapter has been adapted with minor modifications from the following peer-reviewed, published article:

Andres, C. M., Fox, M.L. & Kotov, N. A. Traversing Material Scales: Macroscale LBL-Assembled Nanocomposites with Microscale Inverted Colloidal Crystal Architecture. *Chemistry of Materials* 24, 9-11, (2012).

CHAPTER IV

Conclusion

6.1 Improvements to LBL Processing for Broad Impact Use

The realization of the incredible potential of nanomaterials will only be realized with the development of material processing techniques that allow for exploitation of their nanoscale material properties. In general, current material processing methods are not suitable for sustainable nanomanufacturing as they are limited in their ability to process a diverse range of building blocks across multiple length scales and dimensions.^[15] Material processing techniques capable of providing multiscale and multi-dimensional control to an extensive range of materials in a sustainable fashion is needed for the realization of widespread applications of nanomaterials in next-generation materials and devices.^[30] Layer by layer (LBL) assembly has been very successful at fabricating nanocomposites that transfer a significant amount of the nanoscale properties to macroscale materials through nanoscale control over structure.^[39, 40, 42-44] The technique is applicable to a wide variety of material building blocks and is performed in a relatively sustainable manner.^[34,44,46-53] The traditional dip-coating approach of LBL however, limits the incorporation of these materials into advanced functional devices, First, while

providing structural control over thickness in one direction on the nanoscale,^[46] the rinsing steps limit the ability to selectively pattern the materials. Second, a significant amount of water is used during the rinsing steps, and it can be fairly time consuming compared to traditional material processing approaches. Throughout the scope of this thesis I have provided several improvements to the prospect of LBL as a broad impact material processing technique through the introduction of controllable multiscale and multi-dimensional architectures to the traditionally planar nanocomposites. To as much as possible, the introduction of advanced structure has been performed with processing techniques that allow for the versatility and sustainability of LBL to be maintained or improved upon.

The impressive properties of LBL nanocomposites will only evolve into actual functional devices if controlled spatial arrangement of the materials can be achieved, Advanced structural control was introduced into LBL assembled nanocomposites with the applications of inkjet printing, self-folding mechanisms and template-based 3D assembly. In all cases the nanoscale structural control in the z-direction was maintained providing opportunities for gradient stratified structures and controlled surface functionality. Inkjet printing of LBL assembled composites^[166] allows for variable nanoparticle coverage for a much-improved degree of control over the multilayer structure while also providing microscale X-Y patterning for the realization of unique 2D patterns. As compared to alternative approaches for multilayer printing where the thickness of individual strata is seldom smaller than 100 μm ,^[130, 133-135] inkjet LBL allows for stratified multilayered structured to be achieved with nanoscale accuracy. Such 2D patterning is applied to

controllably transform 2D LBL nanocomposites into 3D mechanically responsive material with the deposition of stimuli-responsive LBL materials. Nanocomposite architectures with permanent 3D structure were realized through LBL deposition onto 3D templates and subsequent template removal. Beginning with simple lithographically patterned substrates,^[168] the approach was advanced to macroscale structures that had controllable nano-, micro- and macroscale features,^[167] a significant achievement for the traditionally thin film processing technique.

Within this document several applications of LBL nanocomposites have been suggested including paper-based electronics, neural implants, soft robotics, high-throughput microcontainers, and tissue engineering scaffolds, all of which will require a unique combination of material building blocks and substrates. Throughout the development of the processing techniques listed, strict attention was paid toward developing methodologies that maintain or expand upon the versatile nature of LBL assembly. The vast range of materials that can be deposited with the patterning methods presented is currently unavailable with other patterning techniques such as traditional lithography or printing of conventional materials.^[43, 91-95] In addition, substrates such as paper, which serve as renewable materials readily available and inherently biodegradable or substrates used in traditional microfabrication techniques can be incorporated with inkjet deposition. With all patterning approaches investigated, none rely on specific chemistries such as photochemistry that would inherently limit the selection of materials demonstrated in traditional LBL to be patterned in such a manner.

Finally, reducing the time and water demands of the LBL deposition process is an important step for the realization of commercial applications. The main contributors to long production times in LBL are the depositions steps that rely on the mass transport of the macromolecular species to the surface and the intermittent rinsing steps between each deposition. In the case of inkjet LBL the majority of rinsing steps and any additional steps needed for patterning were eliminated simultaneously for a significant decrease in production time when considering patterned surfaces of relatively small-scale.^[166] For 3D substrates, the creation of an accelerated deposition machine allowed for a decrease in the time for sufficient mass transport to occur, while also decreasing the amount of rinse water necessary by creating a more efficient rinsing strategy.^[167]

6.2 Future Direction

While significant improvements have been made towards the material processing of nanocomposites for the introduction of novel material property combinations into advanced devices, several limitations still exist for large-scale implementation. Inkjet printing offers a continuously additive fabrication technique with simple introduction of multiple computer-generated patterns, however traditional lithography and nanoimprinting can provide smaller feature sizes. Disparately, the multiscale structural control of template-based LBL for the fabrication of 3D architectures provides greater control over feature size than that of current 3D printing approaches. Technically, inkjet LBL could be used to create

3D structures with nanoscale control over thickness, however the production time makes this processing approach infeasible for even a relatively thin 3D structure of several mm. Inkjet deposition of LBL materials is most likely only applicable for the strategic use of stimuli-responsive materials for the generation of truly 3D structures. Novel strategies to decrease the feature size of additive patterning techniques, while simultaneously accelerating the production speed will provide the necessary processing conditions for the realization of broad impact nanocomposite architectures.

In the meantime, the techniques presented within provide multi-dimensional and multiscale control of nanocomposites unavailable by other means. Such levels of control allow for the in depth investigation of structure-property relationships. In some cases theoretical models exist without sufficient approaches to produce the described structures. Here such structures could be fabricated in order to validate theoretical predictions. In other cases, such as the mechanical motion of natural materials where several different building blocks are arranged into hierarchical structures, it is not always clear which structural and chemical aspects are responsible for functionality, or in some cases restricting functionality. The ability to finely tune compositional and structural features for the realization of such relationships will allow for a deeper understanding of how such material systems can be mimicked, optimized or overcome.

BIBLIOGRAPHY

1. *MIT 150 Exhibition*. Feb. 13, 2013]; Available from: <http://museum.mit.edu/150/123>.
2. *Intel 22nm 3-D Tri-Gate Transistor Technology*. 2011; Available from: <http://newsroom.intel.com/docs/DOC-2032>.
3. Ritchie, R.O., *The conflicts between strength and toughness*. *Nature Materials*, 2011. **10**(11): p. 817-822.
4. Lilley, S., *Men, machines and history; a short history of tools and machines in relation to social progress*. Past and present, studies in the history of civilization, v. 71948, London: Cobbett Press. 240 p.
5. Semaw, S., et al., *2.5-million-year-old stone tools from Gona, Ethiopia*. *Nature*, 1997. **385**(6614): p. 333-336.
6. Lubbock, J., *Pre-historic times, as illustrated by ancient remains, and the manners and customs of modern savages* 1865, London Edinburgh: Williams and Norgate. xxiii, [1], 512 p.
7. Cahn, R.W., *The coming of materials science*. Pergamon materials series ;v. 52001, Amsterdam: New York : Pergamon. xvii, 568 p.
8. Ferry, J.D., *Viscoelastic properties of polymers* 1980, New York: Wiley. xxiv, 641 p.
9. Meikle, J.L., *American plastic: a cultural history* 1995, New Brunswick, N.J.: Rutgers University Press. xiv, 403 p.
10. Pagliaro, M. and I. Wiley online, *Nano-age how nanotechnology changes our future* 2010, Weinheim: Wiley-VCH.
11. Ozin, G.A., A.C. Arsenault, and C. Royal Society of, *Nanochemistry: a chemistry approach to nanomaterials* 2005, Cambridge, UK: Royal Society of Chemistry. xl, 628 p.
12. Iijima, S. and T. Ichihashi, *Single-Shell Carbon Nanotubes of 1-nm Diameter*. *Nature*, 1993. **363**(6430): p. 603-605.
13. O'Connell, M., *Carbon nanotubes: properties and applications* 2006, Boca Raton, FL: CRC Taylor & Francis. 319 p.
14. Roco, M.C., et al., *Nanotechnology Research Directions for Societal Needs in 2020 Retrospective and Outlook*. Science Policy Reports ;12011, Dordrecht: WTEC.
15. *National Nanotechnology Initiative Strategic Plan, 2011*: <http://www.nano.gov>.

16. Levinson, H.J. and E. Society of Photo-optical Instrumentation, *Principles of lithography*. Lithography2010, Bellingham, Wash.: SPIE Press. xiii, 494 p.
17. Leong, T.G., A.M. Zarafshar, and D.H. Gracias, *Three-Dimensional Fabrication at Small Size Scales*. Small, 2010. **6**(7): p. 792-806.
18. Sengul, H., T.L. Theis, and S. Ghosh, *Toward sustainable nanoproducts: An overview of nanomanufacturing methods*. Journal of Industrial Ecology, 2008. **12**(3): p. 329-359.
19. Weiner, S. and H.D. Wagner, *The material bone: Structure mechanical function relations*. Annual Review of Materials Science, 1998. **28**: p. 271-298.
20. Sayle, T.X.T., P.E. Ngoepe, and D.C. Sayle, *Simulating Mechanical Deformation in Nanomaterials with Application for Energy Storage in Nanoporous Architectures*. ACS Nano, 2009. **3**(10): p. 3308-3314.
21. Lakes, R., *Foam Structures with a Negative Poisson's Ratio*. Science, 1987. **235**(4792): p. 1038-1040.
22. Sigmund, O. and S. Torquato, *Design of materials with extreme thermal expansion using a three-phase topology optimization method*. Journal of the Mechanics and Physics of Solids, 1997. **45**(6): p. 1037-1067.
23. Hollister, S.J., *Porous scaffold design for tissue engineering*. Nature Materials, 2005. **4**(7): p. 518-524.
24. Philippi, P.C. and H.A. Souza, *Modeling Moisture Distribution and Isothermal Transfer in Heterogeneous Porous Material*. International Journal of Multiphase Flow, 1995. **21**(4): p. 667-691.
25. Vrettos, N.A., H. Imakoma, and M. Okazaki, *Transport properties of porous media from the microgeometry of a three-dimensional voronoi network*. Chemical Engineering and Processing, 1989. **26**(3): p. 237-246.
26. Campbell, I., D. Bourell, and I. Gibson, *Additive manufacturing: rapid prototyping comes of age*. Rapid Prototyping Journal, 2012. **18**(4): p. 255-258.
27. Hon, K.K.B., L. Li, and I.M. Hutchings, *Direct writing technology-Advances and developments*. Cirp Annals-Manufacturing Technology, 2008. **57**(2): p. 601-620.
28. *Ensuring American Leadership in Advanced Manufacturing*, 2011.
29. *Advanced Manufacturing Portal*. Feb. 13, 2013]; Available from: <http://www.manufacturing.gov/>.
30. *Capturing Domestic Competitive Advantage in Advanced Manufacturing*, 2012.
31. Merhari, L., *Hybrid Nanocomposites for Nanotechnology Electronic, Optical, Magnetic and Biomedical Applications*2009, Boston, MA: Springer-Verlag US.
32. Kojima, Y., et al., *Mechanical Properties of Nylon 6 Clay* Journal of Materials Research, 1993. **8**(5): p. 1185-1189.
33. Tjong, S.C., *Structural and mechanical properties of polymer nanocomposites*. Materials Science & Engineering R-Reports, 2006. **53**(3-4): p. 73-197.
34. LeBaron, P.C., Z. Wang, and T.J. Pinnavaia, *Polymer-layered silicate nanocomposites: an overview*. Applied Clay Science, 1999. **15**(1-2): p. 11-29.
35. Decher, G., *Fuzzy nanoassemblies: Toward layered polymeric multicomposites*. Science, 1997. **277**(5330): p. 1232-1237.

36. Schlenoff, J.B. and S.T. Dubas, *Mechanism of polyelectrolyte multilayer growth: Charge overcompensation and distribution*. *Macromolecules*, 2001. **34**(3): p. 592-598.
37. Sukhorukov, G.B., et al., *Layer-by-layer self assembly of polyelectrolytes on colloidal particles*. *Colloids and Surfaces a-Physicochemical and Engineering Aspects*, 1998. **137**(1-3): p. 253-266.
38. Ferreira, M. and M.F. Rubner, *Molecular-Level Processing of Conjugated Polymers. 1. Layer-by-Layer Manipulation of Conjugated Polyions*. *Macromolecules*, 1995. **28**(21): p. 7107-7114.
39. Podsiadlo, P., et al., *Ultrastrong and stiff layered polymer nanocomposites*. *Science*, 2007. **318**(5847): p. 80-83.
40. Tang, Z.Y., et al., *Biomedical applications of layer-by-layer assembly: From biomimetics to tissue engineering*. *Advanced Materials*, 2006. **18**(24): p. 3203-3224.
41. Tang, Z., *Nanostructured artificial nacre*. *Nature materials*, 2003. **2**(6): p. 413-418.
42. Mamedov, A.A., et al., *Molecular design of strong single-wall carbon nanotube/polyelectrolyte multilayer composites*. *Nature Materials*, 2002. **1**(3): p. 190-194.
43. Hammond, P.T., *Form and function in multilayer assembly: New applications at the nanoscale*. *Advanced Materials*, 2004. **16**(15): p. 1271-1293.
44. Kotov, N.A., *Layer-by-Layer Assembly of Nanoparticles and Nanocolloids: Intermolecular Interactions, Structure and Materials Perspectives*, in *Multilayer Thin Films 2003*, Wiley-VCH Verlag GmbH & Co. KGaA. p. 207-243.
45. Decher, G. and J.D. Hong. *Build up of ultrathin multilayer films by a self-assembly process. 1. Consecutive adsorption of anionic and cationic bipolar amphiphiles on charged surfaces*. in *3rd European Conf on Organized Organic Thin Films (Ecof 90)*. 1990. Mainz, Fed Rep Ger: Huthig & Wepf Verlag.
46. Ostrander, J.W., A.A. Mamedov, and N.A. Kotov, *Two modes of linear layer-by-layer growth of nanoparticle-polyelectrolyte multilayers and different interactions in the layer-by-layer deposition*. *Journal of the American Chemical Society*, 2001. **123**(6): p. 1101-1110.
47. Mamedov, A.A. and N.A. Kotov, *Free-Standing Layer-by-Layer Assembled Films of Magnetite Nanoparticles*. *Langmuir*, 2000. **16**(13): p. 5530-5533.
48. Chluba, J., et al., *Peptide hormone covalently bound to polyelectrolytes and embedded into multilayer architectures conserving full biological activity*. *Biomacromolecules*, 2001. **2**(3): p. 800-805.
49. Stockton, W.B. and M.F. Rubner. *Molecular layer processing of polyaniline via the use of hydrogen bonding interactions*. in *Symposium on Solid State Ionics IV, at the 1994 MRS Fall Meeting*. 1994. Boston, Ma: Materials Research Soc.
50. Brynda, E. and M. Houska, *Multiple alternating molecular layers of albumin and heparin on solid surfaces*. *Journal of Colloid and Interface Science*, 1996. **183**(1): p. 18-25.
51. Sun, J.Q., et al., *Fabrication of a covalently attached multilayer via photolysis of layer-by-layer self-assembled films containing diazo-resins*. *Chemical Communications*, 1998(17): p. 1853-1854.

52. Thierry, B., et al., *Bioactive coatings of endovascular stents based on polyelectrolyte multilayers*. *Biomacromolecules*, 2003. **4**(6): p. 1554-1571.
53. Sukhorukov, G.B., et al., *pH-controlled macromolecule encapsulation in and release from polyelectrolyte multilayer nanocapsules*. *Macromolecular Rapid Communications*, 2001. **22**(1): p. 44-46.
54. Kotov, N.A., *Ordered layered assemblies of nanoparticles*. *Mrs Bulletin*, 2001. **26**(12): p. 992-997.
55. Mamedov, A.A., et al., *Nanorainbows: Graded semiconductor films from quantum dots*. *Journal of the American Chemical Society*, 2001. **123**(31): p. 7738-7739.
56. Mamedov, A., et al., *Stratified assemblies of magnetite nanoparticles and montmorillonite prepared by the layer-by-layer assembly*. *Langmuir*, 2000. **16**(8): p. 3941-3949.
57. Zhang, J., L.S. Chua, and D.M. Lynn, *Multilayered Thin Films that Sustain the Release of Functional DNA under Physiological Conditions*. *Langmuir*, 2004. **20**(19): p. 8015-8021.
58. Chung, A.J. and M.F. Rubner, *Methods of Loading and Releasing Low Molecular Weight Cationic Molecules in Weak Polyelectrolyte Multilayer Films*. *Langmuir*, 2002. **18**(4): p. 1176-1183.
59. Wood, K.C., et al., *Electroactive Controlled Release Thin Films*. *Proceedings of the National Academy of Sciences of the United States of America*, 2008. **105**(7): p. 2280-2285.
60. Zhang, W., S.S. Liao, and F.Z. Cui, *Hierarchical self-assembly of nano-fibrils in mineralized collagen*. *Chemistry of Materials*, 2003. **15**(16): p. 3221-3226.
61. Granqvist, C.G., *Transparent conductors as solar energy materials: A panoramic review*. *Solar energy materials and solar cells*, 2007. **91**(17): p. 1529-1598.
62. Meyer, W.H., *Polymer Electrolytes for Lithium-Ion Batteries*. *Advanced materials (Weinheim)*, 1998. **10**(6): p. 439-448.
63. Shim, B.S., *Multiparameter Structural Optimization of Single-Walled Carbon Nanotube Composites: Toward Record Strength, Stiffness, and Toughness*. *ACS Nano*, 2009. **3**(7): p. 1711-1722.
64. Zhu, J., *Transparent Conductors from Carbon Nanotubes LBL-Assembled with Polymer Dopant with π - π Electron Transfer*. *Journal of the American Chemical Society*, 2011. **133**(19): p. 7450-7460.
65. Kim, Y., Zhu, Z., Di Prima, M., Su, X., Kim, J., Yoo, S., Yeom, B., Uher, C., Kotov, N. A., *Stretchable Nanoparticle Conductors with Self-Organized Conductive Pathways*. Manuscript Submitted, 2013.
66. Zhang, H.N., et al., *Layered Nanocomposites from Gold Nanoparticles for Neural Prosthetic Devices*. *Nano Letters*, 2012. **12**(7): p. 3391-3398.
67. Kotov, N.A., et al., *Nanomaterials for Neural Interfaces*. *Advanced Materials*, 2009. **21**(40): p. 3970-4004.
68. Moritz, C.T., *Direct control of paralysed muscles by cortical neurons*. *Nature (London)*, 2008. **456**(7222): p. 639-642.

69. Nijboer, F., *A P300-based brain-computer interface for people with amyotrophic lateral sclerosis*. *Clinical neurophysiology*, 2008. **119**(8): p. 1909-1916.
70. Keohan, F., *Fabrication and evaluation of conductive elastomer electrodes for neural stimulation*. *Journal of biomaterials science. Polymer ed.*, 2007. **18**(8): p. 1057-1073.
71. Biran, R., *Neuronal cell loss accompanies the brain tissue response to chronically implanted silicon microelectrode arrays*. *Experimental neurology*, 2005. **195**(1): p. 115-126.
72. Ariga, K., et al., *Alternately assembled ultrathin film of silica nanoparticles and linear polycations*. *Chemistry Letters*, 1997(2): p. 125-126.
73. Kotov, N.A., I. Dekany, and J.H. Fendler, *Layer-by-Layer Self-Assembly of Polyelectrolyte-Semiconductor Nanoparticle Composite Films*. *Journal of Physical Chemistry*, 1995. **99**(35): p. 13065-13069.
74. Kotov, N.A., *Layer-by-layer self-assembly: The contribution of hydrophobic interactions*. *Nanostructured Materials*, 1999. **12**(5-8): p. 789-796.
75. Bucur, C.B., Z. Sui, and J.B. Schlenoff, *Ideal mixing in polyelectrolyte complexes and multilayers: Entropy driven assembly*. *Journal of the American Chemical Society*, 2006. **128**(42): p. 13690-13691.
76. Jomaa, H.W. and J.B. Schlenoff, *Salt-induced polyelectrolyte interdiffusion in multilayered films: A neutron reflectivity study*. *Macromolecules*, 2005. **38**(20): p. 8473-8480.
77. Bharadwaj, S., R. Montazeri, and D.T. Haynie, *Direct determination of the thermodynamics of polyelectrolyte complexation and implications thereof for electrostatic layer-by-layer assembly of multilayer films*. *Langmuir*, 2006. **22**(14): p. 6093-6101.
78. Schlenoff, J.B., S.T. Dubas, and T. Farhat, *Sprayed polyelectrolyte multilayers*. *Langmuir*, 2000. **16**(26): p. 9968-9969.
79. Lee, S.S., et al., *Layer-by-layer deposited multilayer assemblies of ionene-type polyelectrolytes based on the spin-coating method*. *Macromolecules*, 2001. **34**(16): p. 5358-5360.
80. Cho, J., et al., *Fabrication of highly ordered multilayer films using a spin self-assembly method*. *Advanced Materials*, 2001. **13**(14): p. 1076-+.
81. Chiarelli, P.A., et al., *Controlled fabrication of polyelectrolyte multilayer thin films using spin-assembly*. *Advanced Materials*, 2001. **13**(15): p. 1167-+.
82. Merrill, M.H. and C.T. Sun, *Fast, simple and efficient assembly of nanolayered materials and devices*. *Nanotechnology*, 2009. **20**(7): p. 075606.
83. Shim, B.S., et al., *Nanostructured thin films made by diewetting method of layer-by-layer assembly*. *Nano Letters*, 2007. **7**(11): p. 3266-3273.
84. Galiote, N.A. and F. Huguenin, *Lithium ion diffusion into self-assembled films composed from WO₃ and polyallylamine*. *Journal of Physical Chemistry C*, 2007. **111**: p. 14911-14916.
85. DeLongchamp, D.M. and P.T. Hammond, *Fast ion conduction in layer-by-layer polymer films*. *Chemistry of Materials*, 2003. **15**(5): p. 1165-1173.

86. Limem, S., et al., *Multi-material inkjet printing of self-assembling and reacting coatings*. Journal of Macromolecular Science Part a-Pure and Applied Chemistry, 2009. **46**(12): p. 1205-1212.
87. Yang, S.Y. and M.F. Rubner, *Micropatterning of polymer thin films with pH-sensitive and cross-linkable hydrogen-bonded polyelectrolyte multilayers*. Journal of the American Chemical Society, 2002. **124**(10): p. 2100-2101.
88. Cheng, K., et al., *Ink-Jet Printing, Self-Assembled Polyelectrolytes, and Electroless Plating: Low Cost Fabrication of Circuits on a Flexible Substrate at Room Temperature*. Macromolecular Rapid Communications, 2005. **26**(4): p. 247-264.
89. Guo, T.-F., et al., *Vertically Integrated Electronic Circuits via a Combination of Self-Assembled Polyelectrolytes, Ink-Jet Printing, and Electroless Metal Plating Processes*. Langmuir, 2002. **18**(21): p. 8142-8147.
90. Wang, T.C., et al., *Selective Electroless Nickel Plating on Polyelectrolyte Multilayer Platforms*. Langmuir, 2001. **17**(21): p. 6610-6615.
91. Tekin, E., P.J. Smith, and U.S. Schubert, *Inkjet printing as a deposition and patterning tool for polymers and inorganic particles*. Soft Matter, 2008. **4**(4): p. 703-713.
92. Simeone, F.C., C. Albonetti, and M. Cavallini, *Progress in Micro- and Nanopatterning via Electrochemical Lithography*. Journal of Physical Chemistry C, 2009. **113**(44): p. 18987-18994.
93. Roy, S., *Fabrication of micro- and nano-structured materials using mask-less processes*. Journal of Physics D-Applied Physics, 2007. **40**(22): p. R413-R426.
94. Nie, Z.H. and E. Kumacheva, *Patterning surfaces with functional polymers*. Nature Materials, 2008. **7**(4): p. 277-290.
95. Menard, E., et al., *Micro- and nanopatterning techniques for organic electronic and optoelectronic systems*. Chemical Reviews, 2007. **107**(4): p. 1117-1160.
96. Izquierdo, A., et al., *Dipping versus spraying: Exploring the deposition conditions for speeding up layer-by-layer assembly*. Langmuir, 2005. **21**(16): p. 7558-7567.
97. Jiang, C.Y., et al., *Freely suspended gold nanoparticle arrays*. Advanced Materials, 2005. **17**(13): p. 1669-+.
98. Jiang, C.Y., et al., *Freely suspended nanocomposite membranes as highly sensitive sensors*. Nature Materials, 2004. **3**(10): p. 721-728.
99. Jiang, C.Y., S. Markutsya, and V.V. Tsukruk, *Compliant, robust, and truly nanoscale free-standing multilayer films fabricated using spin-assisted layer-by-layer assembly*. Advanced Materials, 2004. **16**(2): p. 157-+.
100. Lu, C.H., et al., *Au nanoparticle-based multilayer ultrathin films with covalently linked nanostructures: Spraying layer-by-layer assembly and mechanical property characterization*. Chemistry of Materials, 2006. **18**(26): p. 6204-6210.
101. Turkevich, J., P.C. Stevenson, and J. Hillier, *A study of the nucleation and growth processes in the synthesis of colloidal gold*. Discussions of the Faraday Society, 1951(11): p. 55.
102. Enustun, B.V. and J. Turkevich, *Coagulation of colloidal gold*. Journal of the American Chemical Society, 1963. **85**(21): p. 3317.

103. Frens, G., *Controlled nucleation for regulation of particle size in monodisperse gold suspensions*. Nature-Physical Science, 1973. **241**(105): p. 20-22.
104. Deegan, R.D., et al., *Capillary flow as the cause of ring stains from dried liquid drops*. Nature, 1997. **389**(6653): p. 827-829.
105. Sommer, A.P. and N. Rozlosnik, *Formation of crystalline ring patterns on extremely hydrophobic supersmooth substrates: Extension of ring formation paradigms*. Crystal Growth & Design, 2005. **5**(2): p. 551-557.
106. Hu, H. and R.G. Larson, *Marangoni effect reverses coffee-ring depositions*. Journal of Physical Chemistry B, 2006. **110**(14): p. 7090-7094.
107. Kuang, M.X., et al., *Research Progress of High-precision Patterns by Directly Inkjet Printing*. Acta Chimica Sinica, 2012. **70**(18): p. 1889-1896.
108. Hammond, P.T. and G.M. Whitesides, *Formation of polymer microstructures by selective deposition of polyion multilayers using patterned self-assembled monolayers as a template*. Macromolecules, 1995. **28**(22): p. 7569-7571.
109. Jiang, X.P., et al., *Polymer-on-polymer stamping: Universal approaches to chemically patterned surfaces*. Langmuir, 2002. **18**(7): p. 2607-2615.
110. Jiang, X.P. and P.T. Hammond, *Selective deposition in layer-by-layer assembly: Functional graft copolymers as molecular templates*. Langmuir, 2000. **16**(22): p. 8501-8509.
111. Lee, S.W., et al., *Nanostructured polyelectrolyte multilayer organic thin films generated via parallel dip-pen nanolithography*. Advanced Materials, 2005. **17**(22): p. 2749-+.
112. Tulpar, A., et al., *Nanoscale patterning of ionic self-assembled multilayers*. Nanotechnology, 2009. **20**(15): p. 5.
113. Pallandre, A., et al., *Binary nanopatterned surfaces prepared from silane monolayers*. Nano Letters, 2004. **4**(2): p. 365-371.
114. Sun, J.Q., M.Y. Gao, and J. Feldmann, *Electric field directed layer-by-layer assembly of highly fluorescent CdTe nanoparticles*. Journal of Nanoscience and Nanotechnology, 2001. **1**(2): p. 133-136.
115. Jang, H., S. Kim, and K. Char, *Multilayer line micropatterning using convective self-assembly in microfluidic channels*. Langmuir, 2003. **19**(8): p. 3094-3097.
116. Maury, P., et al., *Patterning the molecular printboard: patterning cyclodextrin monolayers on silicon oxide using nanoimprint lithography and its application in 3D multilayer nanostructuring*. Nanotechnology, 2007. **18**(4): p. 9.
117. Hua, F., T.H. Cui, and Y. Lvov, *Lithographic approach to pattern self-assembled nanoparticle multilayers*. Langmuir, 2002. **18**(17): p. 6712-6715.
118. Cao, T.B., et al., *Micropatterns of protein and conducting polymer molecules fabricated by layer-by-layer self-assembly and photolithography techniques*. Langmuir, 2003. **19**(20): p. 8127-8129.
119. Shi, F., et al., *Layer-by-layer self-assembly of reactive polyelectrolytes for robust multilayer patterning*. Advanced Materials, 2002. **14**(11): p. 805-809.
120. Hua, F., Y. Lvov, and T.H. Cui, *Spatial patterning of colloidal nanoparticle-based thin film by a combinative technique of layer-by-layer self-assembly and lithography*. Journal of Nanoscience and Nanotechnology, 2002. **2**(3-4): p. 357-361.

121. Gao, C.Y., et al., *Irreversible compression of polyelectrolyte multilayers*. *Macromolecules*, 2004. **37**(24): p. 8836-8839.
122. Lu, Y.X., et al., *Room-temperature imprinting poly(acrylic acid)/poly(allylamine hydrochloride) multilayer films by using polymer molds*. *Langmuir*, 2007. **23**(6): p. 3254-3259.
123. Park, J. and P.T. Hammond, *Multilayer transfer printing for polyelectrolyte multilayer patterning: Direct transfer of layer-by-layer assembled micropatterned thin films*. *Advanced Materials*, 2004. **16**(6): p. 520-+.
124. Wang, L., et al., *Simple, Rapid, Sensitive, and Versatile SWNT- Paper Sensor for Environmental Toxin Detection Competitive with ELISA*. *Nano Letters*, 2009. **9**(12): p. 4147-4152.
125. Shim, B.S., et al., *Smart Electronic Yarns and Wearable Fabrics for Human Biomonitoring made by Carbon Nanotube Coating with Polyelectrolytes*. *Nano Letters*, 2008. **8**(12): p. 4151-4157.
126. Tobjork, D. and R. Osterbacka, *Paper Electronics*. *Advanced Materials*, 2011. **23**(17): p. 1935-1961.
127. Kordas, K., et al., *Inkjet printing of electrically conductive patterns of carbon nanotubes*. *Small*, 2006. **2**(8-9): p. 1021-1025.
128. Bogy, D.B. and F.E. Talke, *Experimental and Theoretical Study of Wave Propagation Phenomena in DDrop-on-Demand Ink Jet Devices*. *Ibm Journal of Research and Development*, 1984. **28**(3): p. 314-321.
129. ; Available from:
http://www.fujifilmusa.com/products/industrial_inkjet_printheads/depositi-on-products/dmp-2800/index.html.
130. Moon, J., et al., *Ink-jet printing of binders for ceramic components*. *Journal of the American Ceramic Society*, 2002. **85**(4): p. 755-762.
131. Wang, T.M., R. Patel, and B. Derby, *Manufacture of 3-dimensional objects by reactive inkjet printing*. *Soft Matter*, 2008. **4**(12): p. 2513-2518.
132. Wong, W.S., et al., *Amorphous silicon thin-film transistors and arrays fabricated by jet printing*. *Applied Physics Letters*, 2002. **80**(4): p. 610-612.
133. Kim, S.-S., et al., *Poly(lactide-co-glycolide)/hydroxyapatite composite scaffolds for bone tissue engineering*. *Biomaterials*, 2006. **27**(8): p. 1399-1409.
134. Sherwood, J.K., et al., *A three-dimensional osteochondral composite scaffold for articular cartilage repair*. *Biomaterials*, 2002. **23**(24): p. 4739-4751.
135. Giordano, R.A., et al., *Mechanical properties of dense polylactic acid structures fabricated by three dimensional printing*. *Journal of Biomaterials Science-Polymer Edition*, 1996. **8**(1): p. 63-75.
136. Li, C., E.T. Thostenson, and T.-W. Chou, *Sensors and actuators based on carbon nanotubes and their composites: A review*. *Composites Science and Technology*, 2008. **68**(6): p. 1227-1249.
137. Stuart, M.A.C., et al., *Emerging applications of stimuli-responsive polymer materials*. *Nature Materials*, 2010. **9**(2): p. 101-113.
138. Shenoy, V.B. and D.H. Gracias, *Self-folding thin-film materials: From nanopolyhedra to graphene origami*. *Mrs Bulletin*, 2012. **37**(9): p. 847-854.
139. Leng, J., et al., *Shape-memory polymers and their composites: Stimulus methods and applications*. *Progress in Materials Science*, 2011. **56**(7): p. 1077-1135.

140. Gibson, P., et al., *Humidity-dependent air permeability of textile materials*. Textile Research Journal, 1999. **69**(5): p. 311-317.
141. Menges, A. and S. Reichert, *Material Capacity: Embedded Responsiveness*. Architectural Design, 2012(216): p. 52-59.
142. Fernandes, R. and D.H. Gracias, *Self-folding polymeric containers for encapsulation and delivery of drugs*. Advanced Drug Delivery Reviews, 2012. **64**(14): p. 1579-1589.
143. Ilievski, F., et al., *Soft Robotics for Chemists*. Angewandte Chemie-International Edition, 2011. **50**(8): p. 1890-1895.
144. Vaia, R. and J. Baur, *Adaptive composites*. Science, 2008. **319**(5862): p. 420-421.
145. Dawson, J., J.F.V. Vincent, and A.M. Rocca, *How pine cones open*. Nature, 1997. **390**(6661): p. 668-668.
146. Harrington, M.J., et al., *Origami-like unfolding of hydro-actuated ice plant seed capsules*. Nature Communications, 2011. **2**.
147. Stamp, N.E., *EFFICACY OF EXPLOSIVE VS HYGROSCOPIC SEED DISPERSAL BY AN ANNUAL GRASSLAND SPECIES*. American Journal of Botany, 1989. **76**(4): p. 555-561.
148. Peart, M.H., *EXPERIMENTS ON THE BIOLOGICAL SIGNIFICANCE OF THE MORPHOLOGY OF SEED-DISPERSAL UNITS IN GRASSES*. Journal of Ecology, 1979. **67**(3): p. 843-863.
149. Elbaum, R., et al., *The role of wheat awns in the seed dispersal unit*. Science, 2007. **316**(5826): p. 884-886.
150. Reyssat, E. and L. Mahadevan, *Hygromorphs: from pine cones to biomimetic bilayers*. Journal of the Royal Society Interface, 2009. **6**(39): p. 951-957.
151. Timoshenko, S., *Analysis of bi-metal thermostats*. Journal of the Optical Society of America and Review of Scientific Instruments, 1925. **11**(3): p. 233-255.
152. Shim, T.S., et al., *Controlled Origami Folding of Hydrogel Bilayers with Sustained Reversibility for Robust Microcarriers*. Angewandte Chemie-International Edition, 2012. **51**(6): p. 1420-1423.
153. Luchnikov, V., O. Sydorenko, and M. Stamm, *Self-rolled polymer and composite polymer/metal micro- and nanotubes with patterned inner walls*. Advanced Materials, 2005. **17**(9): p. 1177-+.
154. Schild, H.G., *Poly (n-isopropylacrylamide) - Experiment, Theory and Application*. Progress in Polymer Science, 1992. **17**(2): p. 163-249.
155. Jager, E.W.H., O. Ingnas, and I. Lundstrom, *Microrobots for micrometer-size objects in aqueous media: Potential tools for single-cell manipulation*. Science, 2000. **288**(5475): p. 2335-2338.
156. Zhang, X.B., et al., *Optically- and Thermally-Responsive Programmable Materials Based on Carbon Nanotube-Hydrogel Polymer Composites*. Nano Letters, 2011. **11**(8): p. 3239-3244.
157. Tokarev, I. and S. Minko, *Stimuli-responsive hydrogel thin films*. Soft Matter, 2009. **5**(3): p. 511-524.
158. Minko, S., *Stimuli-responsive hydrogel thin films*. Soft Matter, 2009. **5**(3): p. 511-524.

159. Hu, Z.B., X.M. Zhang, and Y. Li, *SYNTHESIS AND APPLICATION OF MODULATED POLYMER GELS*. Science, 1995. **269**(5223): p. 525-527.
160. Ma, M.M., et al., *Bio-Inspired Polymer Composite Actuator and Generator Driven by Water Gradients*. Science, 2013. **339**(6116): p. 186-189.
161. Urban, M.W. and I. Wiley online, *Handbook of stimuli-responsive materials* 2011, Weinheim: Wiley-VCH. 1 online resource (xvii, 278 p.).
162. Sukhishvili, S.A., *Responsive polymer films and capsules via layer-by-layer assembly*. Current Opinion in Colloid & Interface Science, 2005. **10**(1-2): p. 37-44.
163. Shen, L.Y., et al., *Humidity Responsive Asymmetric Free-Standing Multilayered Film*. Langmuir, 2010. **26**(22): p. 16634-16637.
164. Ma, Y. and J.Q. Sun, *Humido- and Thermo-Responsive Free-Standing Films Mimicking the Petals of the Morning Glory Flower*. Chemistry of Materials, 2009. **21**(5): p. 898-902.
165. Ma, Y., et al., *Polyelectrolyte Multilayer Films for Building Energetic Walking Devices*. Angewandte Chemie-International Edition, 2011. **50**(28): p. 6254-6257.
166. Andres, C.M. and N.A. Kotov, *Inkjet Deposition of Layer-by-Layer Assembled Films*. Journal of the American Chemical Society, 2010. **132**(41): p. 14496-14502.
167. Andres, C.M., M.L. Fox, and N.A. Kotov, *Traversing Material Scales: Macroscale LBL-Assembled Nanocomposites with Microscale Inverted Colloidal Crystal Architecture*. Chemistry of Materials, 2012. **24**(1): p. 9-11.
168. Andres, C.M., et al., *Nanocomposite Microcontainers*. Advanced Materials, 2012. **24**(34): p. 4597-4600.
169. Zhu, J., et al., *Pseudonegative Thermal Expansion and the State of Water in Graphene Oxide Layered Assemblies*. ACS Nano, 2012. **6**(9): p. 8357-8365.
170. Kohler, R., et al., *Neutron Reflectometry Study of Swelling of Polyelectrolyte Multilayers in Water Vapors: Influence of Charge Density of the Polycation*. Langmuir, 2009. **25**(19): p. 11576-11585.
171. Hsieh, M.C., R.J. Farris, and T.J. McCarthy, *Mechanical properties of layer-by-layer-deposited polyelectrolyte assemblies*. Abstracts of Papers of the American Chemical Society, 1999. **218**: p. U620-U620.
172. Gao, C., et al., *Elasticity of hollow polyelectrolyte capsules prepared by the layer-by-layer technique*. European Physical Journal E, 2001. **5**(1): p. 21-27.
173. Tanaka, Y., J.P. Gong, and Y. Osada, *Novel hydrogels with excellent mechanical performance*. Progress in Polymer Science, 2005. **30**(1): p. 1-9.
174. De, S., C. Cramer, and M. Schonhoff, *Humidity Dependence of the Ionic Conductivity of Polyelectrolyte Complexes*. Macromolecules, 2011. **44**(22): p. 8936-8943.
175. Jin, W.Q., A. Toutianoush, and B. Tieke, *Size- and charge-selective transport of aromatic compounds across polyelectrolyte multilayer membranes*. Applied Surface Science, 2005. **246**(4): p. 444-450.
176. Liu, X.Y. and M.L. Bruening, *Size-selective transport of uncharged solutes through multilayer polyelectrolyte membranes*. Chemistry of Materials, 2004. **16**(2): p. 351-357.

177. Chavez, F.V. and M. Schonhoff, *Pore size distributions in polyelectrolyte multilayers determined by nuclear magnetic resonance cryoporometry*. Journal of Chemical Physics, 2007. **126**(10): p. 7.
178. Yu, H.H., et al., *Fiber optic humidity sensor based on self-assembled polyelectrolyte multilayers*. Journal of Wuhan University of Technology- Materials Science Edition, 2001. **16**(3): p. 65-69.
179. Su, P.G. and K.H. Cheng, *Self-assembly of polyelectrolytic multilayer thin films of polyelectrolytes on quartz crystal microbalance for detecting low humidity*. Sensors and Actuators B-Chemical, 2009. **142**(1): p. 123-129.
180. Ge, S., *Absorption, Desorption, and Transport of Water in Polymer Electrolyte Membranes for Fuel Cells*. Journal of the Electrochemical Society, 2005. **152**(6): p. A1149.
181. Tosto, S., *Water adsorption/desorption in proton-conducting ionomer membranes: The model case of sulfonated and silylated poly-ether-ether-ketone*. Solid state ionics, 2012. **209-210**: p. 9-14.
182. Kim, J., et al., *Designing Responsive Buckled Surfaces by Halftone Gel Lithography*. Science, 2012. **335**(6073): p. 1201-1205.
183. Nishino, T., *All-Cellulose Composite*. Macromolecules, 2004. **37**(20): p. 7683-7687.
184. Nogi, M., *Optically Transparent Nanofiber Paper*. Advanced materials (Weinheim), 2009. **21**(16): p. 1595-1598.
185. *Kevlar 49 Fibres: Thermal Expansion Coefficients from High Temperature X-Ray Data*, 2000. p. 331.
186. Randall, C.L., et al., *3D lithographically fabricated nanoliter containers for drug delivery*. Advanced Drug Delivery Reviews, 2007. **59**(15): p. 1547-1561.
187. Syms, R.R.A., et al., *Surface tension-powered self-assembly of micro structures - The state-of-the-art*. Journal of Microelectromechanical Systems, 2003. **12**(4): p. 387-417.
188. Leong, T., et al., *Spatially controlled chemistry using remotely guided nanoliter scale containers*. Journal of the American Chemical Society, 2006. **128**(35): p. 11336-11337.
189. Ionov, L., *Soft microorigami: self-folding polymer films*. Soft Matter, 2011. **7**(15): p. 6786-6791.
190. Fernandez, J.G. and A. Khademhosseini, *Micro-Masonry: Construction of 3D Structures by Microscale Self-Assembly*. Advanced Materials, 2010. **22**(23): p. 2538-2541.
191. Randall, C.L., et al., *Three-dimensional microwell arrays for cell culture*. Lab on a Chip, 2011. **11**(1): p. 127-131.
192. Kwon, J., et al., *SU-8-based immunoisolative microcontainer with nanoslots defined by nanoimprint lithography*. Journal of Vacuum Science & Technology B, 2009. **27**(6): p. 2795-2800.
193. Azam, A., et al., *Self-folding micropatterned polymeric containers*. Biomedical Microdevices. **13**(1): p. 51-58.
194. Wang, Y., A.S. Angelatos, and F. Caruso, *Template synthesis of nanostructured materials via layer-by-layer assembly*. Chemistry of Materials, 2008. **20**(3): p. 848-858.

195. Caruso, F., *Nanoengineering of particle surfaces*. Advanced Materials, 2001. **13**(1): p. 11-+.
196. Ariga, K., J.P. Hill, and Q.M. Ji, *Layer-by-layer assembly as a versatile bottom-up nanofabrication technique for exploratory research and realistic application*. Physical Chemistry Chemical Physics, 2007. **9**(19): p. 2319-2340.
197. Quinn, J.F., et al., *Next generation, sequentially assembled ultrathin films: beyond electrostatics*. Chemical Society Reviews, 2007. **36**(5): p. 707-718.
198. Peyratout, C.S. and L. Dahne, *Tailor-made polyelectrolyte microcapsules: From multilayers to smart containers*. Angewandte Chemie-International Edition, 2004. **43**(29): p. 3762-3783.
199. Zhang, X., H. Chen, and H.Y. Zhang, *Layer-by-layer assembly: from conventional to unconventional methods*. Chemical Communications, 2007(14): p. 1395-1405.
200. Ras, R.H.A., et al., *Ultrathin hybrid films of clay minerals*. Physical Chemistry Chemical Physics, 2007. **9**(8): p. 918-932.
201. Podsiadlo, P., B.S. Shim, and N.A. Kotov, *Polymer/clay and polymer/carbon nanotube hybrid organic-inorganic multilayered composites made by sequential layering of nanometer scale films*. Coordination Chemistry Reviews, 2009. **253**(23-24): p. 2835-2851.
202. Caruso, F., R.A. Caruso, and H. Mohwald, *Nanoengineering of inorganic and hybrid hollow spheres by colloidal templating*. Science, 1998. **282**(5391): p. 1111-1114.
203. Sukhorukov, G.B., et al., *pH-Controlled Macromolecule Encapsulation in and Release from Polyelectrolyte Multilayer Nanocapsules*. Macromolecular Rapid Communications, 2001. **22**(1): p. 44-46.
204. Jang, W.S., I. Rawson, and J.C. Grunlan, *Layer-by-layer assembly of thin film oxygen barrier*. Thin Solid Films, 2008. **516**(15): p. 4819-4825.
205. Hua, F., T. Cui, and Y.M. Lvov, *Ultrathin Cantilevers Based on Polymer,àCeramic Nanocomposite Assembled through Layer-by-Layer Adsorption*. Nano Letters, 2004. **4**(5): p. 823-825.
206. Kiryukhin, M.V., et al., *Fabrication and mechanical properties of microchambers made of polyelectrolyte multilayers*. Soft Matter, 2011. **7**(14): p. 6550-6556.
207. Kiryukhin, M.V., et al., *Adhesion of Polyelectrolyte Multilayers: Sealing and Transfer of Microchamber Arrays*. Langmuir, 2012. **28**(13): p. 5678-5686.
208. Talapin, D.V., et al., *Highly Luminescent Monodisperse CdSe and CdSe/ZnS Nanocrystals Synthesized in a Hexadecylamine,àTrioctylphosphine Oxide,àTrioctylphospine Mixture*. Nano Letters, 2001. **1**(4): p. 207-211.
209. Podsiadlo, P., et al., *Layer-by-layer assembly of nacre-like nanostructured composites with antimicrobial properties*. Langmuir, 2005. **21**(25): p. 11915-11921.
210. Li, J., et al., *Multidirectional Hierarchical Nanocomposites Made by Carbon Nanotube Growth within Layer-by-Layer-Assembled Films*. Chemistry of Materials, 2011. **23**(4): p. 1023-1031.
211. Langer, R. and J.P. Vacanti, *Tissue Engineering*, 1993, American Association for the Advancement of Science. p. 920-926.

212. Ratner, B.D., *Biomaterials science : an introduction to materials in medicine* 2004, Amsterdam ; Boston: Elsevier Academic Press. xii, 851.
213. Sharma, B. and J.H. Elisseeff, *Engineering structurally organized cartilage and bone tissues*. *Ann Biomed Eng*, 2004. **32**(1): p. 148-59.
214. Liu, X. and P.X. Ma, *Polymeric scaffolds for bone tissue engineering*. *Ann Biomed Eng*, 2004. **32**(3): p. 477-86.
215. Kotov, N., *Inverted colloidal crystals as three-dimensional cell scaffolds*. *Langmuir*, 2004. **20**(19): p. 7887-7892.
216. An, Y.H. and R.A. Draughn, *Mechanical testing of bone and the bone-implant interface / edited by Yuehuei H. An, Robert A. Draughn* 2000, Boca Raton: CRC Press. 624 p.
217. Muggli, D.S., A.K. Burkoth, and K.S. Anseth, *Crosslinked polyanhydrides for use in orthopedic applications: Degradation behavior and mechanics*. *Journal of Biomedical Materials Research*, 1999. **46**(2): p. 271-278.
218. Gartner, L.P. and J.L. Hiatt, *Color textbook of histology* 2001, Philadelphia: W.B. Saunders. 577.
219. Johnson, A.J.W. and B.A. Herschler, *A review of the mechanical behavior of CaP and CaP/polymer composites for applications in bone replacement and repair*. *Acta Biomaterialia*, 2011. **7**(1): p. 16-30.
220. Sommerfeldt, D.W. and C.T. Rubin, *Biology of bone and how it orchestrates the form and function of the skeleton*. *European Spine Journal*, 2001. **10**: p. S86-S95.
221. Liu, H. and L.C. Brinson, *Reinforcing efficiency of nanoparticles: A simple comparison for polymer nanocomposites*. *Composites Science and Technology*, 2008. **68**(6): p. 1502-1512.
222. Rho, J.-Y., T.Y. Tsui, and G.M. Pharr, *Elastic properties of human cortical and trabecular lamellar bone measured by nanoindentation*. *Biomaterials*, 1997. **18**(20): p. 1325-1330.
223. Chen, Y.M., et al., *Cultivation of endothelial cells on adhesive protein-free synthetic polymer gels*. *Biomaterials*, 2005. **26**(22): p. 4588-4596.
224. Stevens, M., *Exploring and engineering the cell surface interface*. *Science*, 2005. **310**(5751): p. 1135-1138.
225. Wei, G., *Structure and properties of nano-hydroxyapatite/polymer composite scaffolds for bone tissue engineering*. *Biomaterials*, 2004. **25**(19): p. 4749-4757.
226. Wei, G., *Macroporous and nanofibrous polymer scaffolds and polymer/bone-like apatite composite scaffolds generated by sugar spheres*. *Journal of biomedical materials research. Part A*, 2006. **78a**(2): p. 306-315.
227. Liao, S.S., F.Z. Cui, and Y. Zhu, *Osteoblasts adherence and migration through three-dimensional porous mineralized collagen based composite: nHAC/PLA*. *Journal of Bioactive and Compatible Polymers*, 2004. **19**(2): p. 117-130.
228. Muschler, G.F., C. Nakamoto, and L.G. Griffith, *Engineering principles of clinical cell-based tissue engineering*. *J Bone Joint Surg Am*, 2004. **86-A**(7): p. 1541-58.
229. Stein, A., F. Li, and N.R. Denny, *Morphological control in colloidal crystal templating of inverse opals, hierarchical structures, and shaped particles*. *Chemistry of Materials*, 2008. **20**(3): p. 649-666.

230. Ashby, M.F., *Materials selection in mechanical design*. 4th ed 2011, Amsterdam: Butterworth-Heinemann.
231. Xu, B., et al., *Making negative Poisson's ratio microstructures by soft lithography*. *Advanced Materials*, 1999. **11**(14): p. 1186-1189.
232. Campbell, M., et al., *Fabrication of photonic crystals for the visible spectrum by holographic lithography*. *Nature*, 2000. **404**(6773): p. 53-56.
233. Lin, S.Y., et al., *A three-dimensional photonic crystal operating at infrared wavelengths*. *Nature*, 1998. **394**(6690): p. 251-253.
234. Moon, J.H., J. Ford, and S. Yang, *Fabricating three-dimensional polymeric photonic structures by multi-beam interference lithography*. *Polymers for Advanced Technologies*, 2006. **17**(2): p. 83-93.
235. Wendel, B., et al., *Additive Processing of Polymers*. *Macromolecular Materials and Engineering*, 2008. **293**(10): p. 799-809.
236. Gattass, R.R. and E. Mazur, *Femtosecond laser micromachining in transparent materials*. *Nature Photonics*, 2008. **2**(4): p. 219-225.
237. Smay, J., et al., *Directed colloidal assembly of 3D periodic structures*. *Advanced Materials*, 2002. **14**(18): p. 1279.
238. Lewis, J.A., *Direct ink writing of 3D functional materials*. *Advanced Functional Materials*, 2006. **16**(17): p. 2193-2204.
239. Deubel, M., et al., *Direct laser writing of three-dimensional photonic-crystal templates for telecommunications*. *Nature Materials*, 2004. **3**(7): p. 444-447.
240. Jackman, R.J., et al., *Design and fabrication of topologically complex, three-dimensional microstructures*. *Science*, 1998. **280**(5372): p. 2089-2091.
241. Gratson, G.M., M.J. Xu, and J.A. Lewis, *Microperiodic structures - Direct writing of three-dimensional webs*. *Nature*, 2004. **428**(6981): p. 386-386.
242. De Geest, B.G., et al., *Polyelectrolyte microcapsules for biomedical applications*. *Soft Matter*, 2009. **5**(2): p. 282-291.
243. Gu, Y.Q. and J.G. Huang, *Fabrication of natural cellulose substance derived hierarchical polymeric materials*. *Journal of Materials Chemistry*, 2009. **19**(22): p. 3764-3770.
244. Strydom, S.J., et al., *Preparation and characterization of directly compactible layer-by-layer nanocoated cellulose*. *International Journal of Pharmaceutics*. **404**(1-2): p. 57-65.
245. Vlasov, Y.A., N. Yao, and D.J. Norris, *Synthesis of photonic crystals for optical wavelengths from semiconductor quantum dots*. *Advanced Materials*, 1999. **11**(2): p. 165-169.
246. Huang, L.M., et al., *Fabrication of ordered porous structures by self-assembly of zeolite nanocrystals*. *Journal of the American Chemical Society*, 2000. **122**(14): p. 3530-3531.
247. Lee, J., S. Shanbhag, and N.A. Kotov, *Inverted colloidal crystals as three-dimensional microenvironments for cellular co-cultures*. *Journal of Materials Chemistry*, 2006. **16**(35): p. 3558-3564.
248. Cuddihy, M.J. and N.A. Kotov, *Poly(lactic-co-glycolic acid) Bone Scaffolds with Inverted Colloidal Crystal Geometry*. *Tissue Engineering Part A*, 2008. **14**(10): p. 1639-1649.

249. Wang, D. and F. Caruso, *Fabrication of heterogeneous macroporous materials based on a sequential electrostatic deposition process*. Chemical Communications, 2001(5): p. 489-490.
250. Wang, Y.J. and F. Caruso, *Macroporous zeolitic membrane bioreactors*. Advanced Functional Materials, 2004. **14**(10): p. 1012-1018.
251. Arsenault, A.C., et al., *Tailoring Photonic Crystals with Nanometer-Scale Precision Using Polyelectrolyte Multilayers*. Langmuir, 2004. **21**(2): p. 499-503.
252. Ma, W., H. Otsuka, and A. Takahara, *Poly(methyl methacrylate) grafted imogolite nanotubes prepared through surface-initiated ARGET ATRP*. Chemical Communications. **47**(20): p. 5813-5815.
253. Lvov, Y.M., et al., *Halloysite Clay Nanotubes for Controlled Release of Protective Agents*. Acs Nano, 2008. **2**(5): p. 814-820.
254. <http://probes.invitrogen.com/media/pis/mp07581.pdf>.